

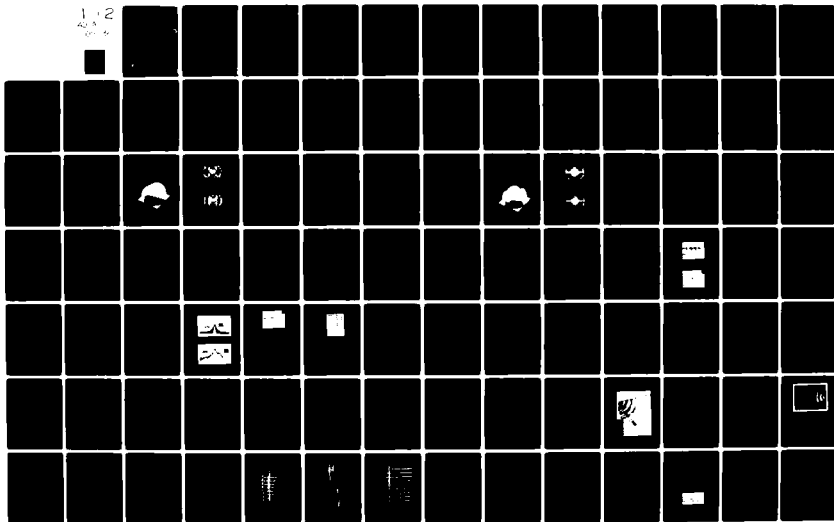
AD-A108 236

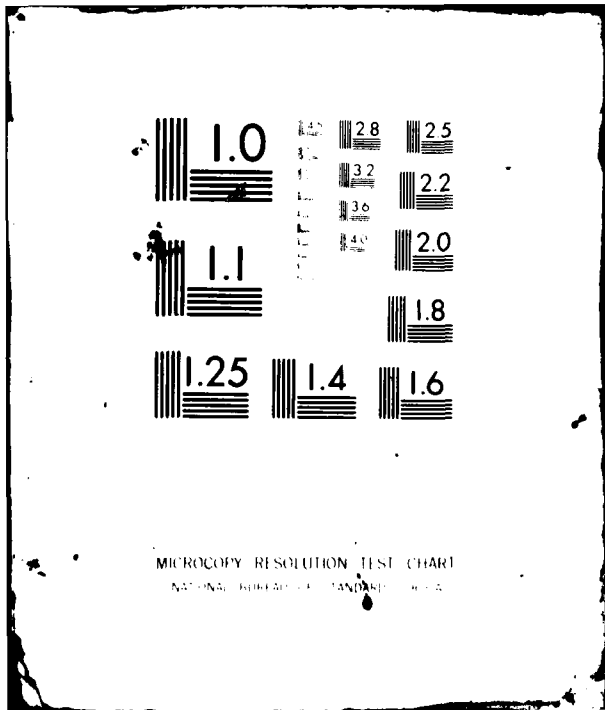
NATIONAL OCEANIC AND ATMOSPHERIC ADMINISTRATION BOUL--ETC F/G 17/9
DEVELOPMENT OF A CLEAR AIR RADAR TO DETECT METEOROLOGICAL HAZAR--ETC(U)
SEP 81 R B CHADWICK, K P MORAN, W C CAMPBELL
AFGL-TR-81-0268

UNCLASSIFIED

NL

1 2
4 3
10 9





LEVEL

AFGL-TR-81-0268

AD A108236

**DEVELOPMENT OF A CLEAR AIR RADAR
TO DETECT METEOROLOGICAL HAZARDS
AT AIRPORTS**

R. B. Chadwick
K. P. Moran
W. C. Campbell
K. B. Earnshaw
T. R. Detman

NOAA/ERL/Wave Propagation Laboratory
Boulder, Colorado 80303

21 September 1981

Final Report
1 October 1978 - 21 September 1981

SD
DTIC
ELECTED
DEC 8 1981
H

Approved for public release; distribution unlimited

DIS FILE COPY

**AIR FORCE GEOPHYSICS LABORATORY
AIR FORCE SYSTEMS COMMAND
UNITED STATES AIR FORCE
HANSCOM AFB, MASSACHUSETTS 01731**

81 12 08 295

406292

Qualified requestors may obtain additional copies from the
Defense Technical Information Center. All others should
apply to the National Technical Information Service.

Unclassified

SECURITY CLASSIFICATION OF THIS PAGE (When Data Entered)

REPORT DOCUMENTATION PAGE		READ INSTRUCTIONS BEFORE COMPLETING FORM
1. REPORT NUMBER AFGL-TR-81-0268	2. GOVT ACCESSION NO. AD-A108 236	3. RECIPIENT'S CATALOG NUMBER
4. TITLE (and Subtitle) DEVELOPMENT OF A CLEAR AIR RADAR TO DETECT METEOROLOGICAL HAZARDS AT AIRPORTS		5. TYPE OF REPORT & PERIOD COVERED Final Report 1 Oct 1978 - 21 Sept 1981
7. AUTHOR(s) R. H. Chadwick K. B. Earnshaw K. P. Moran T. R. Detman W. C. Campbell		6. CONTRACT OR GRANT NUMBER(s) ESD-0-0890
9. PERFORMING ORGANIZATION NAME AND ADDRESS NOAA/ERL/Wave Propagation Laboratory Boulder Colorado 80303		10. PROGRAM ELEMENT, PROJECT, TASK AREA & WORK UNIT NUMBERS 62101F 667006AB
11. CONTROLLING OFFICE NAME AND ADDRESS Air Force Geophysics Laboratory Hanscom AFB, Massachusetts 01731 Monitory Ralph J. Donaldson, Jr/LYR		12. REPORT DATE 21 September 1981
14. MONITORING AGENCY NAME & ADDRESS (if different from Controlling Office)		13. NUMBER OF PAGES 113
		15. SECURITY CLASS. (of this report) Unclassified
		15a. DECLASSIFICATION DOWNGRADING SCHEDULE
16. DISTRIBUTION STATEMENT (of this Report) Approved for public release; distribution unlimited.		
17. DISTRIBUTION STATEMENT (of the abstract entered in Block 20, if different from Report)		
18. SUPPLEMENTARY NOTES		
19. KEY WORDS (Continue on reverse side if necessary and identify by block number) Wind shear Clutter suppression Clear air radar Wake vortex detection FM-CW Doppler radar Airport hazards		
20. ABSTRACT (Continue on reverse side if necessary and identify by block number) To be useful in detecting meteorological hazards such as low-level wind shear near airports, a radar must be able to: (1) detect backscatter from both clear air and rain; (2) operate at short ranges and low elevation angles; and (3) measure Doppler frequencies caused by air motion. The development of a radar with these characteristics is described and the results of testing this radar at airports are presented. Special emphasis is placed on the problems of low elevation angle operation and clutter suppression. The importance of		

DTIC
SELECTED
 AUG 8 1981

TABLE OF CONTENTS

	Page
1. CLEAR AIR RADAR LANDING AID	1
1.1 Introduction	1
1.2 Recommendations	2
1.3 Previous Work	4
1.4 Brief Description of Contents	6
1.5 Chapter 1 Bibliography	8
2. ANTENNA IMPROVEMENTS	10
2.1 Introduction	10
2.2 Splash-Plate Feeds	10
2.3 Near Field Measurements	13
2.4 Antenna Isolation	22
2.5 Alternate Design for Dual Antenna System	32
2.6 Single-Antenna FM-CW Radar	34
2.7 Summary of Antenna Work	40
2.8 Chapter 2 Bibliography	41
3. CLUTTER SUPPRESSION	42
3.1 Introduction	42
3.2 Pre-Detection Saturation	42
3.3 Post-Detection Saturation	45
3.4 Frequency Stabilization	48
3.5 Range Spreading of Strong Return Signals	52
APPENDIX A -- FREQUENCY DOMAIN ANALYSIS OF GROUND CLUTTER SUPPRESSOR.	56
APPENDIX B -- RANGE SPREADING OF LARGE TARGETS	62
4. INTERFERENCE CONSIDERATIONS	70
4.1 Introduction	70
4.2 Interference from Hard Targets	70
4.3 Interference from Biological Targets	77
4.4 Interference from Hydrometeors	78
4.5 Interference from Wake Related Return	80
4.6 Summary of Problem Areas	85
4.7 Chapter 4 Bibliography	87
5. AIRPORT OPERATIONS AT OTIS AIR FORCE BASE, MASSACHUSETTS	88
5.1 Introduction	88
5.2 Wind Shear Measurements in Rain	89
5.3 Comparison of Tower Measurements and Radar Measurements of Low-Level Winds	98
5.4 Summary of Experimental Results	105
6. SUMMARY AND OBSERVATIONS	106

CHAPTER 1 -- CLEAR AIR RADAR LANDING AID

R.B. Chadwick

1.1 Introduction

The purpose of this project was to demonstrate the feasibility of a short-range clear-air radar as a landing aid at airports. The major use for such a radar would be as a remote sensor of wind shear in the approach zone. An unexpected shift in wind speed on the final landing approach can cause problems for large jets. The relative wind speed or "headwind" determines the lift on the wings and if this lift changes unexpectedly during the final seconds of a landing approach, the aircraft will undershoot or overshoot the intended touch-down point. In a study of accidents on final approach, it was found that "... more than 20% of the runoffs and more than 10% of the undershoot cases were due to wind difficulties. Many of these cases were believed to be related to low-level turbulence and wind shear," Narrcoo (1974). Until the problem of low-level wind shear was studied in detail, many of the accidents on final approach were blamed on "pilot error." During the past decade, fatal crashes due to low-level wind shear have averaged about one per year for large jet aircraft.

Small amounts of wind shear are not hazardous, but they can still cause missed approaches where the aircraft must go around and make a second approach. In the past, this was mainly a nuisance, but in this era of expensive jet fuel and high airport congestion, the economic aspects of missed approaches become important. Data showing nine missed approaches in a two hour period on January 4, 1971 at JFK International Airport are shown in Badner (1979). This was for a measured shear of only 0.03 s^{-1} in the lowest 300 m. These nine missed approaches added 144 minutes to the flying time of these aircraft, which would have added \$7,200 in fuel costs at today's rate of about \$3,000/h. This does not include the salaries of the aircraft personnel or the inconvenience of the delay to the passengers. If the pilot knows the height and wind speed difference across the shear layer, it is easy to correct the aircraft speed for the anticipated shear so the landing can be made on the initial approach. It is standard procedure at commercial airports today for pilots who have landed to notify the tower if they experienced wind shear on the final approach. This information is relayed to

incoming pilots so they can take appropriate action. The problem with this procedure is that the information is only a "snapshot" of a changing situation. A much better procedure would be to continuously monitor the wind shear and relay any changes in the situation to the pilot. This appears to be well within the state-of-the-art of today's remote sensors.

A by-product of this study was the relative ease with which short-range clear-air radar can detect return associated with the turbulent wakes of the aircraft. It is not clear just what physical phenomena causes the backscatter, but it is clear that it relates to the aircraft wake and can be detected by radar. A part of the aircraft wake is the wingtip vortex which is a recognized hazard to small aircraft and in one case has caused the crash of a large jet. The standard procedure to avoid the vortex problem is to keep the aircraft spacing large and avoid mixing large and small planes. However, commercial aviation is straining this procedure at many congested airports and the problem is aggravated by the wide range of private aircraft which use these airports. A similar problem potentially exists at military airports. In an emergency situation, many aircraft of widely differing size may need to use the same airfield in a relatively short time interval and wingtip vortices from large aircraft could be hazardous to small aircraft. A device to monitor for hazardous vortices would clearly be useful in this situation.

1.2 Recommendations

These recommendations fall into two categories. The first set of recommendations relate to the actual hardware involved in an FM-CW Doppler radar. The second set concern future research and development needed to develop the concepts into an operational system. The results we have obtained so far are entirely positive and there seem to be no technical reasons why a short-range clear-air radar such as the FM-CW Doppler radar could not be developed into an operational system for measuring wind shear at airports.

The present experimental FM-CW radar was built in 1973 using equipment designed years earlier. So, all of the technology in this experimental radar system is at least a decade old. There are some new concepts available today which should

be tried before an operational prototype is designed. The first item is a solid-state power transmitter. A decade ago, solid state devices could only develop fractions of a Watt at S-band. Now devices which develop 40 W are available. A solid state transmitter would offer two major improvements over the traveling-wave-tube (TWT) transmitter we presently use. First, it should have much greater reliability which is a key element of any operational system. Second, it should have lower output noise. The output noise of the transmitter is a key element in a CW radar because this noise couples into the receiver and can decrease sensitivity. The noise and reliability of the transmitter have been major problems in our experimental radar. There is an important difference between a TWT amplifier and a high power solid state amplifier. The TWT amplifier is a class A amplifier which means that the amplification is the same over each full cycle of the signal. High power solid state amplifiers are usually class C amplifiers, which means the gain is zero over some part of the 360° cycle of the input signal. Class A amplifiers are necessary when both signal amplitude and frequency are important, but a class C amplifier can be used when only frequency is important. Thus, it is felt that a class C power amplifier can be used in the FM-CW radar, but this should be verified experimentally. So, we recommend that a solid-state power amplifier be acquired and tested on the present experimental radar.

A second recommendation relates to the signal processor. In the past decade, audio frequency spectrum analyzers have all become digital Fast Fourier Transform (FFT) devices. In fact, the analog spectrum analyzer we use has not been manufactured for over five years. A programmable FFT device offers much greater flexibility than we presently have. It would be possible to perform arithmetic operations such as weighting or digital filtering on the data before the FFT. Also, we would be able to have any number of output points. Presently, we only have 500. Since a signal processor similar to what we have used is no longer available, experience with an FFT signal processor would be essential before designing an operational prototype. We recommend that an array processor be purchased and software developed to do weighting, digital filtering, and FFTs on the radar output.

A third recommendation relates to the range spreading phenomenon discussed in Chapter three. This is when a strong return in one range cell spreads into other range cells. This is not a problem with stationary targets, but is definitely a problem with large moving targets such as aircraft. Preliminary results in Chapter

three show that the range spreading can be greatly reduced through signal processing. We recommend that after an array processor is acquired, a study be undertaken to determine the best way to reduce range spreading.

The present experimental FM-CW radar was never built with airport operation in mind. It also was not designed to be moved great distances. A prototype device specifically designed to be moved from airport-to-airport should be designed and built. This device should use an offset antenna arrangement to reduce returns from moving targets in sidelobes. It should also be easily moved so that siting characteristics of different airports could be determined.

However, before this prototype is designed, its precise use should be specified. Our research has shown that short-range clear-air radars can also detect returns from aircraft wakes. It should be decided if it is desirable for the prototype radar to be used for wake vortex detection as well as wind shear detection. If this is desirable, more basic research into the interaction of electromagnetic waves and turbulent aircraft wakes is needed. It would be essential to know exactly what part of the wake causes the return. The frequency and polarization dependence must be determined. Also, some idea of the radar cross section of the turbulent wake is needed. Once these things have been determined, a prototype system to detect both hazardous wind shear and wake vortices could be designed. It is likely that a system to detect both hazards would be somewhat different from a system to detect just wind shear. So, we recommend that a decision be made as to whether it is desirable for the same radar to detect both hazardous wind shear and hazardous wake effect. If so, we recommend a program for basic research in radar detection of wake vortices. If not, we recommend the design and construction of a prototype radar specifically designed for wind shear detection at airports.

1.3 Previous Work

During the past decade, there has been considerable progress in probing of the clear atmosphere with radar. Much of this work has been toward the upper atmosphere, but a substantial amount has been directed to clear-air probing of the boundary layer. Hardy and Katz (1969) used a large, high power radar to outline convective processes in lower atmosphere. In addition, they have shown that

the tropopause could be detected by radar. Utterston (1969) collected and quantified the theory of scattering from refractive-index irregularities in the turbulent atmosphere and his frequently referenced result for radar cross section of the clear air is

$$\eta = 0.38 C_n^2 \lambda^{-4}$$

where C_n^2 is the radio refractive index structure constant and λ is the radar wavelength. This shows that the backscatter phenomena is relatively independent of wavelength so that frequency can be selected according to other criteria. Richter (1969) conceived and developed the idea of a short-range high-resolution radar to study the height of inversion layers. The spectacular results from his FM-CW radar located in southern California revealed an unexpectedly rich structure in the inversion layers there and much work on the nature of waves in the clear air followed, Gossard et al. (1970). Richter's design for the FM-CW radar was soon copied and a second unit, operated in the high plains meteorological regime of Colorado, showed similarities and differences with the maritime results obtained in California, Bean et al. (1971). There were sharp-edged layers in the lowest 500 m, as in California, but there were more diffuse layers above 1 km and there appeared to be more air-borne insects in Colorado than on the Southern California coast.

The next step was to introduce Doppler processing into the FM-CW radar and this was done using two different techniques. The first, Strauch et al. (1976) required off-line processing of the recorded data to obtain velocity spectra. The second, Chadwick et al. (1976) used a commercial spectrum analyzer rather than a computer to determine the velocity spectra. The advantage of this approach was that it required no additional equipment beyond that needed in Richter's original design for an FM-CW radar. Also, the outputs were available in real time. The signal processing involved in this second approach was described by Chadwick and Strauch (1979). About the same time that the FM-CW Doppler results were reported, Hennington et al. (1976) reported clear-air wind measurement with a large pulse-Doppler radar.

Up to this point, radar measurements in the clear-air had been mainly of scientific interest. Then, it became obvious that this technology was applicable as a landing aid at airports. The primary interest here was a device to monitor

for hazardous wind shear. Some of the recent publications relating use of clear air radars at airports are: Strauch (1979), Strauch and Sweezy (1980), Chadwick et al. (1978), and Chadwick, Moran, and Campbell (1979). The work described in these last two publications was supported by the Air Force Geophysics Laboratory (AFGL) and is closely related to the work reported on here. This work was started in November 1976 with the purpose of monitoring C_n^2 for an extended period. Measurements of C_n^2 commenced in March 1977 and extended to February 1978. Data was acquired for a total of 160 days at three different sites in Colorado and reduced to histograms and curves relating frequency of occurrence to time of day and month of year. That work was reported in Chadwick et al. (1978) and in Chadwick and Moran (1980) and the main conclusion was that radar detection of hazardous wind shear at airports was indeed feasible. However, it was noted that a capability to operate the radar in the Doppler mode at low elevation angles was necessary. Preliminary work on this low elevation capability was reported in Chadwick et al. (1978) and results were presented in Campbell et al. (1980). That work was successfully completed and is reported on here. This report can be considered a continuation of the first AFGL report, Chadwick et al. (1978).

1.4 Brief Description of Contents

This first chapter is a brief introduction to the wind shear problem. Specific recommendations and a discussion of previous work are included.

The second chapter concentrates on the antenna improvements specifically designed to reject ground clutter at low angles. The design we used and the pattern measurements are given. Some results from bench tests on a circulator-canceller, designed to allow single antenna operation, are given.

Chapter three describes the electronic approach to eliminating ground clutter. Receiver saturation is divided into two classes, pre-detection and post-detection saturation. Both of these are discussed, and it is shown that post-detection is the more prevalent and is amenable to solutions using digital filter techniques. It is demonstrated that to achieve full clutter cancelling capability the transmitted signal must be frequency stabilized. Cases are presented with and without the ground clutter suppressor and with and without frequency stabilization. The

recently discovered problem of range spreading, which is a type of saturation, is also discussed.

Chapter four presents some siting and systems considerations along with some experimental results. Of interest here are the echoes which we believe to be related to the turbulent wakes of large aircraft.

Chapter five presents results from a field experiment conducted in Massachusetts at Otis AFB. Two types of data are presented. The first is from a wind shear layer in stratiform rain. The second is from clear air scattering recorded at low elevation angles. Wind profiles are determined and compared with tower measurements.

The report concludes with Chapter six, a brief summary and some observations on the present status of the low-level wind shear problem.

CHAPTER 1 -- BIBLIOGRAPHY

- Narrcoo, M.E., (1974), "A status report on low level turbulence and wind shear effects on aircraft," ICAO Bulletin, Sept. 1974.
- Badner, J., (1979), "Low-level wind shear: A critical review," NOAA Tech. Memo., NWS FCST-23, April 1979.
- Hardy, K. and I. Katz (1969), "Probing the clear atmosphere with high power high resolution radars," Proc. IEEE, Vol. 57, p 468-480.
- Ottersten, H. (1969), "Radar backscattering from the turbulent clear atmosphere," Radio Sci., Vol. 4, p 1251-1255.
- Richter, J.H. (1969), "High resolution tropospheric radar sounding," Radio Sci., Vol. 4, p 1261-1268.
- Gossard, E.E., J.H. Richter and D. Atlas (1970), "Internal waves in the atmosphere from high-resolution radar measurements," J. Geophys. Res., Vol. 75, p 3523-3526.
- Bean, B.R., R.E. McGavin, R.B. Chadwick and B.D. Warner (1971), "Preliminary results of utilizing the high resolution FM radar as a boundary layer probe," Boundary Layer Meteorol., Vol. 1, p 466-473.
- Strauch, R.G., W.C. Campbell, R.B. Chadwick and K.P. Moran (1976), "Microwave FM-CW Doppler radar for boundary layer probing," Geophysical Research Letters, Vol. 3, No. 3, p 193-196, March 1976.
- Chadwick, R.B., K.P. Moran, R.G. Strauch, G.E. Morrison and W.C. Campbell, "A new radar for measuring winds," Bull. Amer. Meteorol. Soc., Vol. 57, p 1120-1125, Sept. 1976.
- Chadwick, R.B. and R.G. Strauch (1979), "Processing of FM-CW Doppler signals from distributed targets," IEEE Trans. on Aerospace and Electronic Systems, Vol. AES-15, No. 1, pp 185-189.
- Hennington, L., R.J. Doviak, D. Sirmans, D. Zurnic and R.G. Strauch (1976), "Measurements of winds in the optically clear air with microwave pulse-Doppler radar," Proc. of 17th Conf. on Radar Meteorol. p 342-348.
- Strauch, R.G. (1979), "Applications of meteorological Doppler radar for weather surveillance near air terminals," IEEE Trans. on Geoscience Electronics, Vol. GE-17, No. 4, p 105-112.
- Strauch, R.G. and W.B. Sweezy (1980), "Wind shear detection with pulse Doppler," FAA Tech. Report No. FAA-RD-80-26, Jan. 1980.
- Chadwick, R.B., K.P. Moran, G.E. Morrison and W.C. Campbell (1978), "Measurements showing the feasibility for radar detection of hazardous wind shear at airports," Air Force Geophysics Laboratory Tech. Report No. AFGL-TR-78-0160, Feb. 1978.

Chadwick, R.B., K.P. Moran and W.C. Campbell (1979), "Design of a wind shear detection radar for airports," IEEE Trans. on Geoscience Electronics, Vol. GE-17, No. 4, p 137-142.

Chadwick, R.B. and K.P. Moran (1980), "Long-term measurements of C^2 in the boundary layer," Radio Science, Vol. 15, No. 2, p 355-362 Marⁿ-Apr. 1980.

Campbell, W.C., R.B. Chadwick, K.B. Earnshaw and K.P. Moran (1980), "Low elevation angle wind measurements by FM-CW radar," Proc. of 19th Conference on Radar Meteorology, p 722-726, April 1980.

CHAPTER 2 -- ANTENNA IMPROVEMENTS

K.E. Earnshaw and R.B. Chadwick

2.1 Introduction

While there are many approaches which can be used to achieve low elevation angle capability, the place to start is to reduce the antenna sidelobes as much as is practically possible. Ground reflections that are discriminated against by the antenna are kept out of the electronics processing and thus cause no problem. Also improvements in the antenna pattern add to clutter suppression improvements in the electronics and so both should be pushed to the fullest extent possible.

We considered different levels of antenna improvement and decided that the most cost-effective approach was to redesign the feed system for the present antennas. The philosophy behind this design procedure is described below along with the measurements concepts used to arrive at a practical, rugged antenna system which could be used to make calibrated atmospheric measurements.

A proposed dual antenna concept is advanced below which should be both mechanically and electrically superior to the present improved antenna system. The utilization of this new concept would require a new reflector structure as well as new feeds.

Another antenna improvement would be to use the same antenna for both transmitting and receiving. This chapter concludes with a section describing the possible approaches to achieving single antenna operation and the related experimental work.

2.2 Splash-Plate Feeds

There were two major requirements for the improved antenna system. First, the sidelobe level must be such that a significant portion of the ground clutter is rejected. Second, polarization must be adjustable so as to minimize the ground

return. Additional requirements are that the improvements must be rugged and reasonably simple to realize.

A number of antenna types were considered. An offset paraboloid reflector gives the best sidelobe response and is very attractive but would have required that the entire system be rebuilt. The resources to do this were not available, however, a conceptual design for an offset paraboloid antenna system that may be desirable for an operational system is discussed below.

Another antenna improvement considered was to replace the feed system with an improved version. The original feed was a horn supported by a tripod structure with a coaxial line carrying the signals outside the antenna. It was certain that the feed system could be improved somewhat, but there would still be supports, a coaxial line, and the feed horn blocking the aperture. We felt that reflections from these structures were causing many of the sidelobes of the old antenna system, and perhaps a different approach was necessary.

A back fed unsupported feed system has no metal supports to cause reflections or sidelobes and this seemed like a reasonable approach. One version of this type of feed is the splash-plate feed or Cassagrain feed with unity magnification. This feed is rugged and easy to manufacture, however it has reduced efficiency. Since the primary requirement is on the sidelobes rather than antenna gain, it was felt that the reduced aperture efficiency could be tolerated. Another disadvantage of splash-plate feeds is that the design and focusing are empirical. However, this was not considered a major disadvantage as the National Bureau of Standards indoor near-field antenna range was available for trial and error design.

The basic geometry behind a splash plate feed is shown in Fig. 2.1. On transmission the microwave signal propagates up the waveguide, hits the metal reflector and is reflected out the openings back toward the reflector. The waveguide can be either rectangular or circular. For rectangular guide, the opening is along the H-axis (long side of guide) and the short sides of the guide are used to support the splash plate reflector. For circular guide, the reflector is held in place by a dielectric cylinder attached to the guide and the opening extends completely around the guide.

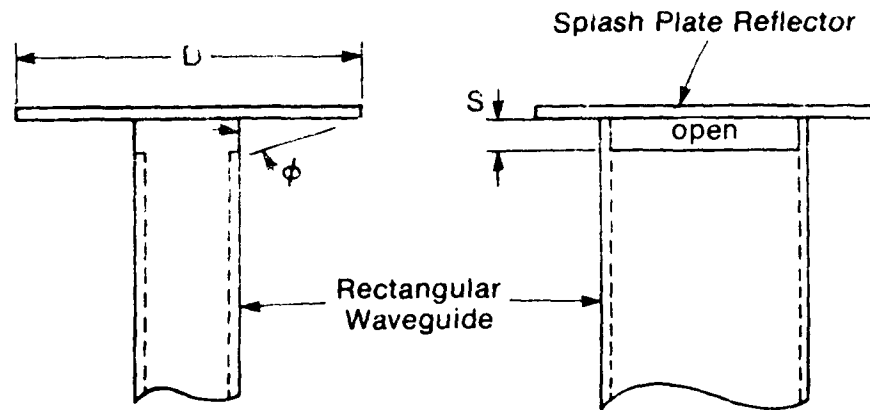


Figure 2.1--Splash plate feed geometry.

Because of the empirical nature of splash-plate feed design, it was decided to base this design on feed structures which had been previously built. Four such designs were available. The first was an S-band rectangular feed and 15' diameter antenna used at the National Air Facilities Experimental Center (NAFEC) near Atlantic City, N.J., Strauch (1979). The second was an X-band rectangular feed and 21" diameter antenna, Studd (1966). The third was an X-band circular feed and 5' diameter antenna designed at Bell Telephone Laboratories over twenty years ago, Hogg (1979). The fourth was a circular feed at an unspecified frequency, James and Malik (1975). The dimensions for each of these feeds are given in Table 2.1 along with those of the final design of the feed built for the FM-CW radar.

Table 2.1--Characteristics of several splash-plate antenna systems

	freq. (MHz)	D/ λ	S/ λ	ϕ (deg)	Antenna Diameter (ft)	Aperture Efficiency	Sidelobe Level (dB)	Return Loss (dB)
NAFEC (rectangular)	2800	0.94	0.08	78.2	15	.35	-27	-21
Studd (rectangular)	9375	1.11	0.13	125	1.75	.55	-26	-27.6
BTL (circular)	11000	2.85	1.01	46.6	5	.62	-22	-30
James & Malik (circular)		4	2	17.7				-20.8
FM-CW (rectangular)	2945	1.40	0.11	78.8	8	.50	-27	-22

None of these five feed systems are exactly like that shown in Fig. 2.1. The NAFEC antenna and the FM-CW antenna both have a small deflection plate near the opening as shown in Fig. 2.2. In addition, the NAFEC feed has a metallic structure above the reflector plate to reduce the edge currents on the plate. On the Studd feed, the reflector plate is not flat, but rather has skirts on the edge of the reflector. These skirts extend below the opening resulting in an angle ϕ greater than 90° . Both the James and Malik and BTL designs have a structure on the bottom of the reflector designed to improve the VSWR of the feed. The FM-CW splash-plate, rather than being circular, is elliptical with the major axis in the E-plane. The precise geometry for the FM-CW splash-plate feed is shown in Fig. 2.2.

2.3 Near Field Measurements

The approach used for the FM-CW feed design was to reproduce the NAFEC design and measure the feed pattern on the National Bureau of Standards indoor antenna range. This measurement facility is described in detail by Newell and Crawford (1974). Measuring the feed pattern of a back-fed feed is not easy as the structure is mounted backwards, i.e., the light end is attached to a holder and the heavy end is cantilevered. If no additional supporting structure is used to support the heavy end of the feed, the welds that attach the splash-plate to the waveguide will immediately break. To circumvent this problem, a support of dry spruce wood was constructed to hold the feed structure. This entailed a piece of spruce running along the edges of the waveguide. The initial measurements gave some peculiar results. It was later decided that these results were due to dielectric waveguide action in the dry spruce along the sides of the waveguide. This necessitated rebuilding the support structure entirely out of extruded styrofoam, thin nylon cord, and considerable ingenuity. The effort proved successful as the feed horn did not sag as it was rotated through 90° to make both E-plane and H-plane adjustments.

The feed patterns were measured at a number of discrete frequencies ranging from 2.2 to 4.5 GHz. These amplitude and phase measurements in the E-plane are shown in Fig. 2.3. Even though the NAFEC antenna was designed at 2.8 GHz, it was felt that the response at 3.8 GHz would give better feed patterns when used with a

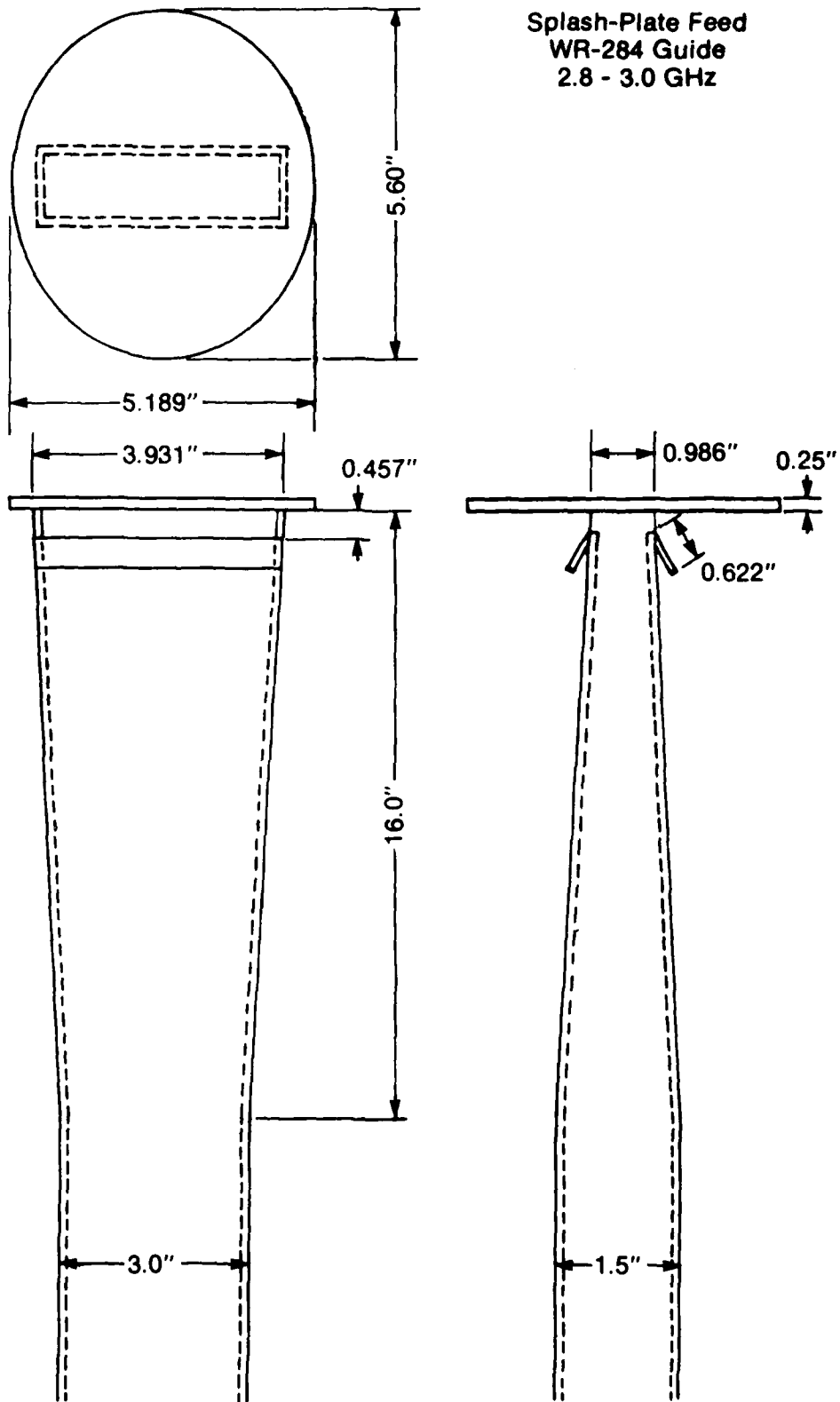


Figure 2.2--FM-CW splash plate feed.

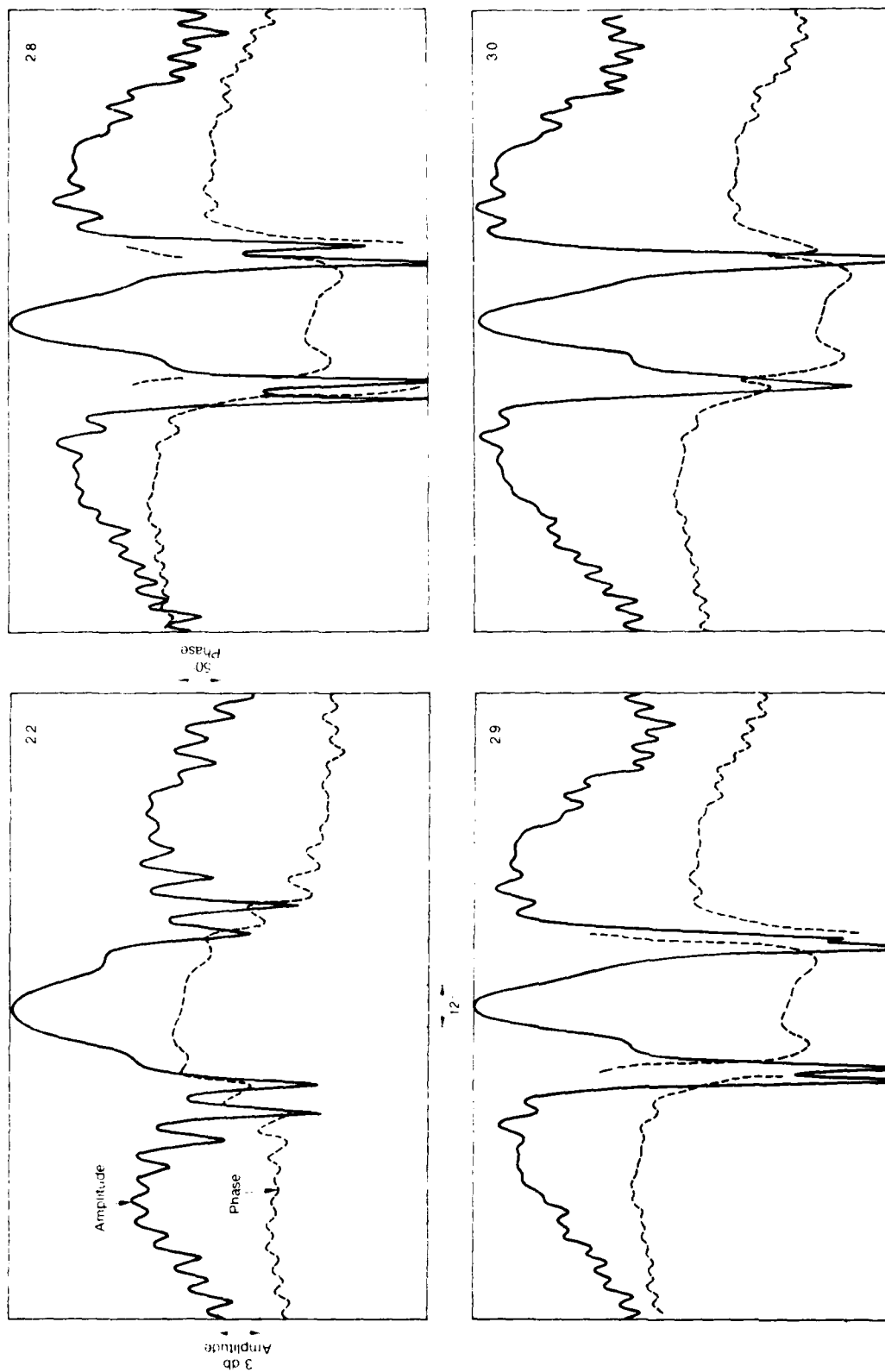


Figure 2.3(a) -- Feed pattern amplitude and phase in E-plane at 2.2, 2.8, 2.9 and 3.0 GHz for design #1.

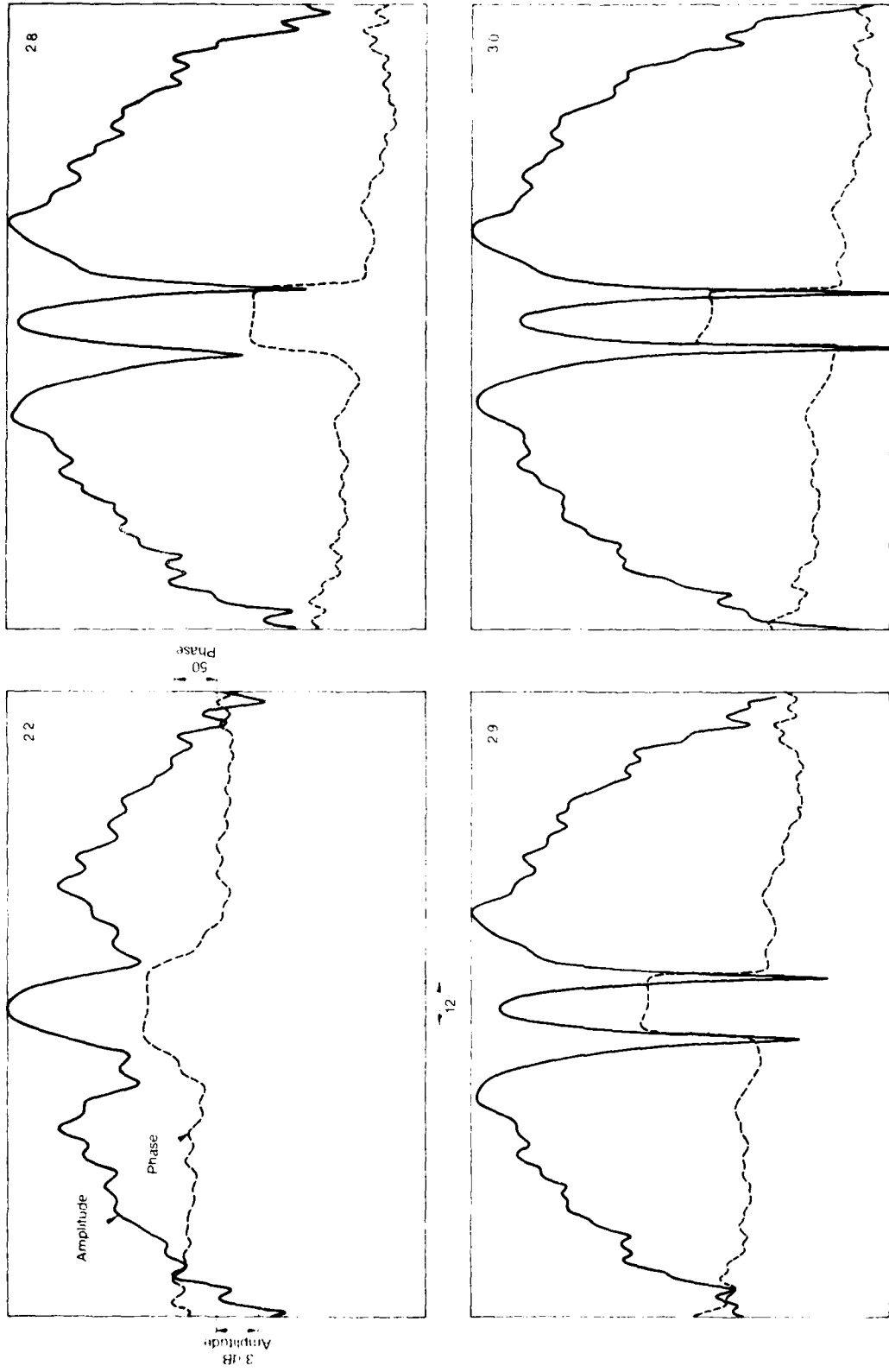


Figure 2.3(b) -- Feed pattern amplitude and phase in H-plane at 2.2, 2.8, 2.9 and 3.0 GHz for design #1.

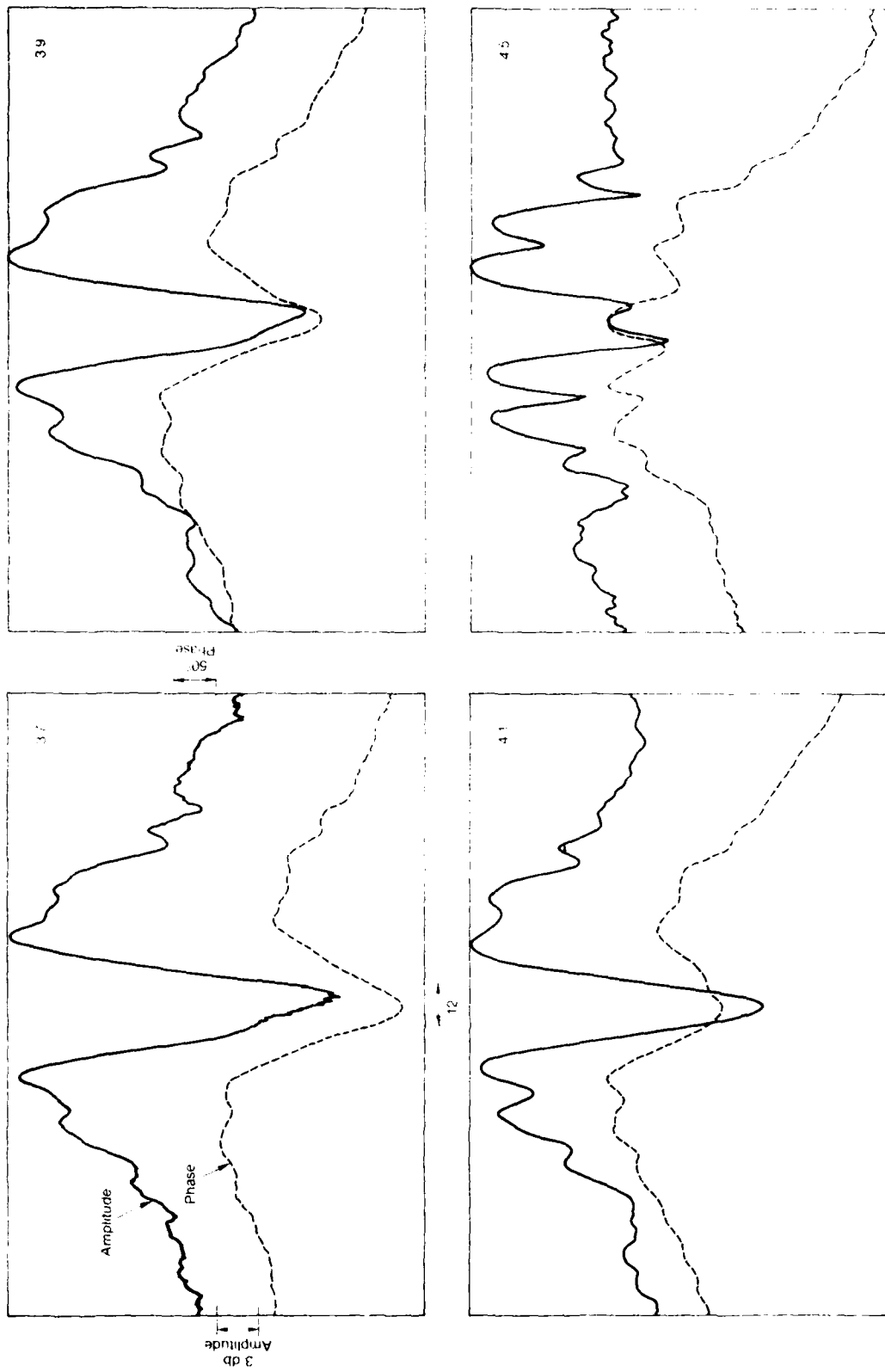


Figure 2.3(c) -- Feed pattern amplitude and phase in E-plane at 3.7, 3.9, 4.1 and 4.5 GHz for design #1.

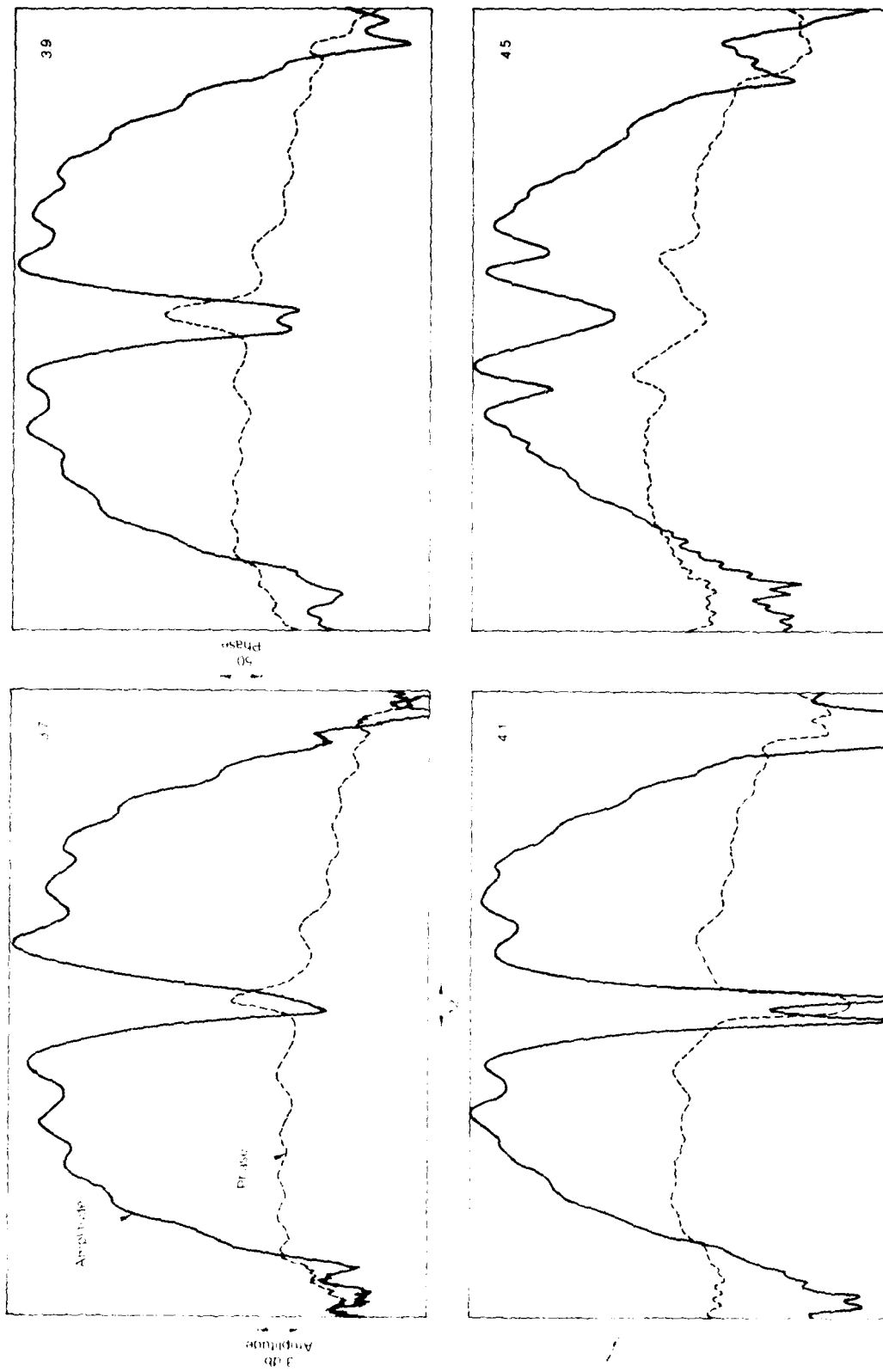


Figure 2.3(d)--Feed pattern amplitude and phase in H-plane at 3.7, 3.9, 4.1 and 4.5 GHz for design #1.

back fed parabolic reflector system. So, this original prototype was frequency scaled from 3.9 to 2.945 GHz and this formed the basis of the final design, which is illustrated in Fig. 2.2.

The feed pattern measurements for the frequency scaled design (design #2) are shown in Fig. 2.4. It was not possible to scale each parameter of the design and so the feed pattern for the scaled version at 2.9 GHz is not exactly the same as that of the original version at 3.9 GHz. The size of the waveguide had to be the same for both designs. In the scaled version the waveguide was tapered near the splash-plate as shown in Fig. 2.2. It is perhaps this difference that accounts for the difference between the original feed pattern and the pattern of the scaled version.

The measurements to this point have been of the feed pattern. These are similar to conventional pattern measurements in that the results are obtained in real time and so, trial and error design procedures can be used. Electrical sizes can be changed by using different types of dielectric inserts in the feed and physical sizes can be changed by using metallic inserts and metallic foil. This allows some adjustment of the feed structure to obtain a better feed pattern.

The next step was to measure the pattern when the feed was mounted in an eight foot parabolic reflector. This is not a real time measurement as the procedure requires a two-dimensional numerical Fourier transform of the complex near-field data obtained in an aperture plane of the reflector antenna. The output of this procedure is a complete two-dimensional plot of the far-field antenna pattern. The cross-polarization response of the antenna can be obtained in the same way.

The near-field measurements necessary to obtain the far field pattern are made by a movable probe which scans the antenna a short distance in front of the aperture and samples the amplitude and phase at sample points. Since the procedure depends strongly on knowing the precise spacing and location of these sample points, the location of the movable probe is continually monitored by a laser distance measuring device.

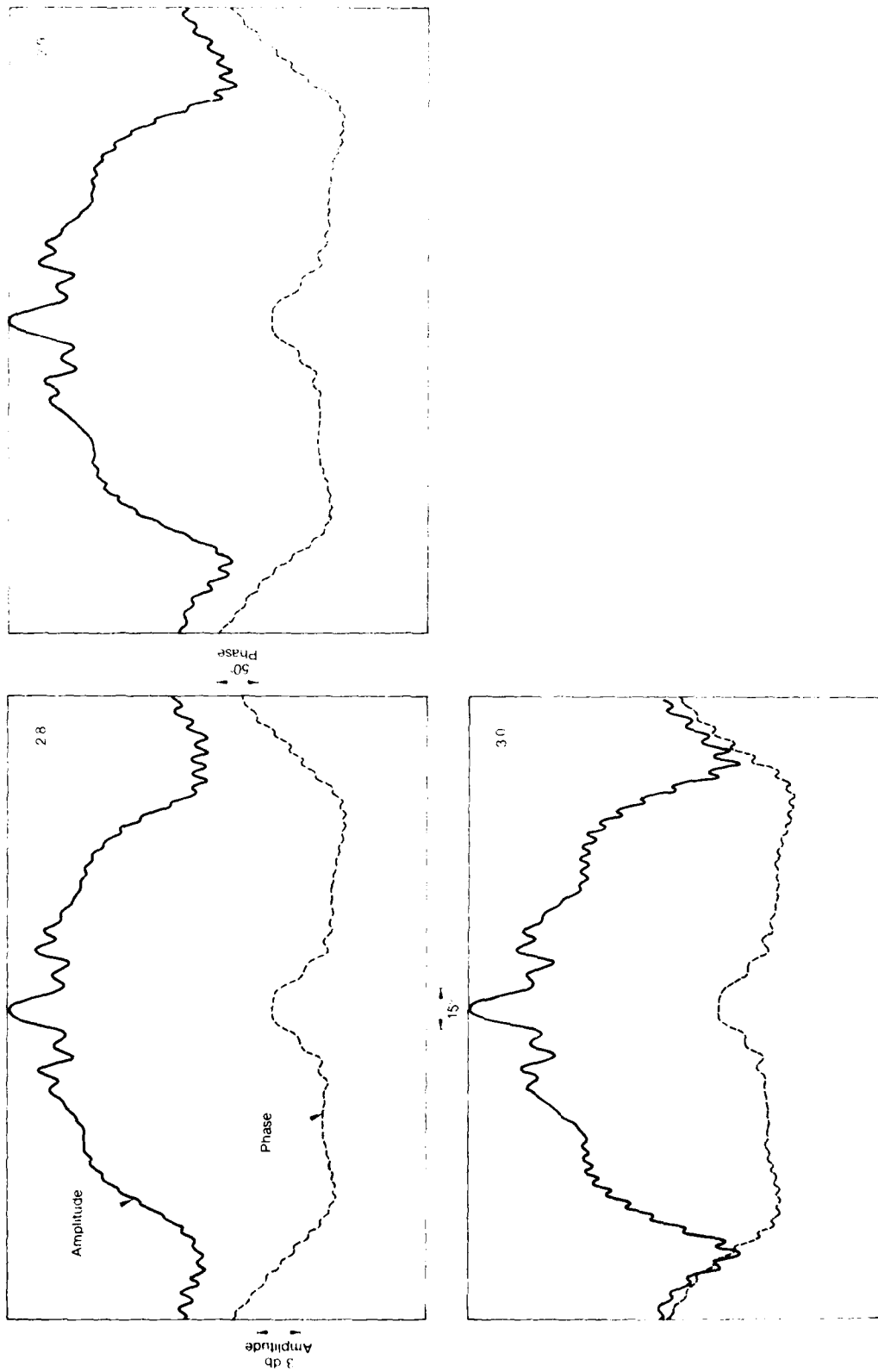


Figure 2.4(a) -- Feed pattern amplitude and phase in E-plane at 2.8, 2.9 and 3.0 GHz for design #2.

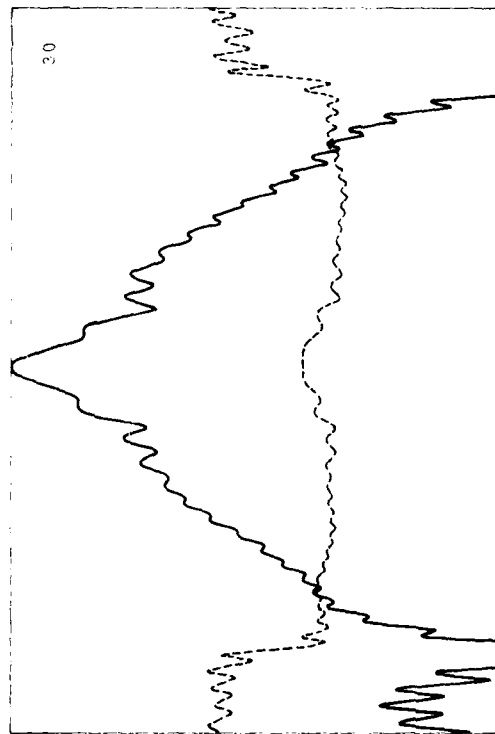
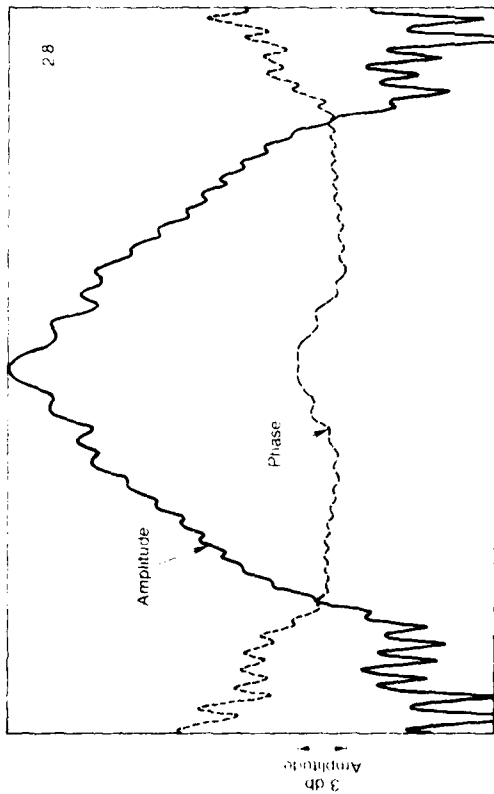
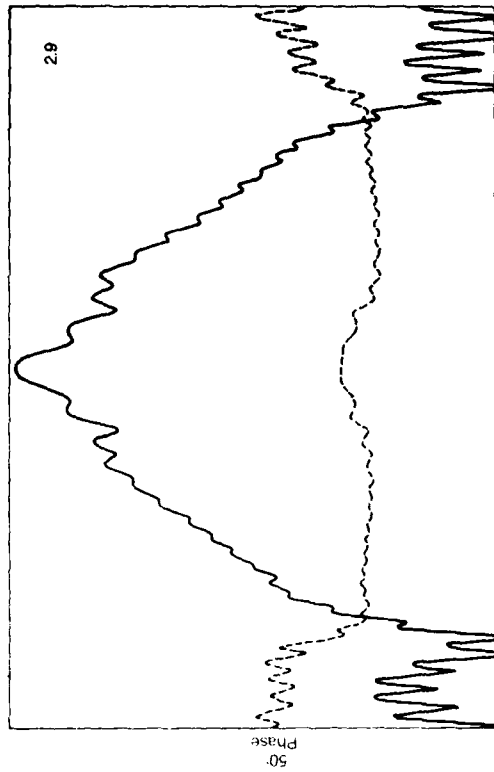


Figure 2.4(b) -- Feed pattern amplitude and phase in H-plane at 2.8, 2.9 and 3.0 GHz for design #2.

The movable probe scans the aperture plane 144 times, acquiring 144 equally-spaced complex samples in each scan. This generates a 144 x 144 complex matrix which is then Fourier transformed to yield the far-field antenna pattern. Two of the near-field scans are shown in Fig. 2.5. Both of the scans are through the center of the aperture plane, Fig. 2.5(a) is in the vertical direction and Fig. 2.5(b) is in the horizontal direction.

The two-dimensional plot of the far-field antenna pattern is shown in Fig. 2.6 which is good for qualitative information. More quantitative information can be obtained from Fig. 2.7 which shows contour plots of the two-dimensional antenna pattern in Fig. 2.6. The contour interval is 6 dB, and in Fig. 2.7(a) the first contour is at -3 dB while in Fig. 2.7(b) the first contour is at -6 dB. Conventional one-dimensional antenna patterns can be obtained by taking cross-sections through the two-dimensional plot. These E-plane and H-plane patterns are shown in Fig. 2.8(a) and (b), and on a more expanded scale in Fig. 2.8(c) and (d).

As expected, the back-fed, splash-plate feed results in an unsymmetric antenna pattern with lower sidelobes in the H-plane. This effect can be used to advantage in this situation as the H-plane can be made perpendicular to the ground and thus reduce returns from ground clutter objects.

Using this near-field measurement technique, the cross-polarization antenna pattern can also be obtained. Figure 2.9 shows a perspective view of the cross-polarization pattern. Figure 2.10 shows contour plots of the cross-polarization pattern.

2.4 Antenna Isolation

An important consideration for any CW radar is the isolation between the transmitting and receiving antenna. When the splash plate feeds are polarized so that the ground clutter is minimized, the coupling between the antennas can be large. In this case, the increase in the cross-coupling was larger than expected which meant that we had to take additional steps to increase the isolation.

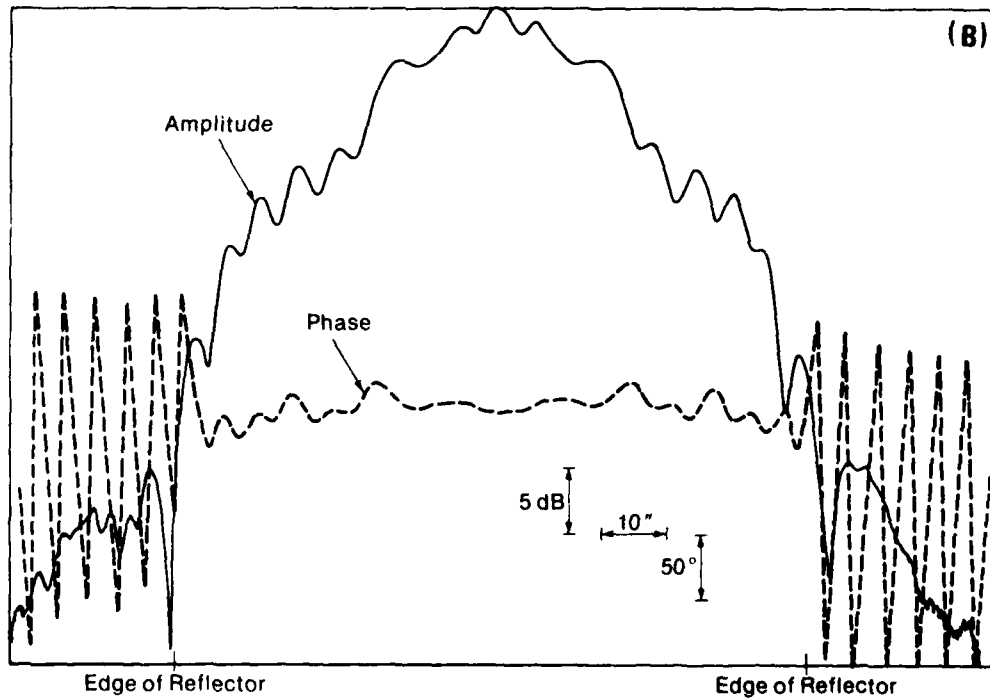
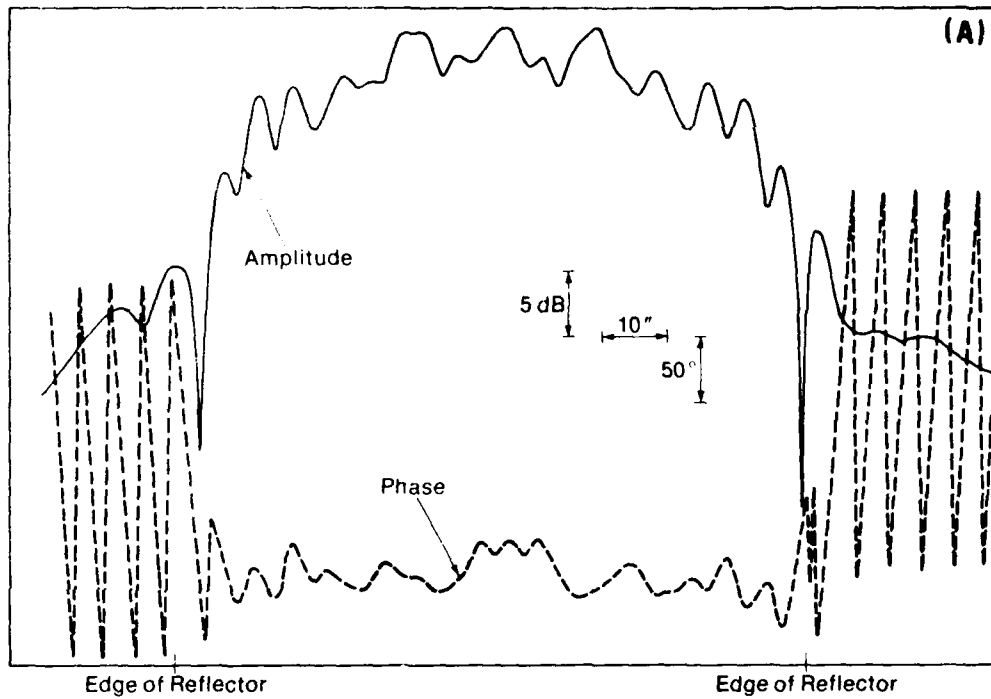


Figure 2.5--Paraboloid reflector near-field amplitude and phase through center of aperture at 2.945 GHz. (a)--vertical direction. (b)--horizontal direction.

$\alpha = 127.385$ $\theta = 114.820$ $\gamma = 47.574$
 Lev: 42.142 Lev: 42.142 Distance Is 1600.8648
 Observer To FunMin FunMax
 X -900.0000 72.0000 2.0000 284.0000
 Y -600.0000 72.0000 2.0000 284.0000
 Z 900.0000 -180.0000 -180.0000 81.0500

NOAA DISH W G FEED MAIN COMP 0579

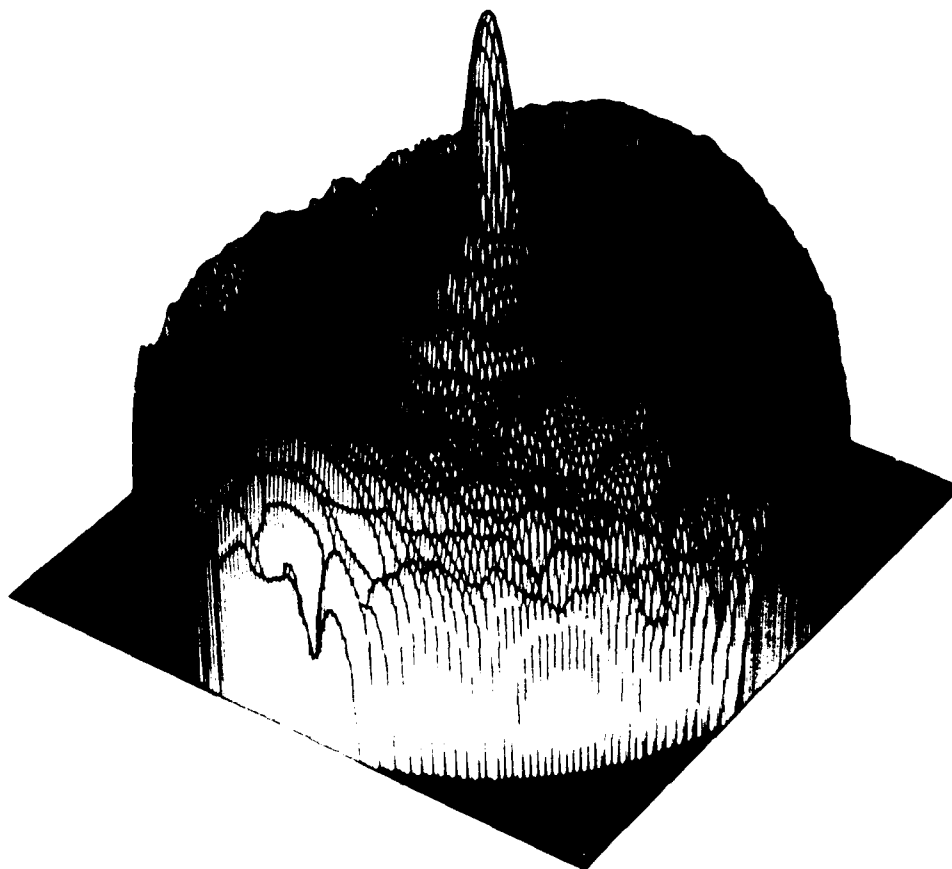
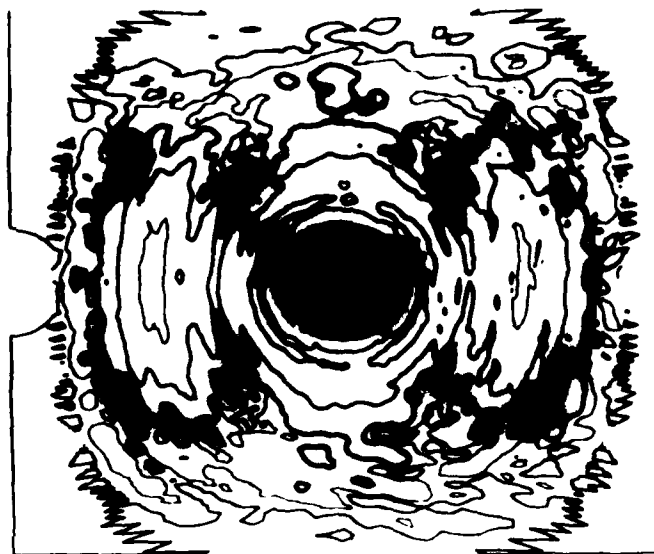
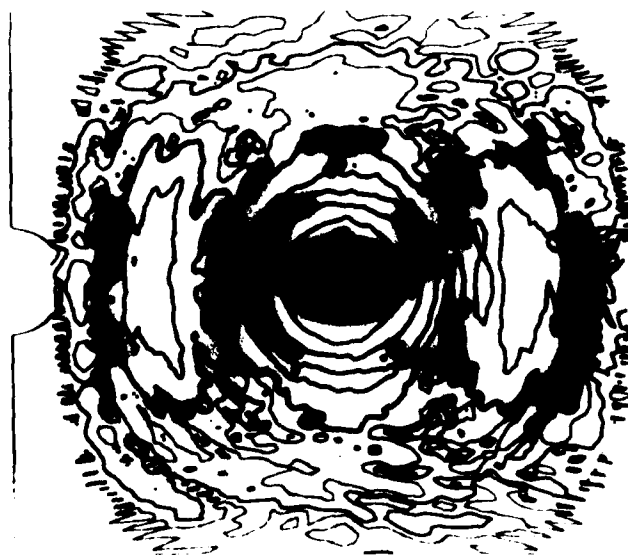


Figure 2.6--Perspective view of far-field antenna pattern.



(A)



(B)

Figure 2.7--Contour plot of antenna pattern.
 (a)--Contours at -3 dB, -9 dB, -15 dB, -21 dB, etc.
 (b)--Contours at 0 dB, -6 dB, -12 dB, -18 dB, etc.

NOAA DISH W G FEED F=2.94925 MAIN COMP

H-PLANE PATTERN

5

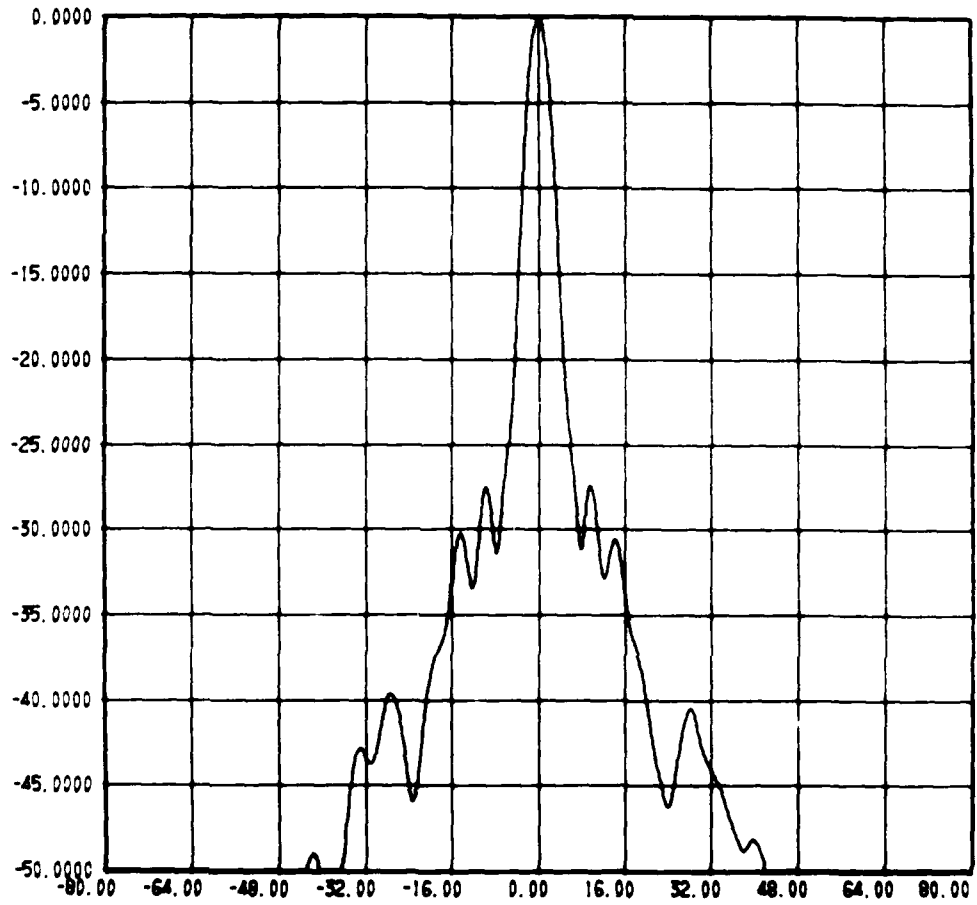


Figure 2.8(a)--Antenna patterns through center of beam — H-plane to 80°.

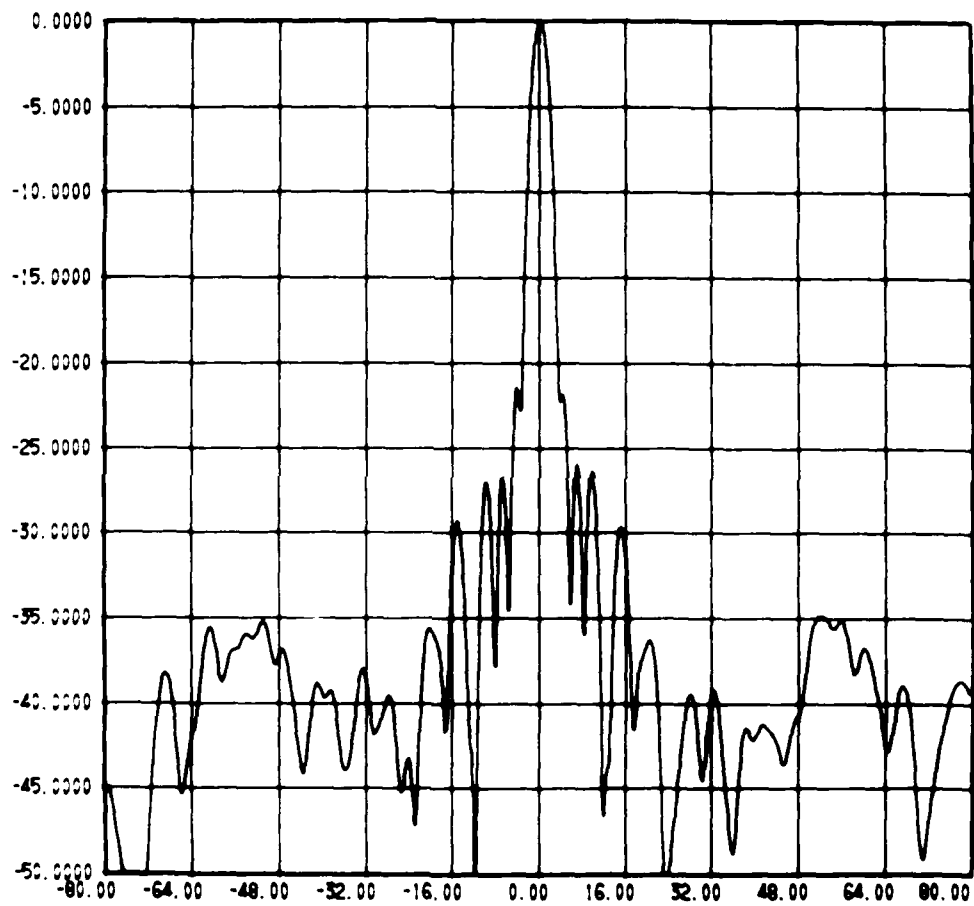


Figure 2.8(b)--Antenna patterns through center of beam — E-plane to 80°.

NOAA DISH W G FEED F=2.94925 MAIN COMP

H-PLANE PATTERN

7

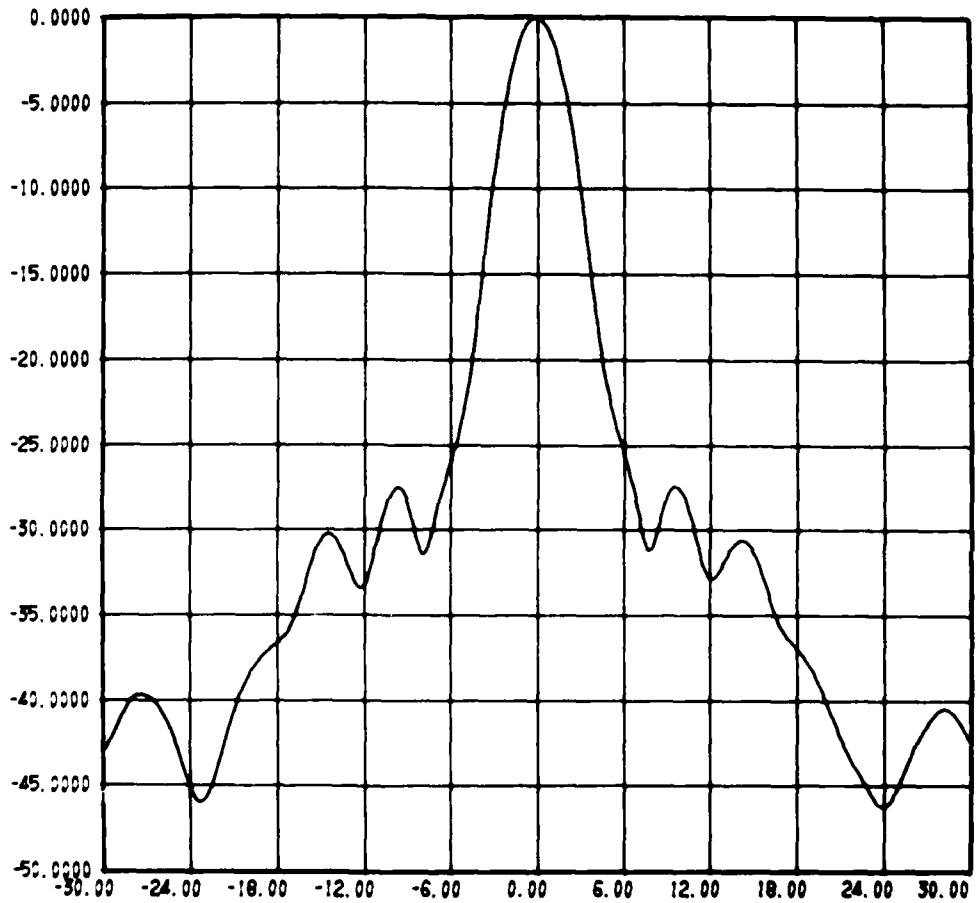


Figure 2.8(c)--Antenna patterns through center of beam — H-plane to 30°.

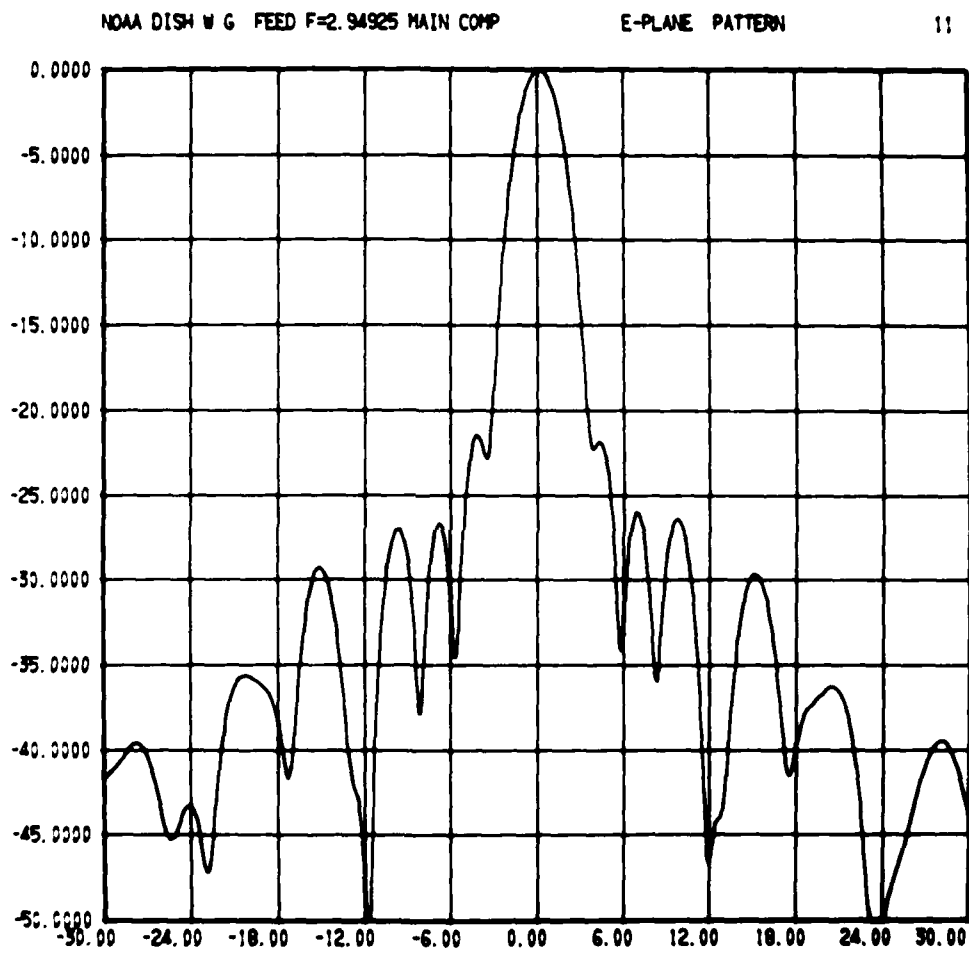


Figure 2.8(d)--Antenna patterns through center of beam — E-plane to 30°.

X= 127.385 Y= 114.820 Z= 47.574
 Lev:42.142 Lev:42.142 Distance is 1600.8648
 Observer θ FwhMin FwhMax
 X -900.0000 72.0000 2.0000 284.0000
 -600.0000 72.0000 2.0000 284.0000
 Z 900.0000 -180.0000 -180.0000 15.5881

WAA DISH & G FEED CRIS COMP 0579

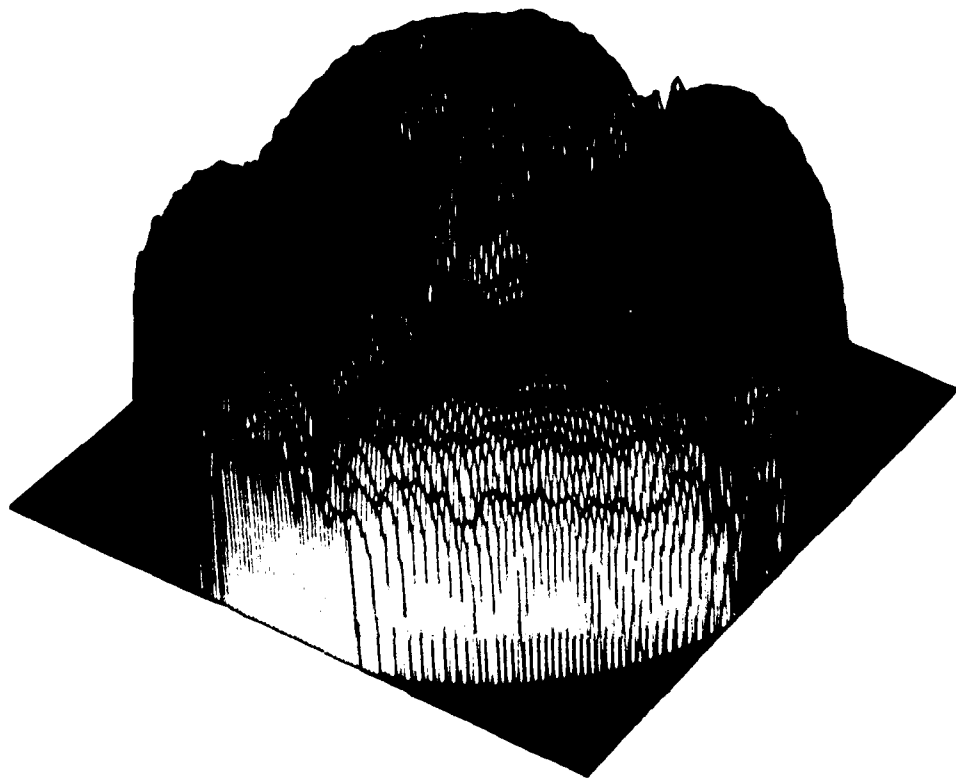


Figure 2.9--Perspective view of cross-polarization pattern.

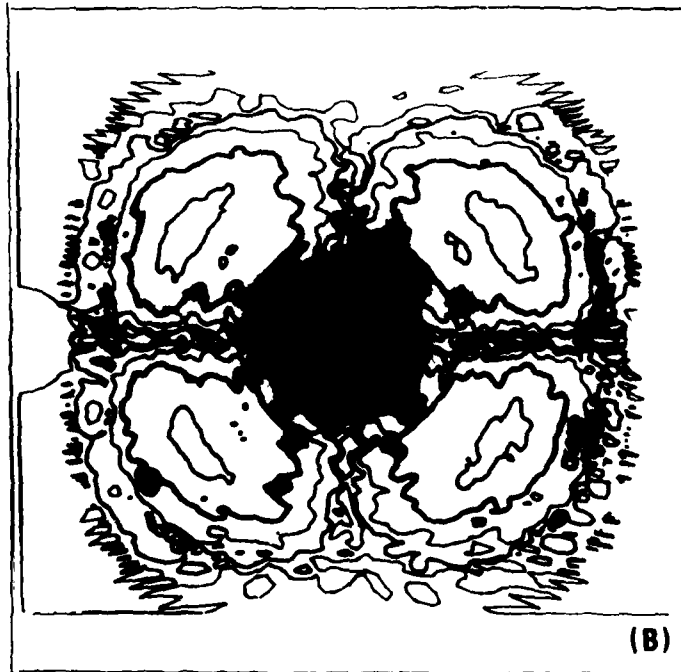
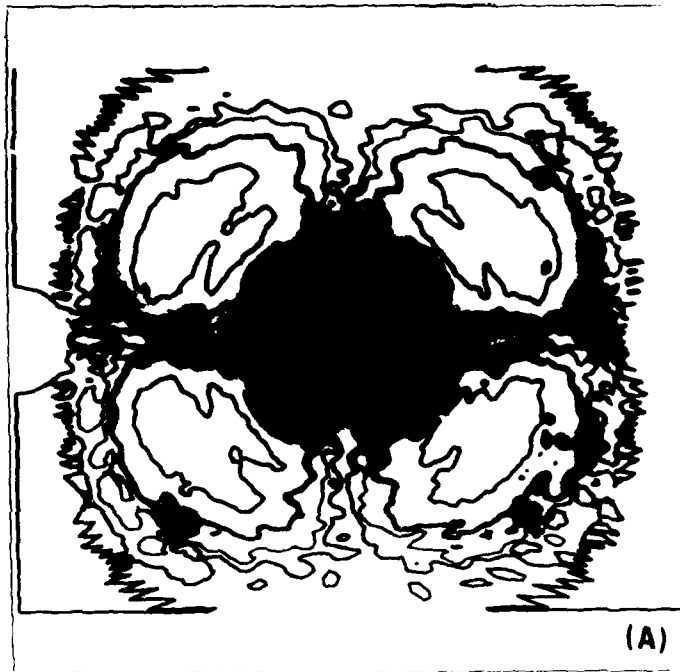


Figure 2.10--Contour plot of cross-polarization antenna pattern.
(a)--Contours at -3 dB, -9 dB, -15 dB, -21 dB, etc.
(b)--Contours at 0 dB, -6 dB, -12 dB, -18 dB, etc.

The approach that we used is to mount a shield of microwave absorber between the two antennas as shown in Fig. 2.11(a). The absorber shield is two sheets of absorber mounted on both sides of a sheet of plywood. The shield is such that a wave passing through it is attenuated about 20 dB. The mounting arrangement was such that the shield could be raised and lowered to select the best height. But as shown in Fig. 2.11(b), the isolation is nearly independent of the height of the absorber shield. However, when a small irregularity (approximately 6") is placed at the top of the absorber shield the isolation is increased greatly and becomes a strong function of height as shown. It is not unrealistic to obtain an isolation of 115 dB using this approach.

The reason for this increased isolation is that there is a path produced by diffraction over the shield. The irregularity produces a second path and the phase of this second path is adjusted (by placement of the top piece) to be 180° out of phase with the first path. The exact placement and size of the top piece is adjusted by trial and error. In this case, the trial and error adjustment is straightforward and quick. The high levels of isolation achieved by this trial and error procedure are repeatable on a day-to-day basis. Some readjustment is necessary on a month-to-month basis. This is perhaps due to changing characteristics of its absorber and some movement in the mechanical support.

2.5 Alternate Design for Dual-Antenna System

The present dual-antenna system uses two eight foot paraboloids with three foot shrouds attached around the edges of the apertures to reduce the sidelobes. This arrangement has three disadvantages: first, the dual antennas have a large "sail" area and thus need a larger pedestal to move them in the wind; second, there must be some arrangement to be sure the beams are parallel; third, the antennas have larger than necessary sidelobes because of aperture blockage. All of these disadvantages can be circumvented by making the dual-antenna system of offset paraboloids. In addition, the problem of mounting the dual-antennas together is eased.

Larger microwave line-of-sight communication antennas are manufactured in sections to facilitate shipment by truck. Twelve foot diameter antennas are made

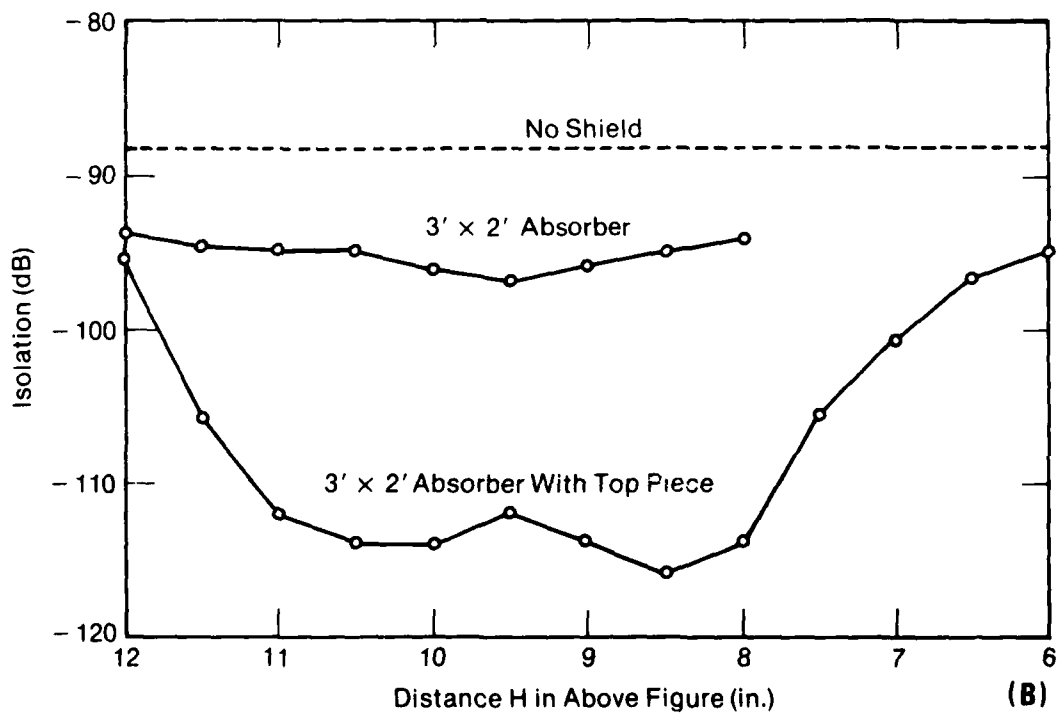
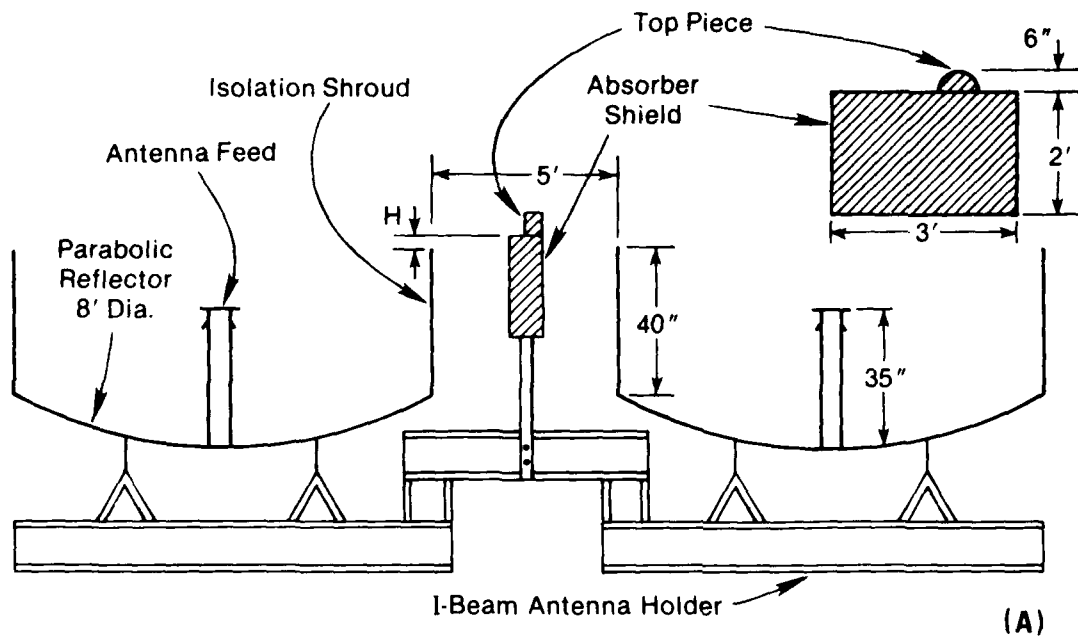


Figure 2.11(a)--Absorber shield placement.
 (b)--Dependence of isolation on absorber shield placement.

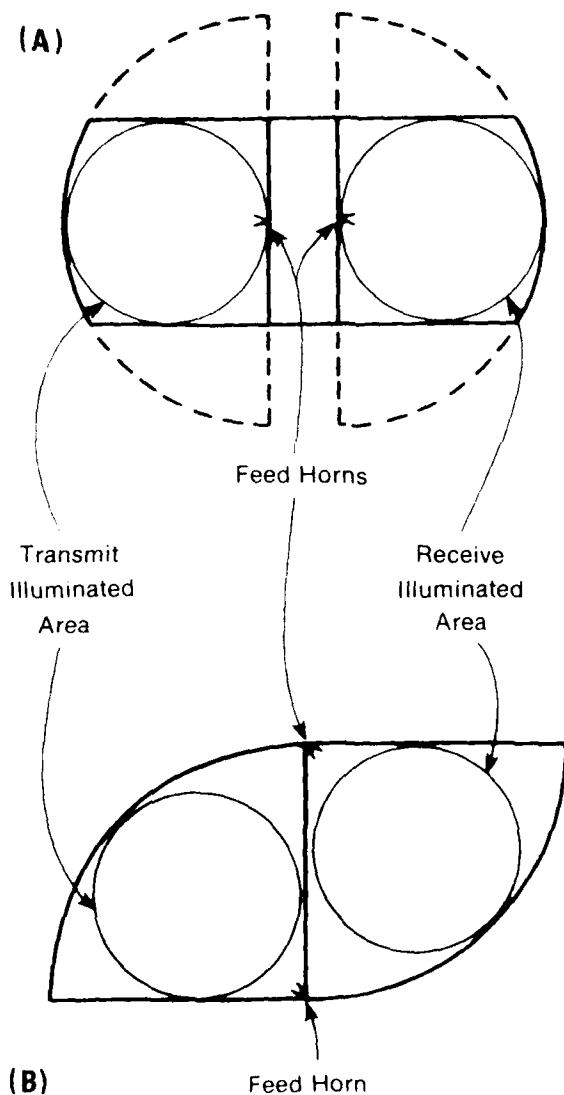


Figure 2.12--Dual offset paraboloid antenna structures using (a)--half antennas. (b)--quarter antennas.

of antenna are rigidly bolted together rather than being attached to a common frame. This dual-antenna system would probably be cheaper and more rugged than one composed of two full paraboloids.

2.6 Single-Antenna FM-CW Radar

The present experimental FM-CW radar uses separate parabolic antennas for transmitting and receiving. This arrangement results in a very close minimum

in halves and fifteen foot diameter ones are made in quarters. By using these sections or portions of these sections and bolting them together in unconventional ways, dual-antenna systems can be realized which are relatively compact and utilize an offset feed. Figure 2.12 shows such an arrangement. A 12 foot diameter antenna is shown in the upper part of Fig. 2.12 with the two halves separated by two feet and the portion shown dotted cut-off and discarded. This does have the disadvantage of requiring a mounting bracket and of wasting a portion of the original antenna. The lower part of Fig. 2.12 shows two quarters of a 15 foot diameter antenna attached together to form a dual antenna system for which the attachment is with a plate rather than a bracket. This would be a much simpler arrangement.

Both of the arrangements in Fig. 2.12 have offset feed structures and thus would have good sidelobe response. The shrouds around the edges of the parabolic surfaces would reduce the sidelobes even further. Also the problem of aligning the beams is reduced because the sections

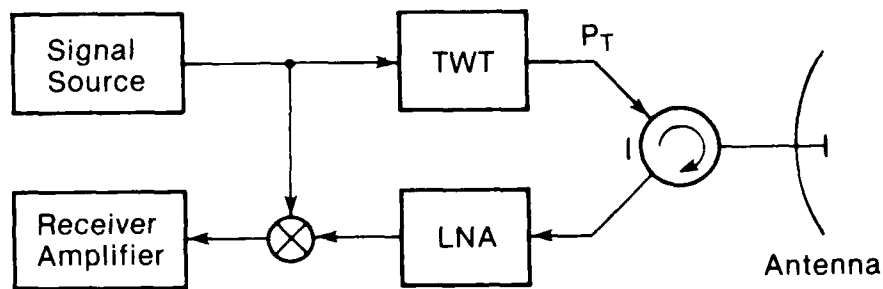


Figure 2.13--Simplified block diagram of FM-CW radar.

range, which is desirable but it also results in a bulky and awkward antenna system. This raises the question as to whether the FM-CW radar can be realized with a single antenna. There seem to be two approaches to achieving this capability. The first is to build a non-reciprocal three-port device which could be connected between the transmitter, the receiver and the antenna. It would allow each of these three elements to be used simultaneously. The second approach is to use 50% duty cycle transmission where the transmitter is turned on and off at a rate much faster than the sweep period. This rate might be on the order of 1 MHz. Then time multiplex the antenna between the transmitter and the receiver. This has the disadvantage of reducing the average power by half and of requiring a redesign of the receiver system. Also this introduces blind range slices within the range bins. This would be important if the radar were to detect point targets, but in this case where the target is distributed, it is not a factor.

The approach we have chosen is to attempt to build a three-port non-reciprocal device and obtain as much isolation as possible. If this isolation is sufficient, then the problem is solved; if not, the device which was developed could be used in the 50% duty cycle scheme. It is likely that a T-R switch would not be fast enough to use as the element to switch between transmitter and receiver.

An estimate of the required isolation can be made by considering the block diagram in Fig. 2.13. The power transmitter is a traveling wave tube (TWT) and has gain G_T , noise figure F_T , and output power P_T . The three-port device has isolation I . The low noise amplifier (LNA) has gain G_r and noise figure F_r . The mixer has a saturation level of S_m . There are two questions which must now be

answered: 1) What value of isolation is necessary so that the leakage signal does not saturate the mixer; and 2) What value of isolation is necessary so that the noise from the TWT is less than the noise from the LNA? The first question is answered by writing the leakage signal power at the input to the mixer and requiring this to be less than the mixer saturation level. The resulting requirement is

$$I > \frac{P_T G_r}{S_m}$$

The second question is answered by finding the noise out of the TWT and that out of the LNA and then transferring both to the input of the LNA. After canceling common terms, the requirement on the isolation is

$$I > \frac{F_T G_T}{F_r}$$

Some typical values of these parameters are given in Table 2.2, and these values in the equations above show that the required isolation is 68 dB. In practice, we have found that isolation values greater than this are needed to make the leakage noise negligible and to insure that the mixer is operated well into the linear region. We have generally used isolation values of 80 dB or larger. It is desirable to have the isolation as large as possible to provide a large margin against a noisy TWT and to allow the low noise amplifier gain to be as large as possible.

Table 2.2--Typical values of parameters associated with isolation calculations

Symbol	Parameter	Value
S_m	mixer saturation level	0 dBm
P_T	transmitted power	+53 dBm
G_r	receiver gain	+15 dB
F_r	receiver noise figure	+ 2 dB
F_T	transmitter noise figure	+30 dB
G_T	transmitter gain	+38 dB

A bench model of a microwave circulator-canceller based on a four-port ferrite circulator was constructed and tested on the National Bureau of Standards network analyzer. When used in the manner we used it, this analyzer can measure isolation to 110 dB with an error of a few tenths of a dB.

The bench model of the circulator used a waveguide circulator based on a four-port design supplied by Merrimac Industries. Figure 2.14 shows the isolation characteristics of this four-port circulator along with those of a three-port circulator. Both of these are high-quality devices as a standard ferrite circulator has an isolation of 20 dB. To further increase the isolation of the four-port device a canceller arm was built around it as shown in Fig. 2.15. The idea here is to re-introduce an attenuated r-f signal that has been phase shifted by 180° so that it will cancel out the leakage signal. This is a fairly common technique and it is possible to achieve an additional isolation of 20 dB.

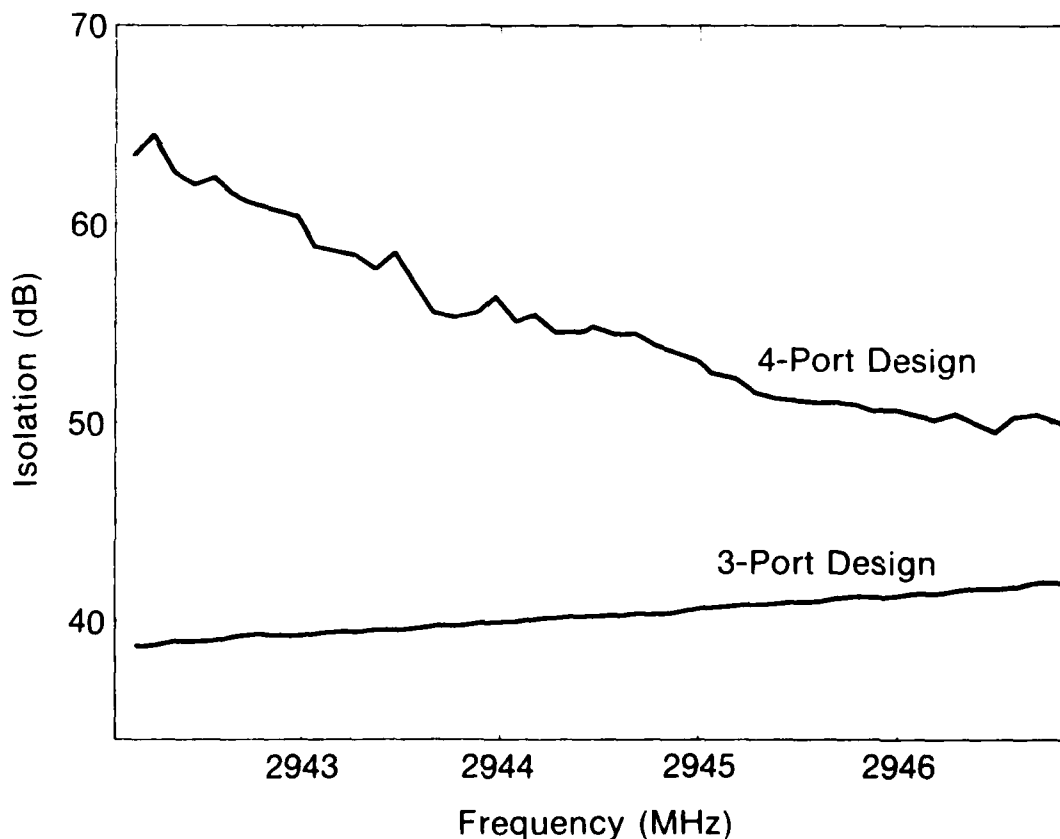


Figure 2.14--Waveguide circulator characteristics.

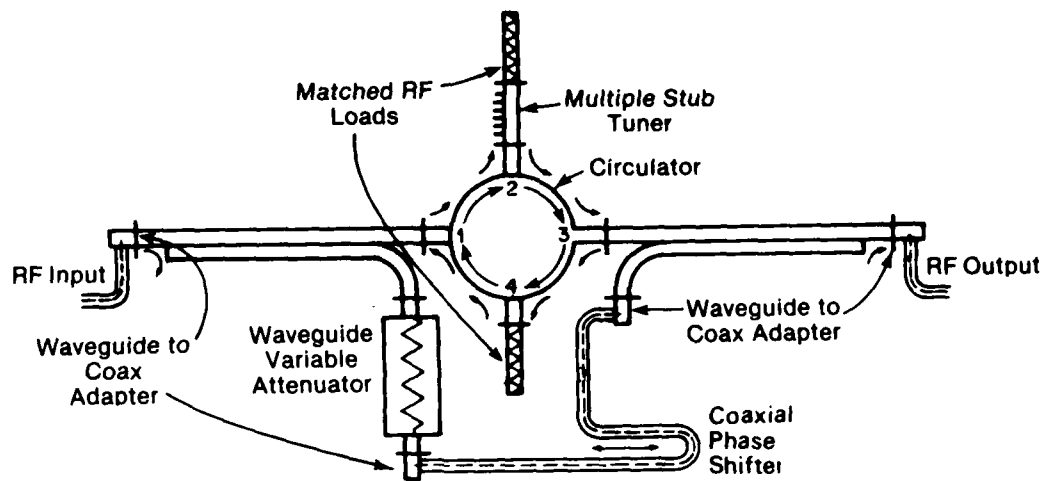


Figure 2.15--Block diagram for bench model of circulator-canceller.

When the bench model of the circulator-canceller was tested on the network analyzer, the isolation as a function of frequency was as shown in Fig. 2.16. For radar work, the important thing is not the isolation at a particular frequency, but rather the isolation over a band of frequencies. This can easily be determined from Fig. 2.16 and is shown in Fig. 2.17 along with the isolation of an ideal non-ferrite two-path canceller. A non-ferrite two-path canceller is a device that splits the signal into two equal amplitude branches and then recombines them. One of the paths has an electrical length that is a half-wavelength longer than the other at the design frequency. This type of canceller is perfect at the design frequency, but has a finite isolation over any band of frequencies. This isolation as a function of bandwidth can be calculated exactly and this is shown for comparison in Fig. 2.17.

The circulator-canceller should ideally be built of all waveguide components to achieve maximum bandwidth. However, it was necessary to construct the canceller arm with coaxial components. The coaxial components have a different dispersion law than the waveguide components and this will result in a larger relative phase change between the circulator arm and the canceller arm for a given frequency change. This will reduce the bandwidth over which a given isolation can be maintained. So, it seems likely that an all-waveguide version of the circulator-canceller would have an even better isolation-bandwidth characteristic than that shown in Fig. 2.17.

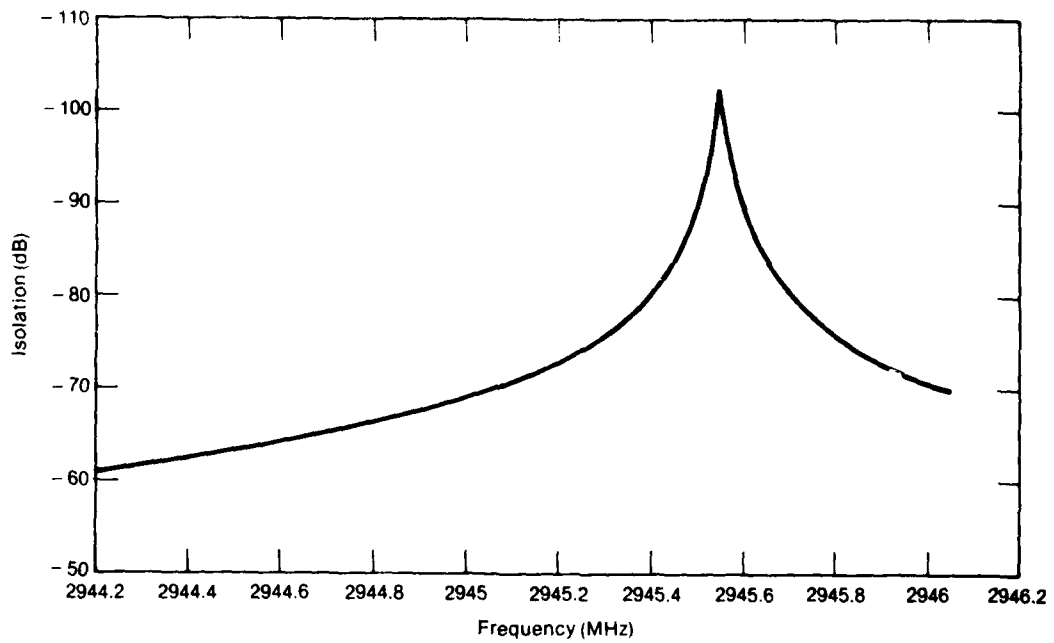


Figure 2.16--Measured isolation of circulator-canceller.

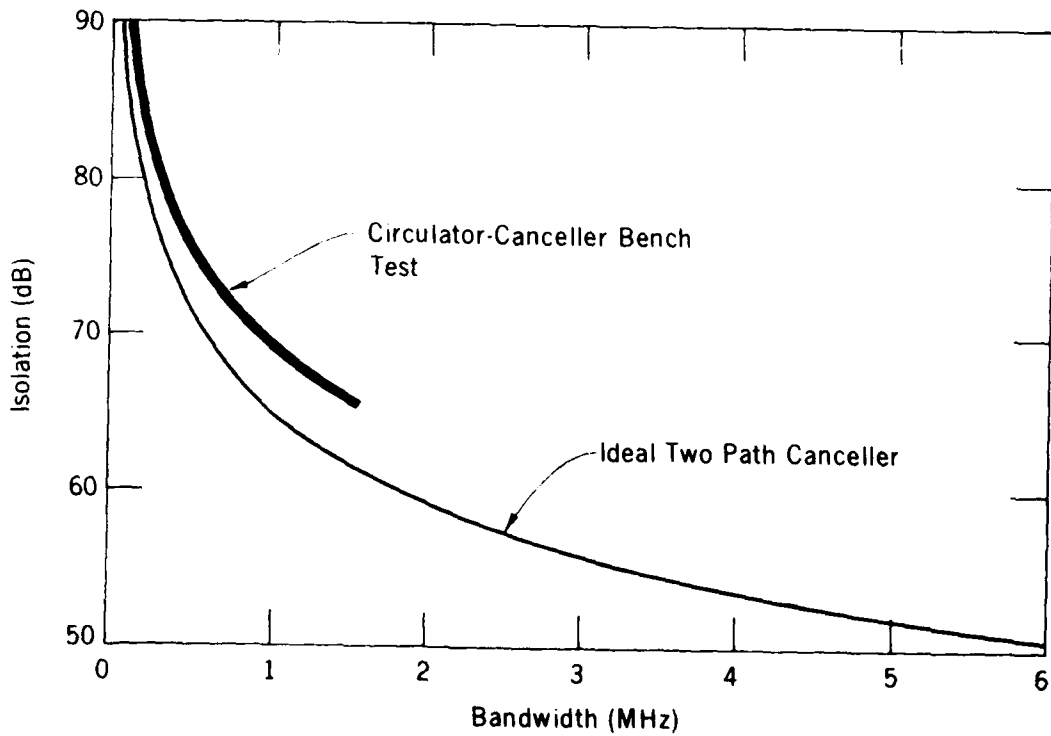


Figure 2.17--Bandwidth-isolation characteristic of the bench-model circulator-canceller and an ideal non-ferrite two path canceller.

The conclusion here is that we were able to increase the isolation of the four-port circulator from 50 dB to 70 dB over a 1 MHz bandwidth by adding the coaxial canceller arm. Figure 2.14 suggests that the circulator has a frequency region where the isolation is greater than 60 dB. It seems likely that we should be able to increase this to 80 dB by using the canceller arm. This is within the range that we have used with the present two-antenna system.

There are ways of changing the radar to reduce the required isolation. From the equations developed above, we see that the transmitted power, receiver gain, transmitter gain, and transmitter noise figure should be made smaller while the mixer saturation level and receiver noise figure could be larger. A practical approach here would be to use a transistor power amplifier with maybe 6 dB lower transmitted power and 10 dB lower noise figure. This in addition with a high level mixer ($S_m = 10$ dBm) should allow operation with an isolation of 70 dB.

Two questions remain. The first concerns the environmental range over which a practical circulator-canceller will work. Our tests so far were done under lab conditions. The second question relates to the return loss of the antenna. The return loss must meet the same requirement as the isolation. Supposedly a well-designed offset paraboloid without a weather cover should be tunable to return losses over the 70-80 dB range (Hogg, 1980).

2.7 Summary of Antenna Work

A splash-plate feed system for the eight foot parabolic reflectors was designed, built, and tested. The final far-field antenna patterns were measured on the NBS near-field antenna range. The antennas and feeds have been used on the FM-CW radar and have worked well. Laboratory measurements of a ferrite circulator-canceller have shown that it may be possible to operate the FM-CW radar (with modifications) in a single-antenna mode.

CHAPTER 2 -- BIBLIOGRAPHY

Strauch, R.G. (1979), Private communication.

Studd, A.C. (1966), "A rear feed for parabolic reflectors," Microwave Journal, p 51-54, Feb. 1966.

Hogg, D.C. (1979), Private communication.

James, G.L. and D.P.S. Malik (1975), "Towards the theoretical design of splash-plate feeds," Electronics Letters, Vol. 11, No. 24, p 593-594, Nov. 1975.

Newell, A.C. and M.L. Crawford (1974), "Planer near-field measurements on high performance array antennas," National Bureau of Standards Report No. NBS-IR-74-380, July 1974.

Hogg, D.C. (1980), Private communication.

CHAPTER 3 -- CLUTTER SUPPRESSION

W.C. Campbell, R.B. Chadwick, and K.P. Moran

3.1 Introduction

A major problem for CW radars is saturation caused by close-in hard targets such as buildings, power lines, etc. This problem is especially severe at low elevation angles where the return can even be from the ground itself. The previous chapter outlined antenna modifications that were designed to improve the rejection of returns from these types of targets. This chapter discusses how these returns can be rejected electronically by the receiver and signal processor.

The large returns from ground targets can saturate the radar receiver in two different ways, pre-detection saturation and post-detection saturation. The causes and consequences of each of these will be discussed below. The majority of this chapter will deal with a system specially designed to prevent post-detection saturation. A special case of rejecting another type of interference, that due to the 60 Hz power line will also be discussed.

3.2 Pre-Detection Saturation

Pre-detection saturation refers to the saturation of any r-f component in the receiver. For an FM-CW radar, this means saturation of either the low noise r-f amplifier or the mixer. This type of saturation is difficult to deal with because signal processing techniques can not be applied at r-f. One must rely solely on the antenna characteristics and the dynamic range of the r-f components. Fortunately, in most applications, the major saturation problem occurs after the mixer as post-detection saturation. However, it is well to be informed as to the various power levels and margins that relate to the pre-saturation problem.

An additional problem which is related to pre-detection saturation is the decrease in sensitivity due to transmitter noise being reflected from large targets into the receiver and being larger than the receiver noise. The potential severity of this problem and the pre-detection problem can be represented by one

graph of the power levels and saturation levels all referred to a common point in the radar system. Any point could be used but the most convenient is the output terminal of the receiving antenna. Of course, this is equivalent to the input terminal of the low-noise r-f amplifier. Figure 3.1 shows the signal levels, noise levels, and equivalent saturation levels at the receiver antenna. The saturation and signal levels are independent of bandwidth while the noise levels are for a 1 MHz bandwidth. Some of these levels are measured and some are calculated. The radar parameters used in these measurements and calculations are given in Table 3.1.

In Fig. 3.1 the range over which we have detected clear air (radio refractive-index fluctuations) returns is indicated. The upper limit was an occasion where there was independent verification by a lidar that the return was not due to scattering from particles. Directly above the range for clear air is a range of calculated power levels for rain. This is for a 150 m rain cell centered at 1 km range which is a rather artificial situation. However, some estimate of return power can be made by noting that for every halving (or doubling) of range the power increases (or decreases) by 6 dB. The case of a uniform rain extending from the antenna to a large distance can not be calculated because of the uncertain antenna gain at close ranges. However, this case is easy to measure and a level for a typical uniform rain is shown.

A range of returns for point targets at 1 km range is also shown. The scale is radar cross section in dB relative to one square meter. Typical point targets such as aircraft, birds, and insects vary greatly in radar cross section with type and aspect angle, so the locations of these targets in Fig. 3.1 are only approximations. We have found that a side view of a commercial jetliner at 500 m will completely saturate the r-f amplifier.

The noise levels in Fig. 3.1 are for the transmitter shot noise leaking between the antennas or being reflected from transmitter to receiver. It is clear that the transmitter noise will usually not desensitize the receiver significantly. Sometimes we have experienced cases when the transmitter becomes unusually noisy and causes degradation of the receiver sensitivity. The precise source of this noise has not been found.

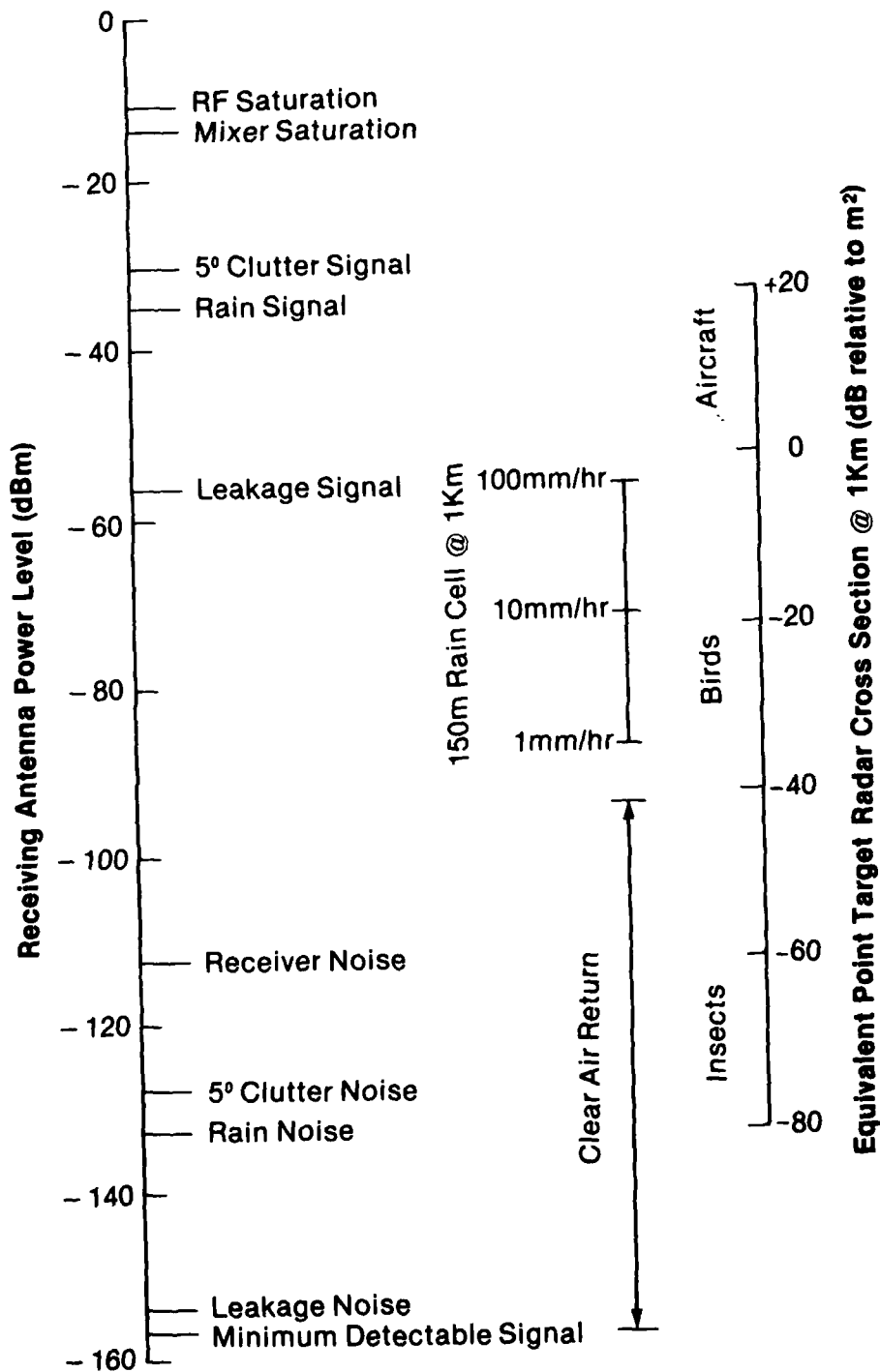


Figure 3.1--Equivalent power levels referred to receiving antenna terminal.

Table 3.1--Radar Parameters

Transmitted power	+53 dBm (200 W)
Transmitter gain	+40 dB
Transmitter noise figure	+30 dB
Antenna isolation @ 90° elevation	+110 dB
Antenna isolation @ 5° elevation	+83 dB
Receiver gain	+21 dB
Receiver noise figure	+2 dB
Cable loss receiver to mixer	-7 dB
Mixer saturation level	0 dBm

The conclusion from Fig. 3.1 is that pre-detection saturation is not a major unsolvable problem in the airport application. Ideally the transmitter shot noise should not desensitize the receiver, but for some unknown reason this occasionally happens. This is not however, an unsolvable problem because a solid state transmitter has inherently lower noise than a vacuum tube transmitter and could be used.

3.3 Post-Detection Saturation

Post-detection saturation is the saturation of any of the electronic equipment after the mixer. In normal applications of the FM-CW radar, this is usually the more important type of saturation and since it is at audio frequencies, is easier to deal with.

The most straight-forward way of avoiding post-detection saturation is by analog filtering in the amplifier chain following the mixer. It is particularly convenient here to filter in such a way as to provide range correction at the same time. A beam-filling distributed target has return power which varies as $(\text{range})^{-2}$. In the audio portion of the FM-CW radar, range is proportional to frequency and so a properly chosen filter can provide range weighting at the same time it is increasing the dynamic range of the receiver. The filter should have a power transfer function which varies as $(\text{frequency})^2$ over the range of interest so that it cancels the $(\text{range})^{-2}$ variation of the beam-filling distributed target. This

is a very simple filter which effectively changes the receiver gain so that close-in returns are not amplified as much as returns from greater ranges. A properly chosen series capacitor will do this. It blocks completely the signal which leaks directly from the transmitting antenna to the receiving antenna.

One disadvantage is that the noise baseline is not a constant since the receiver gain now changes with frequency. A consequence of this is that the noise baseline of a single spectrum changes slightly from in-coming and out-going targets. However, the effect is slight and the difference between the noise level on the in-coming and out-going sides of the spectrum is often less than one quantization level at the output of the signal processor. So far, we have not found this non-constant noise baseline to be a problem.

This simple passive filter works on both moving and stationary targets, but does not discriminate between them. Since the returns which tend to saturate the receiver amplifier are generally from stationary objects, the simple filtering technique is not a complete solution to post-detection saturation. We have found that an active digital filter in conjunction with the simple analog range correction does a very effective job in eliminating post-detection saturation due to ground clutter. The digital active filter is microprocessor-based and designed to estimate the return from stationary targets and subtract this from the total received signal. A brief discussion of the preliminary design was presented in Chadwick et al. (1978) and here we present a characterization of the filter and its response in Appendix A.

The clutter suppressor response has nulls or stop bands at the zero velocity points of each range cell. This suppresses the return, which is near zero velocity, of that range cell. By a proper choice of parameters, we can make the stop-band of the suppressor much less than the resolution of the spectrum analyzer. Then the clutter suppressor has only a negligible effect on atmospheric return and a large effect on stationary clutter return.

An idea of the performance of the ground clutter suppressor can be obtained by considering the time signal at the input and output of the device. Figure 3.2 shows the input and output of the ground clutter suppressor. Note that the suppressor removes predictability. Figure 3.3 shows the radar output in the Doppler

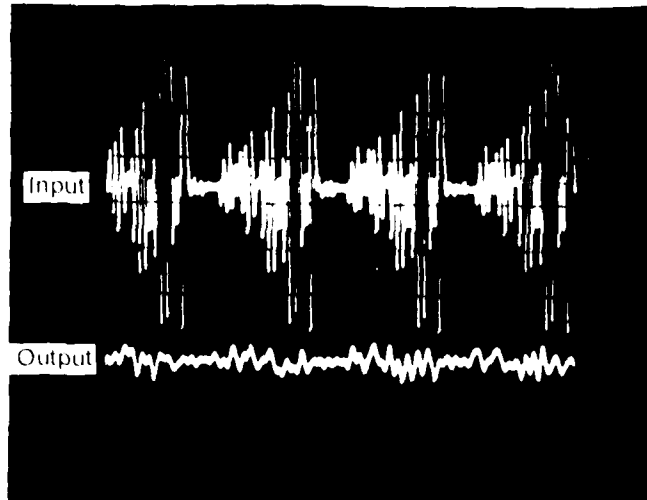


Figure 3.2--Time signal at input and output of ground clutter suppressor.

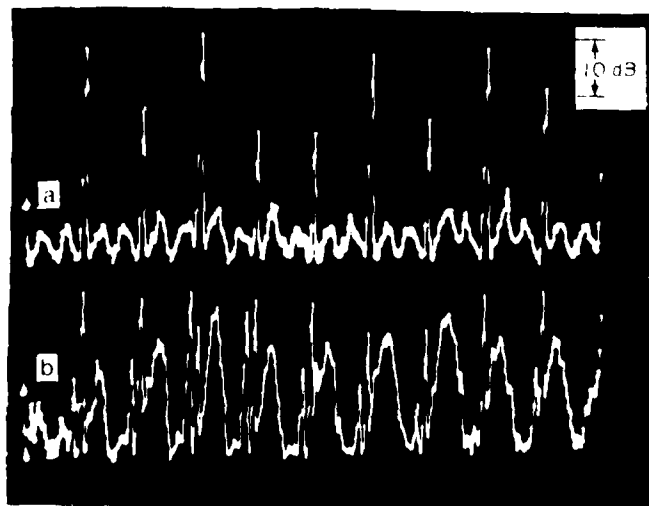


Figure 3.3--Radar output (a) without and (b) with ground clutter suppressor.

mode with and without the ground clutter suppressor. Note that the large returns at zero velocity have reduced the clear-air spectra because of partial saturation of the signal processor. Figure 3.4 shows the radar output in range-only mode looking at an elevated layer. The ground clutter suppressor was inadvertently turned off in the center part of the picture. In this vertically looking case ground clutter is not strong enough to saturate the signal processor, but does saturate portions of the output display. The ground clutter suppressor is very useful for improving and cleaning-up the output display.

3.4 Frequency Stabilization

The clutter suppressor does an excellent job of eliminating stationary returns, however frequency instabilities in the transmitted signal can make returns from stationary targets change from one sweep to the next. The clutter suppressor can not remove these changes. The solution to this problem is to remove these frequency instabilities with a frequency lock loop. This loop would frequency lock the microwave source to a stable frequency synthesizer that is programmed to sweep linearly over a range of frequencies. This sweeper uses direct digital synthesis techniques to generate a signal that sweeps linearly from 595 kHz to 2095 kHz. Because this is a completely digital device, the stability of the output signal depends only on the stability of the clock signal which is very good. The digital sweeper was described in Chadwick et al. (1978). Here we concentrate on the second part of the frequency stabilization equipment, the frequency lock loop.

Figure 3.5 is a block diagram of the frequency lock loop which locks the frequency of the Yttrium-Iron-Garnet (YIG) microwave source to the digital frequency synthesizer. The microwave signal is mixed down to an IF and then compared against the output of the digital frequency synthesizer with a mixer and frequency discriminator. The output of the discriminator is the error signal which could be applied directly to the microwave source to close the feedback loop and correct the microwave frequency. However, the output of the discriminator has some noise associated with it and this noise would result in frequency excursions. If the error signal is integrated, the discriminator noise is reduced. This does reduce

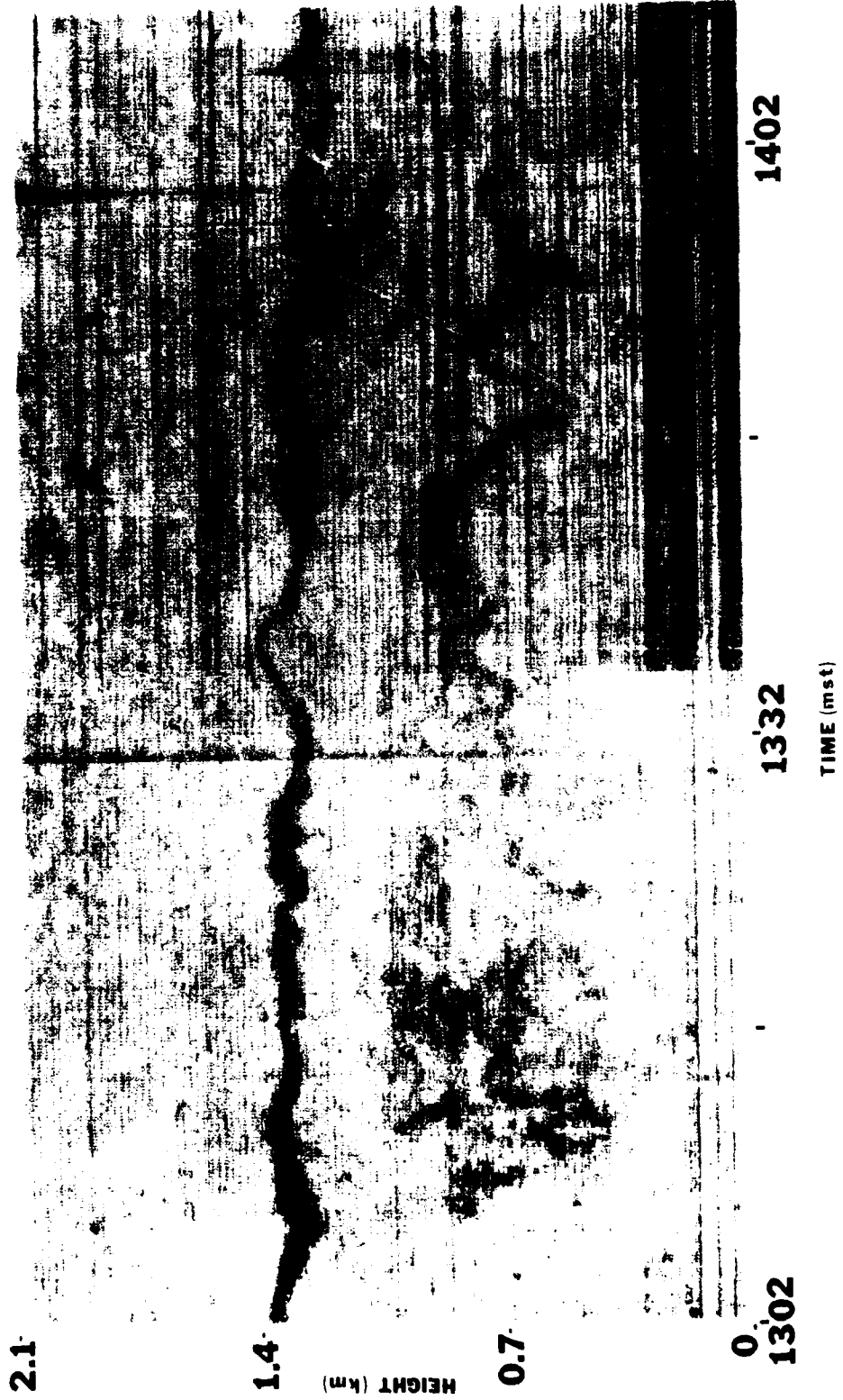


Figure 3.4--Radar output in vertically looking, range-only situation. Return is from elevated layer in clouds. The left portion is with the ground clutter suppressor on.

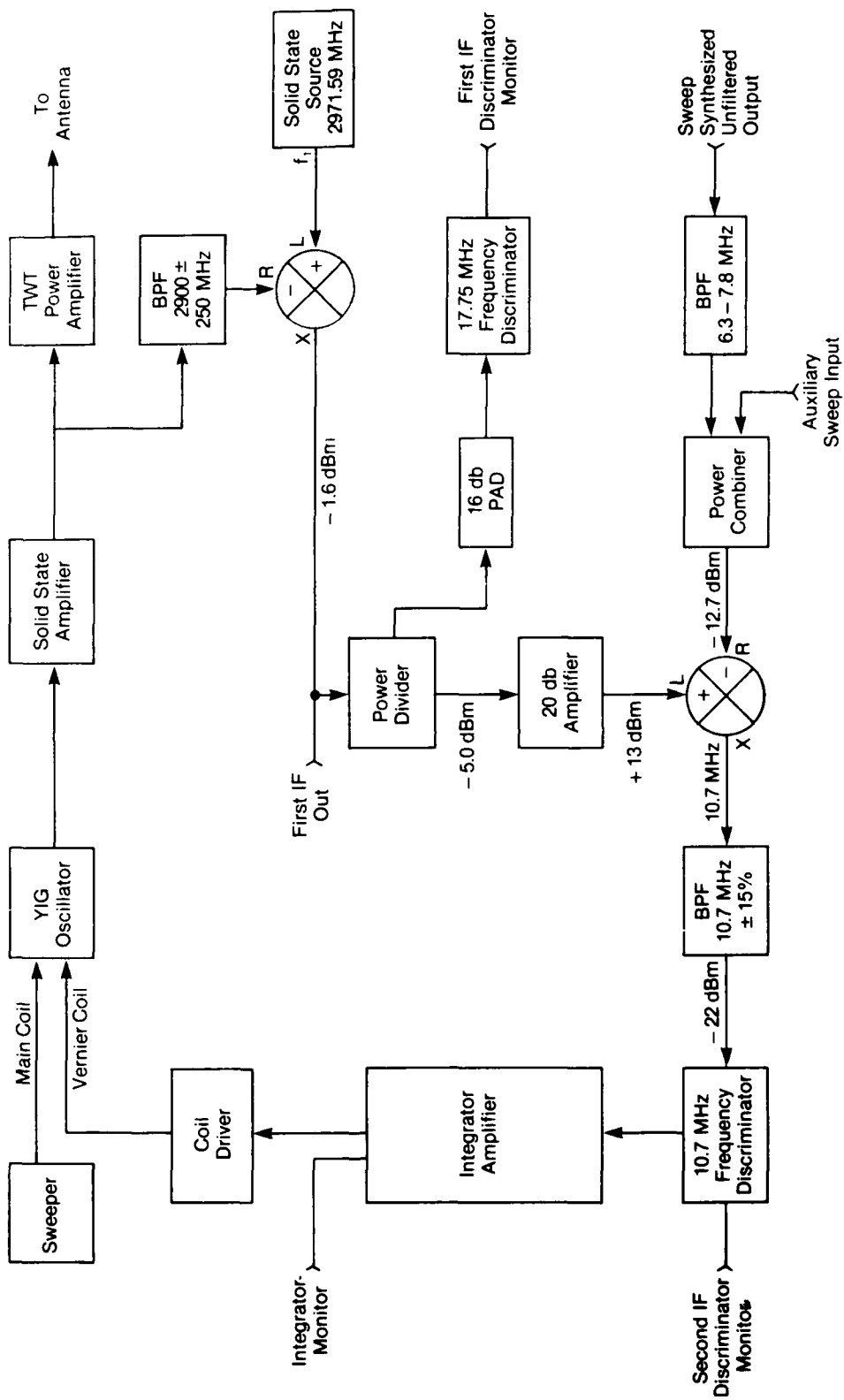


Figure 3.5--Block diagram of frequency stabilization loop.

the loop bandwidth, but the frequency excursions are not rapid and a fast loop is not required to eliminate them.

The manner in which the integrated error term is put into the YIG oscillator is also important. It could be added in electronically and used to drive the main ferrite core coil. However, we found that a better way was to use a small air core coil and add the main signal and the vernier signal magnetically. This results in less of the loop noise being coupled into the YIG oscillator.

The capability of the frequency lock loop is shown in Table 3.2, for the case where frequency is not swept. Although this is not the normal mode of operation, it does facilitate measurement of stability parameters. A convenient parameter is the bandwidth from the peak of the spectrum to a point that is 40 dB below the peak. These bandwidths for different devices are given in Table 3.2. These values are all for non-sweeping operation and show that the loop improves the stability of the YIG oscillator by a factor of 353. A rule-of-thumb is that bandwidths add as sum-of-squares. So the loop, which is composed of the solid state source and digital sweeper could not have a -40 dBC bandwidth less than 39 Hz. Its measured -40 dBC bandwidth is about four times greater than this. The additional bandwidth is probably caused by the noise in the output of the discriminator. A better quality discriminator would probably help the situation, but we have found that the loop with 170 Hz bandwidth is acceptable.

Table 3.2--Bandwidths for -40 dBC Spectral Heights

Device	Bandwidth (Hz)
YIG oscillator	60,000
Solid state source	30
Digital sweeper	25
Frequency locked loop	170

Spectra of the output of the YIG oscillator running open loop and closed loop are shown in Fig. 3.6. Again this is in a non-sweeping condition. Note the scale changes by a factor of 50.

The usefulness of frequency stabilization in a high clutter situation seen at low angles is clearly demonstrated in Fig. 3.7 which shows the radar output with the stabilization loop on and off. This is at a 5° elevation angle with a large tower in the sidelobes. Figure 3.7(a) shows ten side-by-side clear-air spectra obtained in a high clutter situation. The first cell is contaminated by harmonics of 60 Hz power line noise because the sweep frequency was not synchronized with the power line. Note that the clear-air spectra are 15 dB above the noise baseline out to ranges of 3 km. However, when the stabilization loop is turned off and post-detection saturation occurs, the clear-air spectra are no longer visible in the radar output. This has to be post-detection saturation rather than pre-detection saturation because the received power is the same in both cases.

3.5 Range Spreading of Strong Return Signals

In addition to pre-detection and post-detection saturation, there is a third undesirable result of strong return signals. A strong return in one range cell can spread into adjacent range cells. This is a common problem with high duty cycle radars and is usually studied by making use of the radar ambiguity function. In Appendix B we use a different approach which is more closely related to the processing used in the FM-CW radar. A numerical study of range spreading and two possible solutions is presented in Appendix B. Here we will briefly summarize the material in Appendix B.

The main signal processing operation in the FM-CW radar is a spectral or Fourier analysis of the mixed signal. Two important properties of Fourier analysis are: 1) an isolated discontinuity in the time signal results in a broadened or spread frequency spectrum; and 2) a periodic time signal results in a discrete frequency signal with harmonics at multiples of the primary signal. These two effects together cause the range spreading problem. The r-f frequency sweep is periodic and this introduces periodic discontinuities in the mixed signal. At the end of each sweep the frequency must be reset and the mixed signal has a large

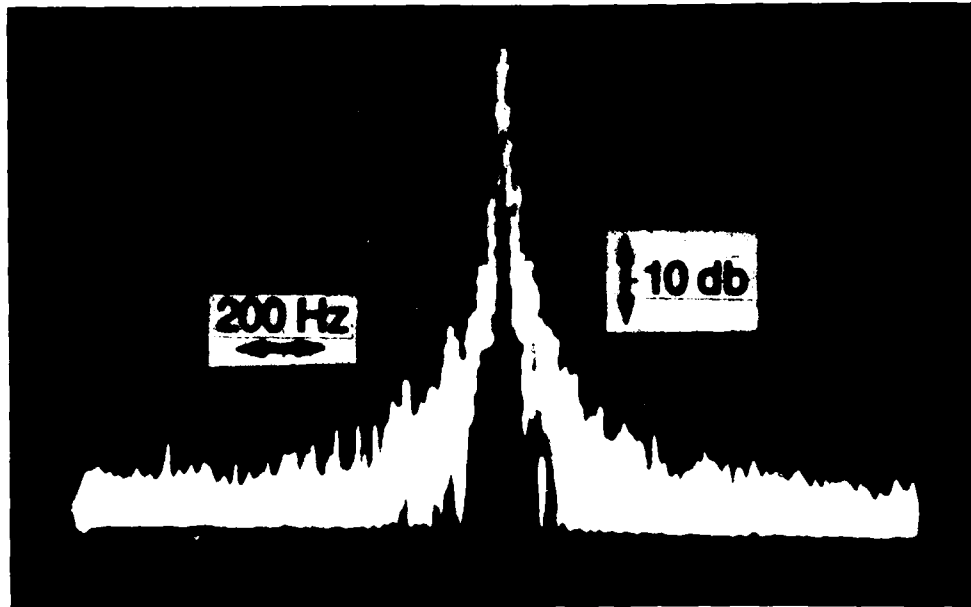


Figure 3.6(a)--Frequency spectrum of VIG oscillator with stabilization.

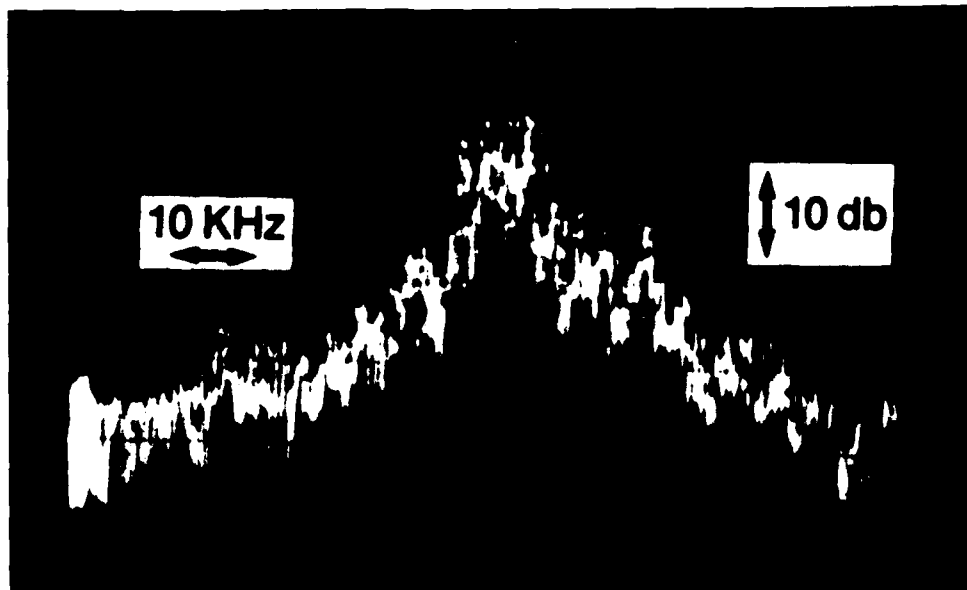


Figure 3.6(b)--Frequency spectrum of VIG oscillator without stabilization.

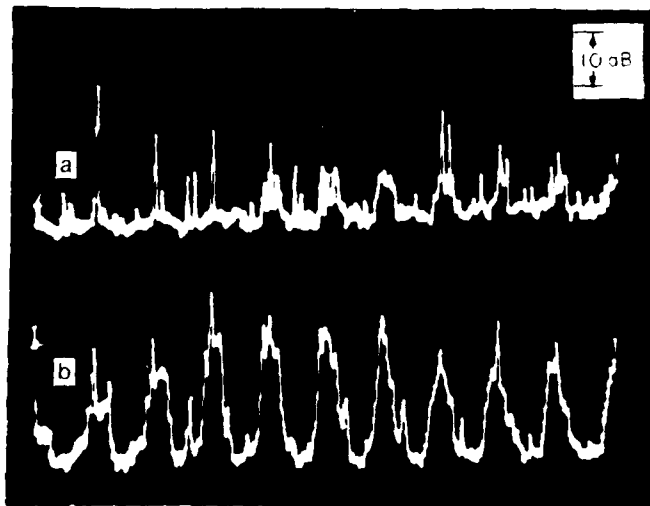


Figure 3.7--Radar output in high clutter situation (a) without and (b) with frequency stabilization.

pulse which must be gated out and this creates a discontinuity. The frequency spectrum of these discontinuities is a discrete spectrum with energy at harmonics of the mixed signal caused by the large return. The envelope of these harmonics has a "1/f" form and so has significant energy far removed from the frequency of the large return signal. The frequency of this large return signal is determined by the range and velocity of the target and thus the harmonics do not necessarily appear at the same frequencies as ground clutter. These harmonics are what we have referred to as range spreading.

An interesting and graphic illustration of range spreading is shown in Fig. 3.8 where an aircraft has a changing radial velocity as it goes through an antenna sidelobe. Because of the large target the return is spread from the true range cell and is replicated in other range cells. But this replication extends to zero frequency where it is "folded" and then makes the other side of the X-type signature in Fig. 3.8.

There are two approaches to eliminating or reducing this range spreading. The first is to reduce or eliminate the discontinuities at the sweep end points. This is similar to the weighting or windowing frequently used in spectral analysis. The second approach is to determine the range spreading and correct for it. This is similar to deconvolution or deblurring used in image processing. Both of these

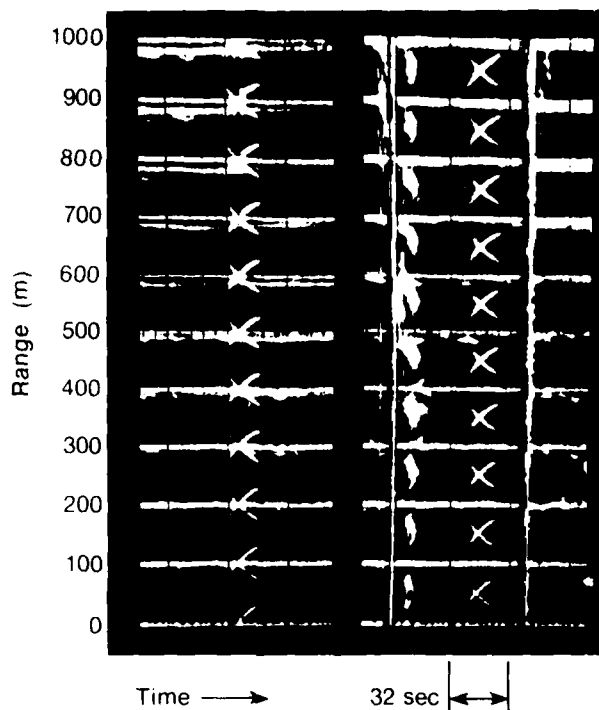


Figure 3.8--Examples of range spreading of aircraft echo causing an "X-echo".

approaches should be pursued since the improvements of each would be additive. However, the only approach used in Appendix B is to reduce the discontinuities.

This range spreading problem is extremely important in the airport environment because of the large aircraft targets. It is also a problem in precise measurement of atmospheric parameters since the spectral shapes are altered in the case of wind shear. This may result in errors up to 10-20% in wind profile and greater errors in measurements of turbulent energy dissipation rate.

APPENDIX A -- FREQUENCY DOMAIN ANALYSIS OF GROUND CLUTTER SUPPRESSOR

A block diagram of the ground clutter suppressor is shown in Fig. A-1. Conventional z-plane notation is used where the sampling interval is 10 μ s. The notation z^{-m} indicates a shift delay of m sampling intervals. In the micro-processor based system m is a variable and if we select $m = 1666$, the total shift delay is $1666 \times 10 \mu$ s or 16.66 ms which is the period of the 60 Hz AC primary power line. This means that all power line harmonics (or any signal that has a periodicity of 16.66 ms) will be subtracted out. This is very useful for a CW radar as the transmitter generally has a 60 Hz ripple on the output signal.

The two multiplier coefficients are given by

$$1 - a = 1/L \quad \text{and} \quad a = 1 - 1/L$$

where $L = 2^N$ and $N = 0, 1, 2 \dots 7$. The divisions by L can now be realized by shifting a binary number towards least significance by N bits. This restricts the values of the coefficients to some specific values, but the increase in speed and the reduction in complexity are well worth it. The plots of frequency response are parameterized by N, the number of binary bit shifts which is selectable from the front panel.

From Fig. A-1, we see that the output is

$$Y(z) = X(z) - U(z)$$

and the feedback term is

$$U(z) = z^{-m} [(1-a) X(z) + a U(z)] .$$

Solving for U(z) and substituting back gives

$$Y(z) = X(z) - \frac{z^{-m}(1-a) X(z)}{1-a z^{-m}} .$$

The transfer function is then the output divided by the input

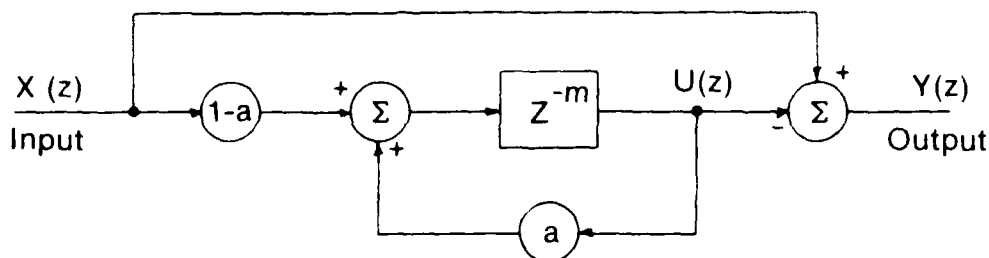


Figure A-1--Block diagram of ground clutter suppressor.

$$H(z) = \frac{Y(z)}{X(z)} = \frac{1-z^{-m}}{1-a z^{-m}}$$

It is clear from above that the parameter a can not take on a value of one.

The frequency response of the filter is obtained by substituting $\cos j\omega + j \sin j\omega$ for z . This results in

$$H(j\omega) = \frac{(1+a)(1-\cos m\omega) + j(1-a) \sin m\omega}{1+a^2 - 2a \cos m\omega}$$

The magnitude (in dB) of this filter is shown in Fig. A-2. It is clear that this is a comb filter and the selection of $m = 1666$ results in the nulls of the filter at harmonics of the 60 Hz power line. This is extremely helpful in the suppression of power line noise. If the parameters of the radar are chosen correctly the returns from stationary clutter will be at the same frequency as the power line harmonics and both will be suppressed by the clutter suppressor.

One advantage of this type of filter is that the null or stop bands can be made very narrow and sharp. This is done by increasing the feedback term, i.e., making the multiplier a larger (or equivalently by increasing N), which increases the time length over which the filter acts. Detailed graphs of the transfer function behavior near the nulls are shown in Fig. A-3.

The spectrum analyzer which operates after the clutter suppressor has a range of frequency resolution with 10 Hz being typical. For N greater than 3, the stop band of the clutter suppressor is much less than the resolution of the spectrum analyzer so that the effect on the atmospheric return is negligible.

With narrow stop bands, it is necessary to synchronize the radar and clutter suppressor so that the clutter remains in the stop band. This is not difficult.

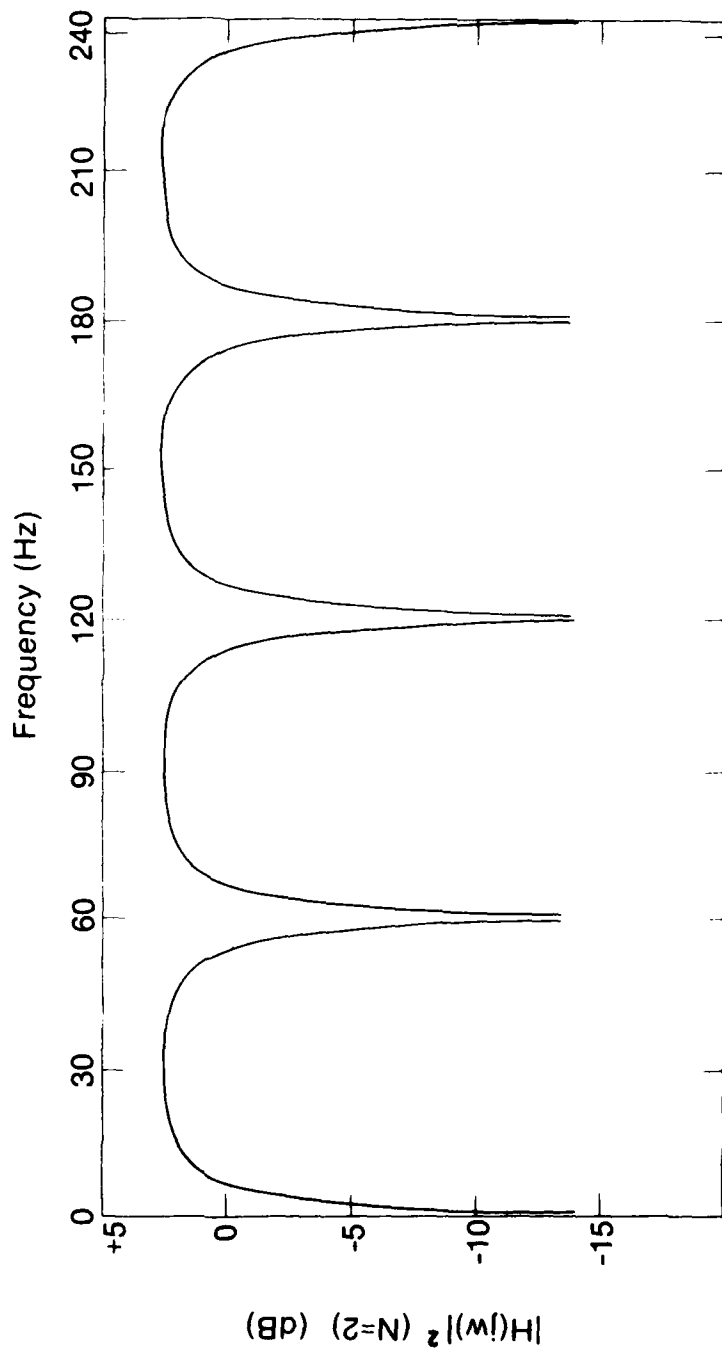


Figure A-2--Magnitude response of ground clutter suppressor.

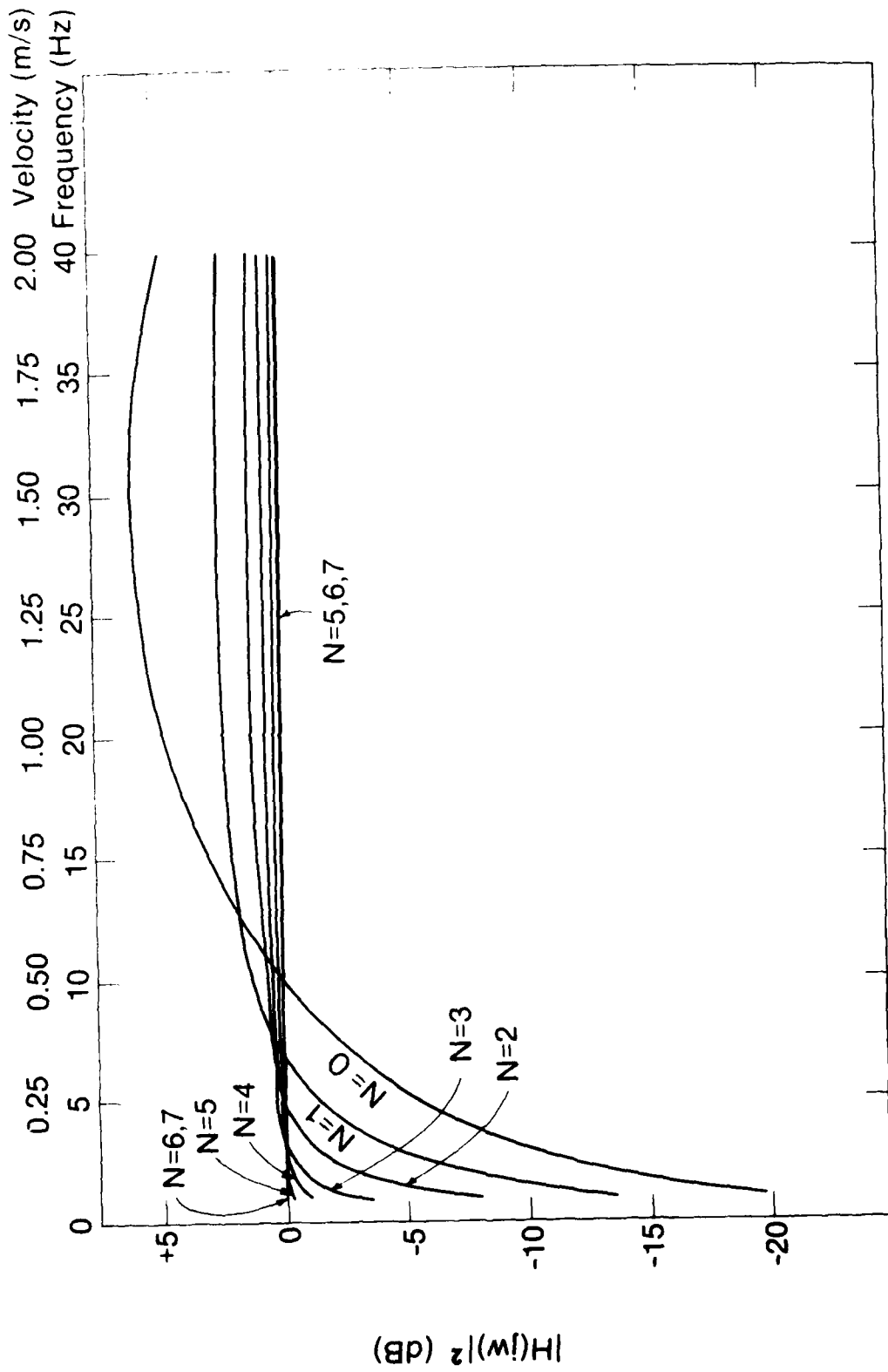


Figure A-3(a) -- Frequency (0-40 Hz) and velocity (0-2 m/s) response of ground clutter suppressor near a null.

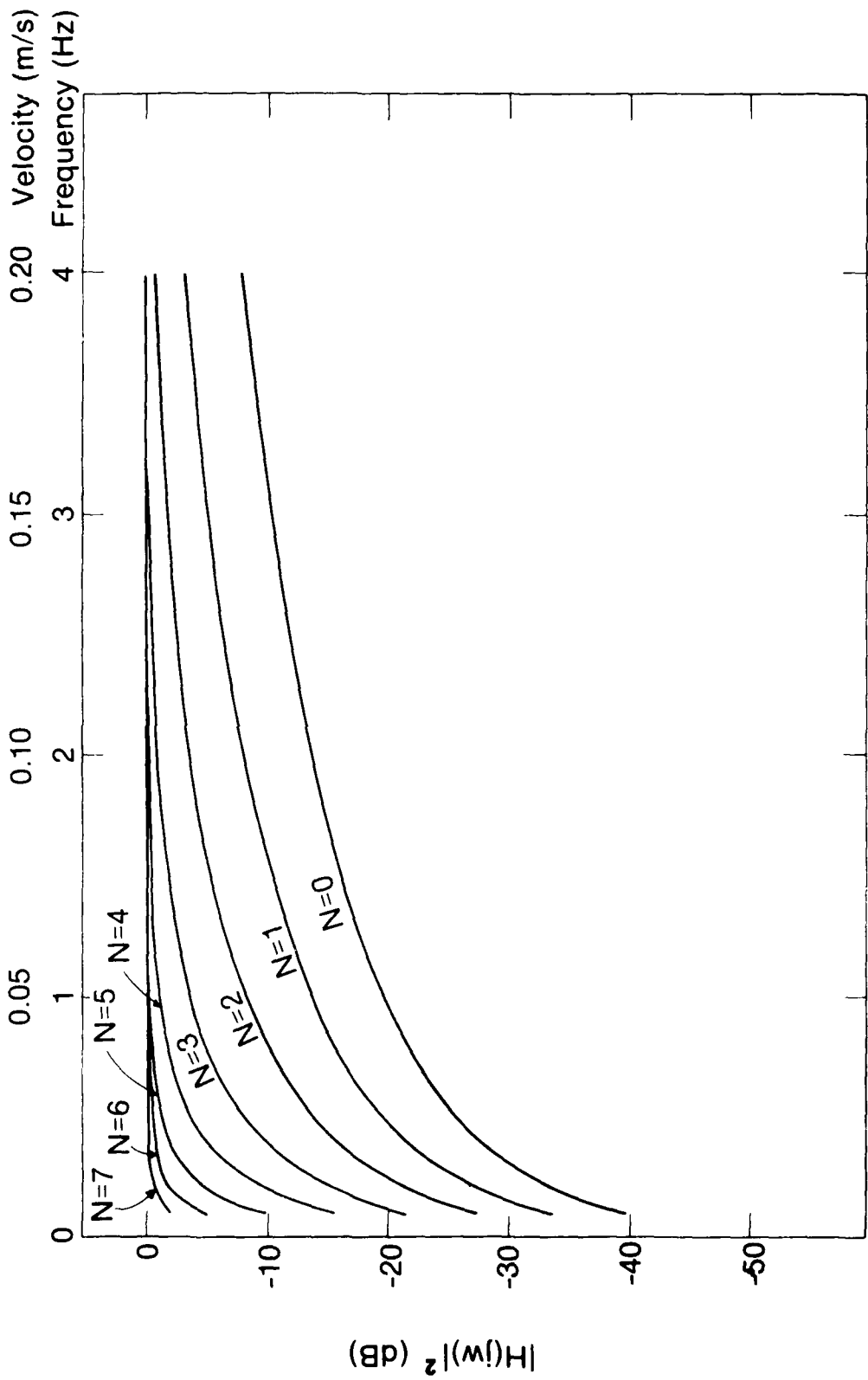


Figure A-5(b) -- Frequency (0-4 Hz) and velocity (0-0.2 m/s) response of ground clutter suppressor near a null.

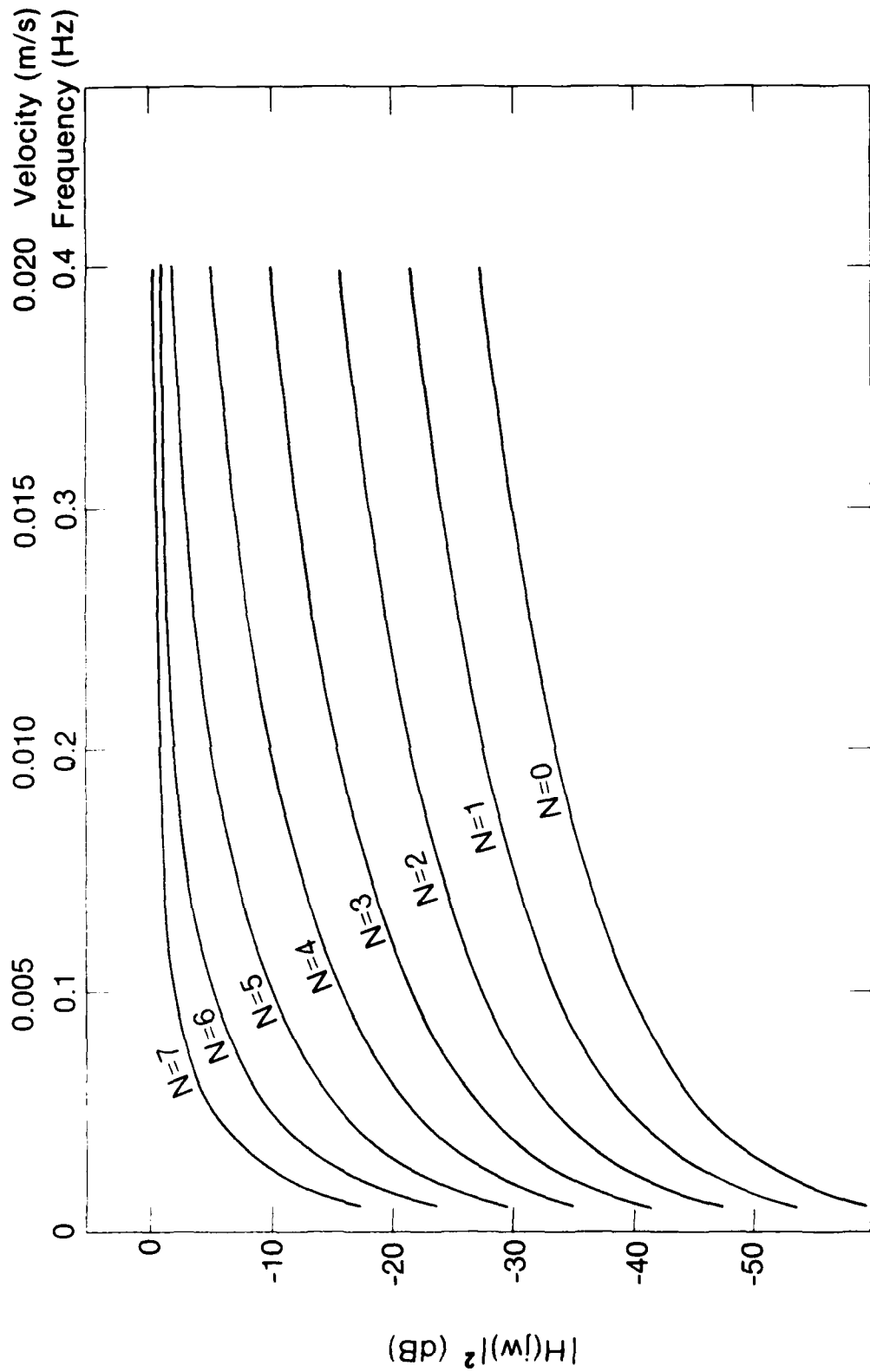


Figure A-3(c) -- Frequency (0-0.4 Hz) and velocity (0-0.02 m/s) response of ground clutter suppressor near a null.

APPENDIX B -- RANGE SPREADING OF LARGE TARGETS

1. The Problem

All high duty cycle radars have the problem that a large return in one range cell can appear in other range cells. In the case of the FM-CW radar, the range cells adjacent to the large target contain a false return that is 13 to 20 dB below the large target return. Range cells further removed from the large target have progressively smaller false returns. We have referred to this effect as range spreading.

In normal operation in the clear air, this range spreading was rarely observed because the return signals were rarely more than 20 dB out of the noise so the spread or false signals were not visible. However, operation at an airport showed that the returns from large jetliners frequently exceeded 20 dB signal-to-noise ratio so the range spread false signals appear in several range gates. An example of this is shown in Fig. 4.7. Just before the 727 jetliner saturates the radar, returns show up in the top four range bins. These returns are due to the range spreading referred to above and the cause will be made clear below.

This range spreading could cause difficulties with any automatic signal processing algorithm designed to differentiate classes of returns. This Appendix shows the reason behind this range spreading phenomena by presenting a numerical example similar to the processing used in the FM-CW radar. Since this numerical work was done on a programmable desk calculator, it is not equivalent to the actual processing done in the radar, but worthwhile conclusions can still be drawn.

2. Cause of Range Spreading in FM-CW Radar

The range spreading is due to the frequency spectra associated with the periodic discontinuities in the mixed signal. Periodic discontinuities have a spectrum which is discrete with a "1/f" type of envelope and it is these components which show up in other range bins.

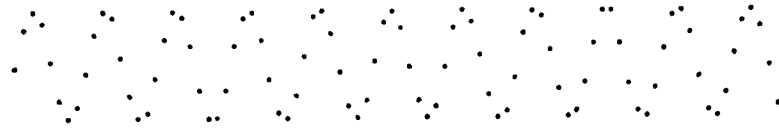
The top graph in Fig. B-1 is made of 88 samples of a continuous sine wave which could represent the mixed signal for a single point target and an r-f sweep with no retraces. From this graph, one could not tell whether the target was moving or not. The top graph in Fig. B-2 could represent a signal with discontinuities at one-quarter, one-half, and three-quarters of the way through the signal. These discontinuities would occur at the retrace times of the frequency of the transmitted signal. In this case, the target is moving at a relatively slow velocity as the phase from one quarter to the next is changing slowly. The output of the radar signal processor is essentially the power spectrum of these signals. Figure B-3 shows power spectra for each of these signals as Q (continuous) and R (discontinuous). The points labeled "X" are where two or more of the points fell on the same location.

The first thing to note is that the spectrum of the continuous signal is not a single line because the beginning and ending points are not continuous. This is not what is referred to above as range spreading. The second thing to note is that the spectrum of the discontinuous signal has discrete peaks with three frequency points between each peak. (The number of points between each peak is equal to the number of discontinuities between the end points of the original signal.) These peaks are the range spreading problem shown with real data in Fig. 4.7.

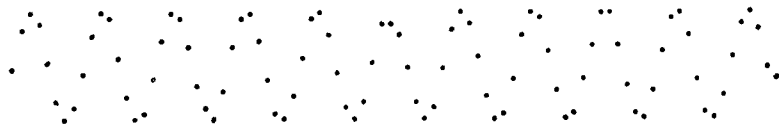
3. Ways to Eliminate Range Spreading

The primary cause of range spreading is that the r-f sweep has to periodically depart from a linear function and this causes discontinuities in the mixed signal. These discontinuities arise irregardless of how fast the frequency retrace occurs and so, adjusting the frequency modulation of the transmitted signal will not solve the problem.

There seem to be two different approaches to eliminating the problem; operating on the mixed signal or operating on the spectrum of this signal. These two approaches are drastically different. Here the main emphasis is on the former, but a few remarks should be made about the latter.



Continuous signal

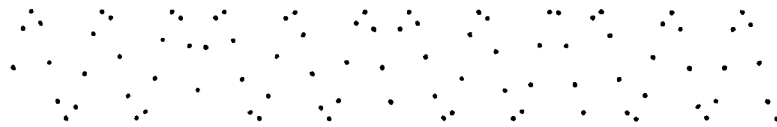


Continuous signal with 3 point average type of weighting

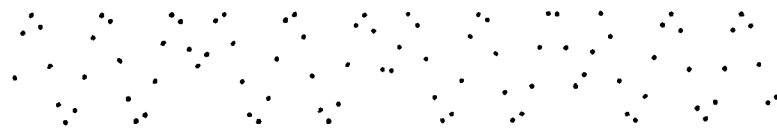


Continuous signal with raised cosine type of weighting

Figure B-1--Continuous signal with two types of weighting.



Discontinuous signal

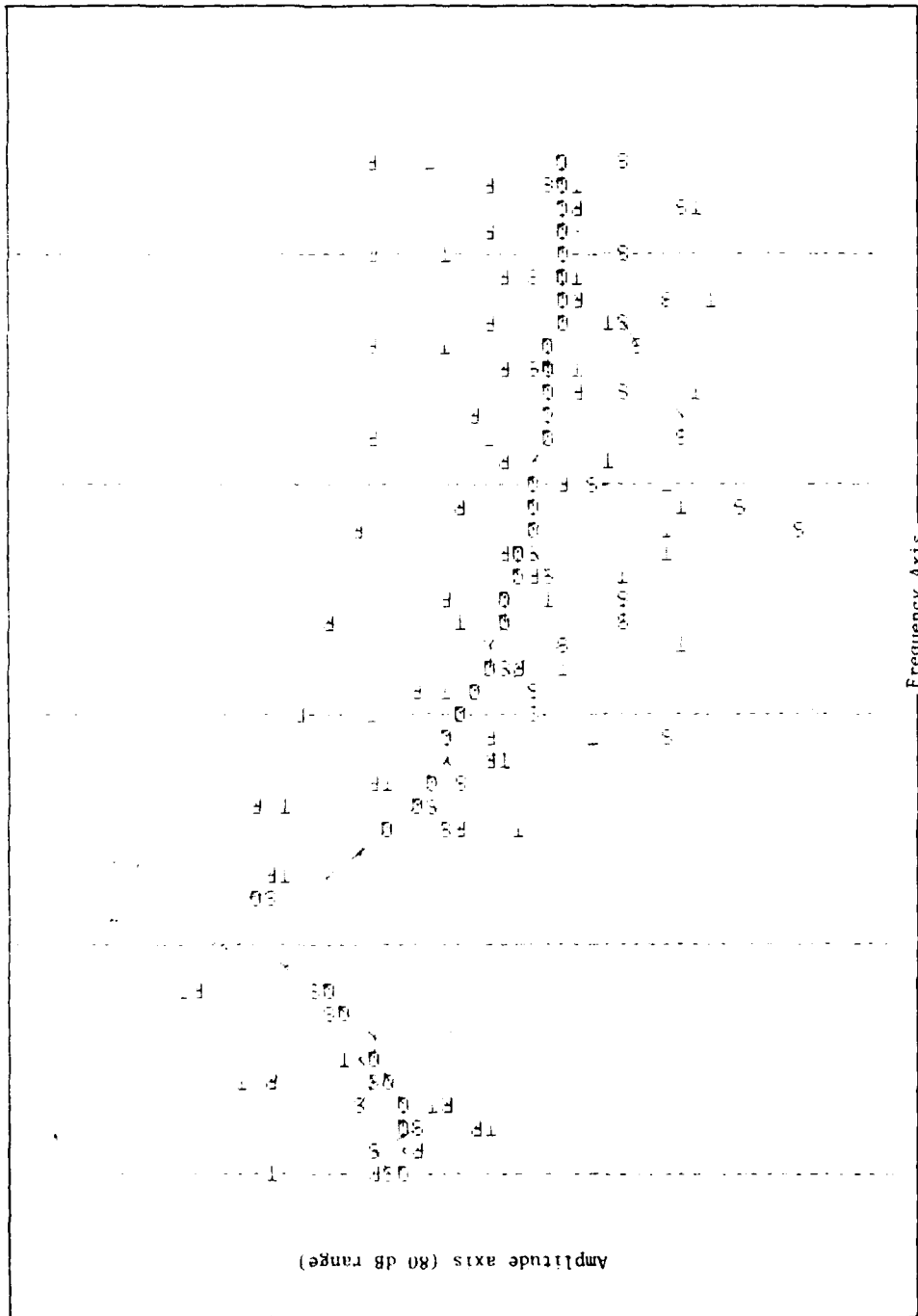


Discontinuous signal with 3 point average type of weighting



Discontinuous signal with raised cosine type of weighting

Figure B-2--Discontinuous signal with two types of weighting.



Frequency Spectra: O for continuous signal; R for discontinuous signal; S for continuous signal with 3 point average weighting; T for discontinuous signal with 3 point average weighting.

Figure B-3--Spectra of 3 point averaged signals.

The main advantage to operating on the radar output or spectrum of the mixed signal is that the data rates at this point in the radar are relatively slow, and complicated operations are feasible. In fact, it would even be possible to do these operations off-line. To reduce the peaks associated with range spreading, one would do a deconvolution on the output spectrum. This is similar to what is done in two dimensional digital image processing. In that instance, it is referred to as deblurring. The only difference here is that the so-called kernel of the resulting integral equation is stochastic. It is difficult to predict, without detailed study, what improvement is possible. The technique should be looked into further because the improvement it gives will probably be in addition to the improvement achieved by the second technique.

The second technique is to operate on the time signal before the spectrum analyzer to reduce the discontinuities, or in other words, weight the input signal. The usual use of weighting in spectral processing (or antenna aperture design) is to reduce undesirable effects associated with the discontinuities at the ends of the time (or space) aperture. Here the purpose is to extend that concept to reducing effects associated with discontinuities anywhere within the time aperture of the spectrum analyzer.

There is a range of approaches to weighting a signal. At one end of this range the philosophy is to change the signal by only a small amount. At the other end of this range, the signal is greatly changed. This Appendix presents some preliminary numerical results, one case with little change to the signal and one case where the signal is heavily changed. The two cases are done for both a continuous signal and a discontinuous signal.

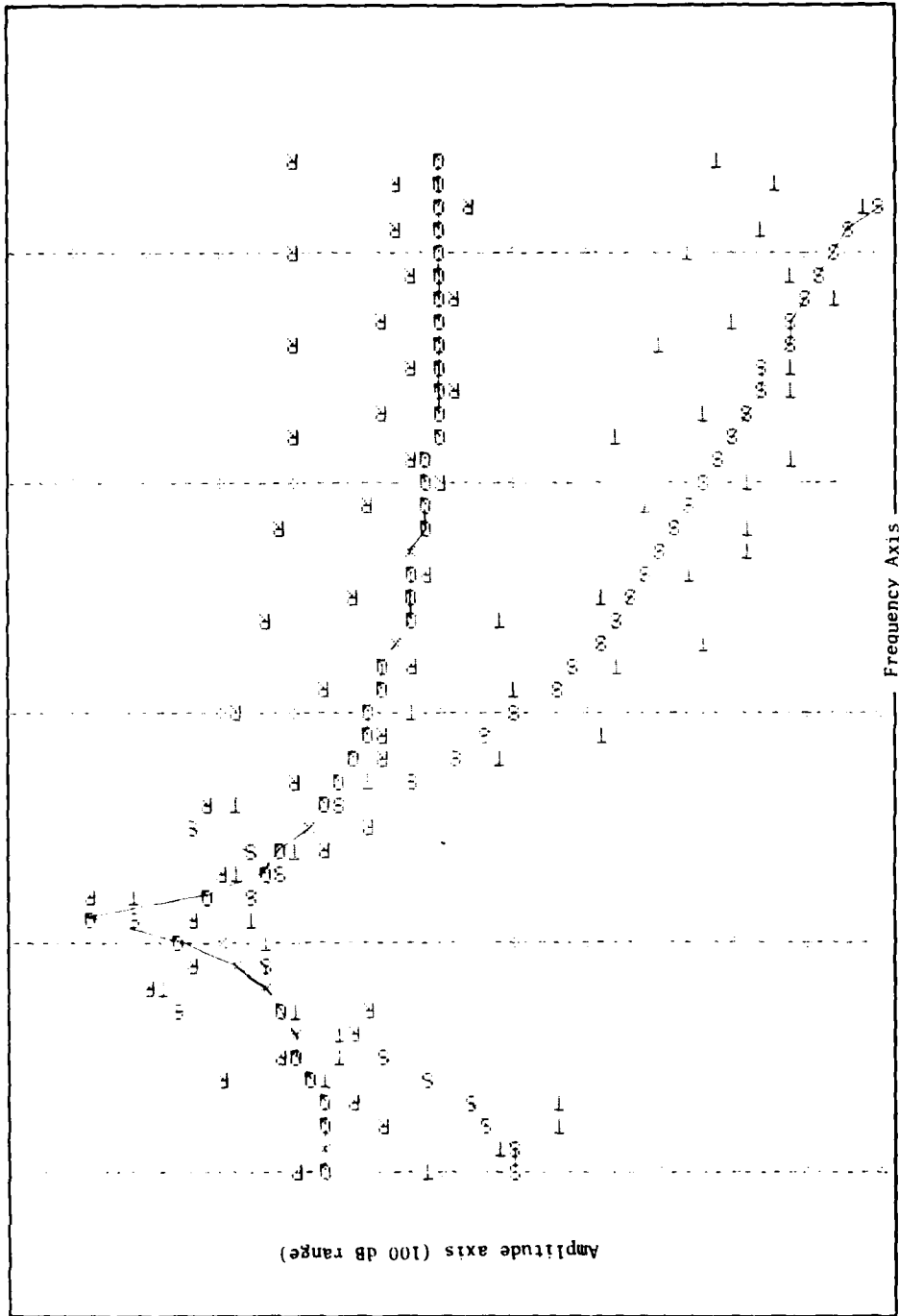
The two types of weighting used here are a three point average weighting and a raised cosine weighting. The three point average type is where the points adjacent to the discontinuity are replaced by a three point average about that point using the original data. For the 88 point time sequence used here, only 8 points or 9% of the data are changed. The raised cosine type of weighting is where the entire sequence is multiplied by another sequence that is a raised cosine curve with zeros occurring at the points of discontinuity. In this case 84 points or 95% of the original data are changed. The difference between these

two approaches is shown in Figs. B-1 and B-2. Figure B-1 shows the continuous signal and the result of operating on that signal with both types of weighting. The effect of the three point average type of weighting is almost imperceptible while the effect of the raised cosine type of weighting is quite drastic. Figure B-2 shows this same thing for the discontinuous signal.

The power spectrum of each of these six sequences can be determined by conventional Fourier transforms and graphs of these six spectra are shown in Figs. B-3 and B-4. The spectra of the continuous and discontinuous sequences are repeated in both figures.

Figure B-3 shows the results of a three point averaging technique. Since this weighting technique only slightly changes the signal, the spectra for the continuous signal before and after weighting should not be greatly different. The difference is that the weighting smooths the discontinuity associated with the ends of the sequence. For the peak and the region around the peak, there is little difference between the Q and S symbols in Fig. B-3. This simple three point averaging technique does surprisingly well in reducing the range spreading peaks, reducing them from 5 to 27 dB in regions removed from the peak. Two disadvantages are that the technique does poorly in low frequency regions (left side of Fig. B-3) and seems to lose effectiveness for high frequencies (right side of Fig. B-3).

Figure B-4 shows the results for the raised cosine weighting. Here the range spreading is reduced by up to 50 dB at high frequencies and 15 dB at low frequencies. However, since the technique makes significant changes to the input sequence, one would expect changes near the spectral peak and a clear picture of this change can be seen by comparing the spectra of the continuous signal with and without raised cosine weighting. These spectra are labeled Q and S in Fig. B-4 and have been connected by a line. The raised cosine weighting technique spreads the simple peak into three separate peaks. This would be unacceptable because measurement of wind shear requires velocity differences between adjacent range cells and the multi-peak response would make it difficult to determine these differences.



Frequency Spectra: O for continuous signal; R for discontinuous signal; S for continuous signal with raised cosine weighting; T for discontinuous signal with raised cosine weighting.

Figure B-4--Spectra of raised cosine weighted signals.

4. Conclusions

The numerical results presented here are for weighting the mixed signal before the spectrum analyzer. Two types of weighting were compared and it was found that a weighting function which drastically changes the signal results in unacceptable behavior near the spectral peak. A weighting technique which weights only near the discontinuities give acceptable results near spectral peaks, but causes problems near zero frequency and only reduces range spreading by 5 dB at high frequencies.

Almost certainly, there is a weighting technique somewhere between the two presented here that combines some of the good features of each. Unfortunately, this type of weighting can not be done on the present equipment. At present, the only type of weighting is that which consists of multiplication by a given function. So, even the simple three point averaging weighting can not be done on the present equipment. Utilizing weighting techniques resembling digital filters (such as the three point averaging technique) require that an array processor be used in place of the present spectrum analyzer.

Exactly how far the range spreading peaks can be suppressed is not clear without more detailed analysis, but suppressions of 20 dB do not seem at all unreasonable.

CHAPTER 4 -- INTERFERENCE CONSIDERATIONS

R.B. Chadwick, K.P. Moran, and T.R. Detman

4.1 Introduction

The distinguishing feature of the FM-CW Doppler radar is the extreme sensitivity it has at short ranges. This is desirable because it can detect and measure atmospheric phenomena that conventional weather radars miss. However, it also means that the FM-CW radar is susceptible to undesirable returns and clutter from these short ranges. These returns can be from hard targets such as aircraft or cars. Also they can be from biological targets such as birds or insects. The atmosphere also introduces interfering returns from hydrometeors. Even the aircraft passage produces interfering returns in the form of wake-related echoes. Each of these sources of interfering returns will be discussed below.

In this chapter, the word interference means any type of received signal that could possibly interfere with automatic data processing algorithms designed to detect hazardous wind shear. This includes the usual use of the word interference which relates to electromagnetic signals from other equipment, but also includes undesirable returns from moving objects near the radar.

4.2 Interference from Hard Targets

A major problem which must be resolved is the interference from moving hard targets such as aircraft and automobiles. This problem is especially severe near airports where there are moving targets with large radar cross section. The major cause of this problem is that the radar can be looking in one direction and return from a large moving target can be received through the antenna sidelobes. The patterns for our antennas are given in Chapter 2 and it is clear that there are significant sidelobes in the E-plane. Perhaps the best way to reduce sidelobes is to use an offset paraboloid antenna structure with a symmetric, near-Gaussian feed pattern and some possible approaches to offset antennas for the FM-CW Doppler radar are given in Chapter 2.

Another way to eliminating this interference is through proper siting of the radar. Unfortunately, site selection is something which is not as easily quantified as design of specific antenna patterns. About the best that can be done is to relate the experiences that we have had in siting the radar in four locations at three different airports: Buckley Air National Guard Base near Denver; Stapleton International Airport in Denver; and Otis Air Force Base in Massachusetts.

Based on these experiences and others not near airports, we have arrived at some rules-of-thumb relating to site locations. Because of some unique features of the FM-CW radar, these rules are somewhat different from those for conventional pulse radars. An important consideration is that the antennas should be as low as possible. The reason for this is that distant objects on or close to the ground are somewhat shielded from view by natural undulations in the earth's surface and are not seen by the radar. At a permanent site, earth berms would be an effective shielding device. These berms would scatter energy back to the receiver, but since this energy is from a stationary target, it would be removable by the clutter suppression technique discussed in Chapter 3.

Sites should be avoided which have line-of-sight views of roads, highways, or railroad tracks. Foliage may shield a roadway from optical line-of-sight, but will have little effect on 10-cm wavelength signals.

We have also found that vertical metal structures such as towers, metal sheds, etc. should be avoided. These structures return so much energy that the clutter suppressor frequently is saturated.

During the summer and fall of 1977 the radar was operated at Buckley Air National Guard Base east of Denver where we were constrained to look away from the main terminal area. The area the radar was viewing consisted of high plains sagebrush with no trucks or automobiles. Buckley is mainly used for training and the aircraft traffic is light. So we experienced little interference from moving targets.

In the fall of 1979, we located the radar on the Rocky Mountain Arsenal adjacent to Denver's Stapleton International Airport. The location was about half a mile north of the north end of runway 35L as shown in Fig. 4.1. This site

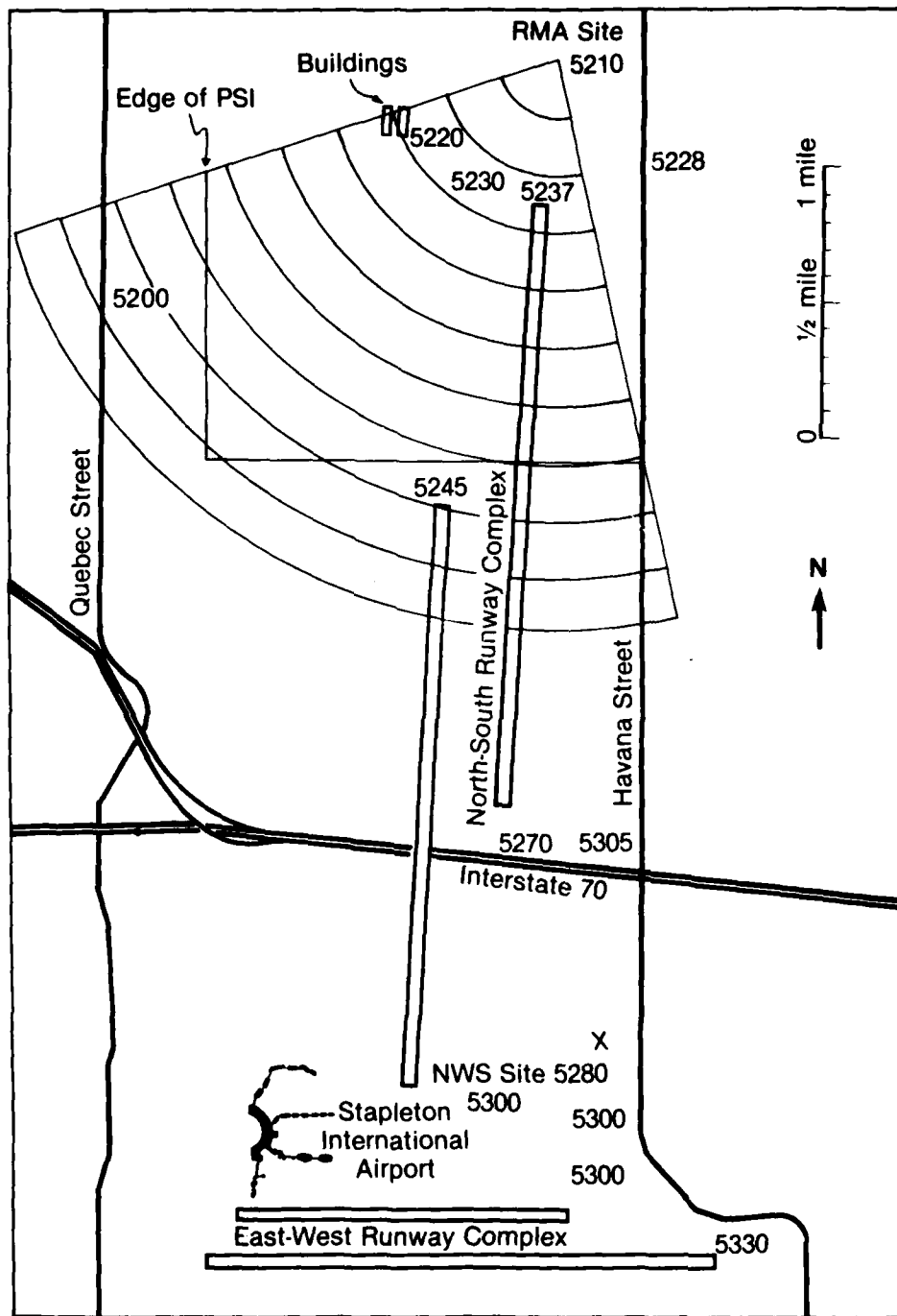


Figure 4.1--Location of two radar sites near Stapleton International Airport. The elevations (in feet) of various locations near the sites are shown.

was located in a natural depression which was ten to twenty feet below the runway area. This provided very effective natural shielding from moving targets. Certain equipment buildings were visible near the end of the runway, but the ground clutter suppressor was able to eliminate these returns because the buildings were stationary. Aircraft on the runways were generally not optically visible from the radar and had no effect on the radar output. A plan shear indicator (PSI) display taken from this location is shown in Fig. 4.2. The maximum range for this PSI is 3530 m and the region covered is shown in Fig. 4.1 where each range bin of 353 m is indicated. The PSI in Fig. 4.2 shows a nearly uniform wind from the northwest with small wind shear in the area under the title box. Notice that along the radial under the title box, the radial wind at 1 km range is about 16 m/s while at 2.4 km range, the radial wind is about 9 m/s. Converting this to vertical shear of the horizontal wind, we obtain a shear of 0.02 s^{-1} , a small value of little consequence. It is pointed out here only to indicate what shear will look like on the PSI. In normal operation, looking for hazardous wind shear, the maximum unambiguous velocity (which is 9 m/s in Fig. 4.2) would be on the order of 20 m/s.

The site where this data was taken was very good because of the natural shielding evident from the elevations in Fig. 4.1. We experienced little difficulty with automobiles or aircraft on the runways. Note in Fig. 4.1 that major roadways were located under the scan area, but no interference is present in the PSI. However, after a month of operation, the FAA erected a tower directly in front of the radar and we were forced to move to a second site which was near the National Weather Service (NWS) balloon launch facility. This site was selected so that radar returns could be compared with temperature profiles measured by balloon. The NWS site is more centrally located with respect to the airport as shown in Fig. 4.1. Because of blockage by the radar trailer we were unable to scan at low angles to the southeast. Whenever we would look to the west (even at relatively high angles) the E-plane sidelobes would be toward a heavily traveled Interstate highway (I-70) which was about one mile away to the north. The automobile traffic on this road was visible optically from the NWS site and was easily seen by the radar. This would have been a major source of interference for automatic data-processing algorithms. The automobile traffic was also easily detected when we looked to the north, but then only at low elevation angles.

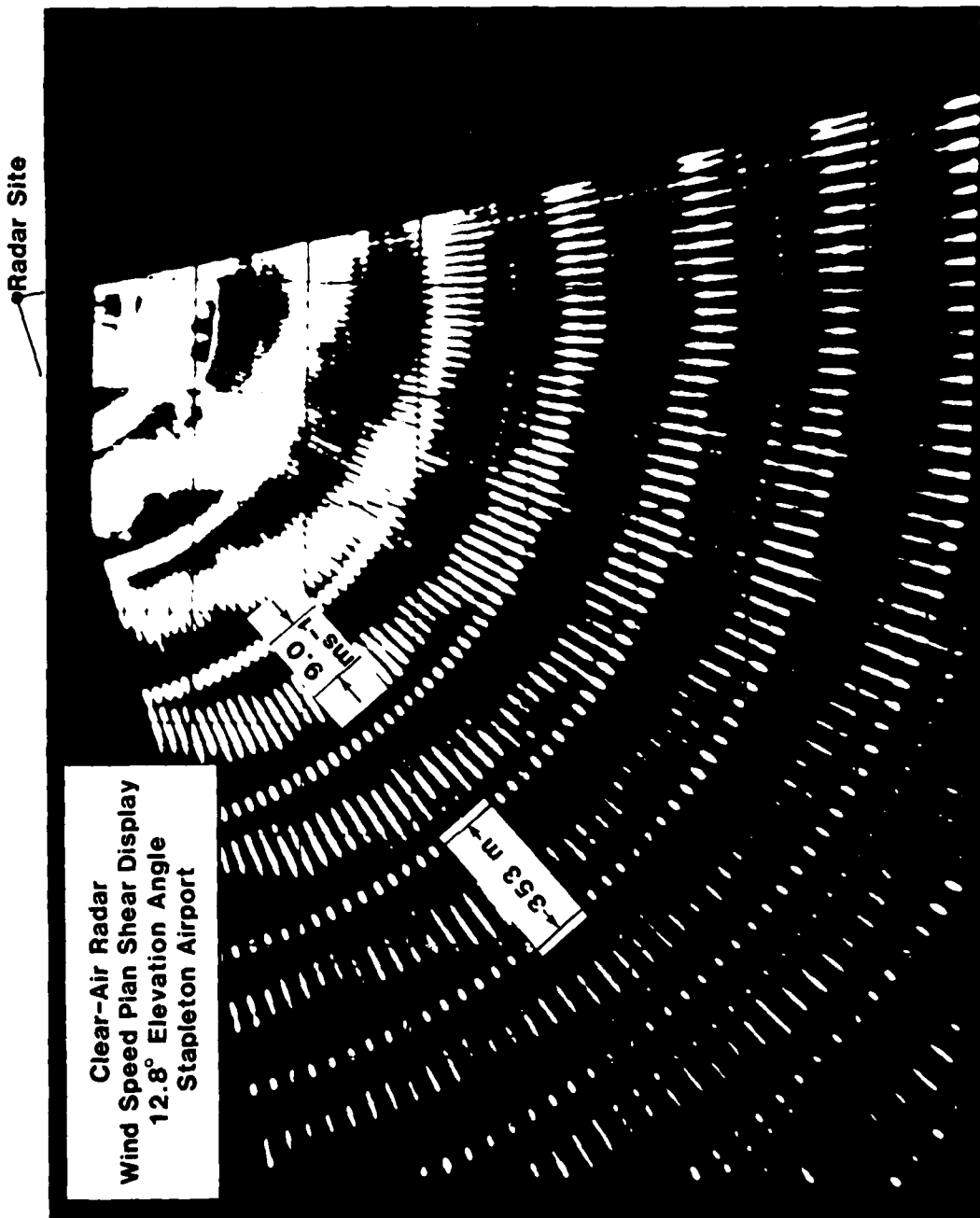


Figure 4.2--PSI display taken at Stapleton International Airport. The region of coverage relative to the airport is shown in Fig. 4.1.

During the spring of 1980, the radar was located at Otis Air Force Base, Massachusetts. This is a very flat region with little chance for natural shielding. There were several lightly traveled roadways within sight of the radar, but the traffic on these roads was not sufficient to cause problems. The main problem was the presence of large metal buildings about one kilometer away in the direction we were operating. In the other direction were a complex of towers and large antennas. The return from the metal buildings was strong enough so that the clutter suppressor was operating beyond its full range. This meant that return from the buildings was present in the output. Since the buildings were stationary, the output components could not be mistaken for atmospheric return by a processing algorithm. However, when the antennas were moved, the return from the metal buildings broadened and, in some cases, could be mistaken for atmospheric return. The movement could be intentional, such as antenna scanning, or it could be unintentional, such as might be caused by wind blowing the antennas. So it is highly desirable to avoid vertical metal structures near the main antenna beam.

A final siting example is from a location not near a large airport, but it does show the importance of natural shielding. The site is at the Boulder Atmospheric Observatory (BAO) about 20 miles east of Boulder, Colorado near the small town of Erie, Colorado. A contour map of the site is shown in Fig. 4.3. The radar was located near the building and looked westward over the town of Erie. A clear-air PSI at an 8° elevation angle is shown in Fig. 4.4. This PSI was taken on a very calm day, so there is little evidence of either wind shear or of even uniform wind. The important thing to note is the terrain as one looks west from the BAO tower. It falls off and provides natural shielding so that the town of Erie is optically shielded from the radar. The radar then does not detect any buildings or traffic in Erie.

Siting is an extremely important aspect of FM-CW radar operation. Because of the CW nature of the device, different siting criteria are important than are normally used for pulsed meteorological radar operation. The most important thing is to employ natural shielding of interfering targets. Low antenna placement will usually result in the greatest amount of natural shielding.

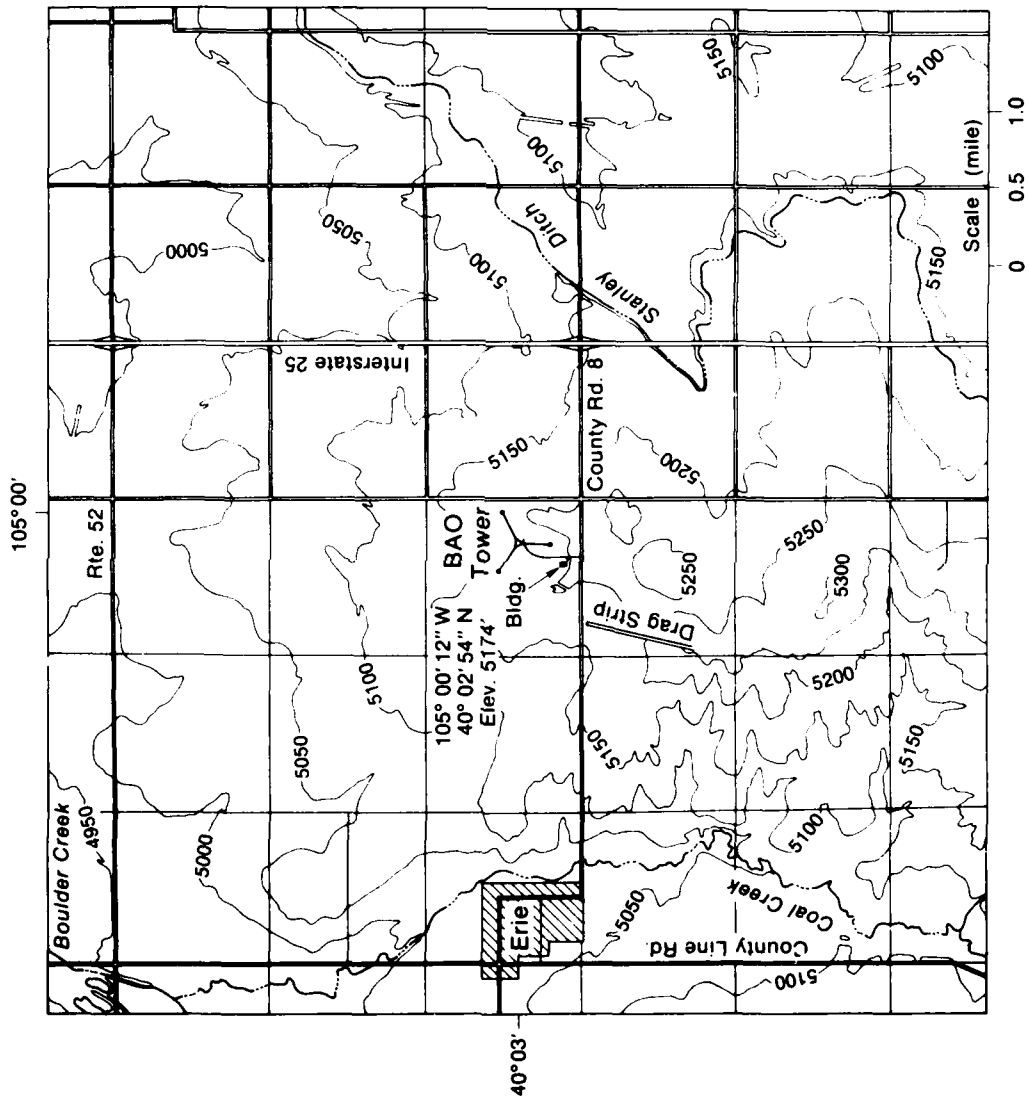


Figure 4.3--Contour map of BAO field site. Radar was located slightly west of building.

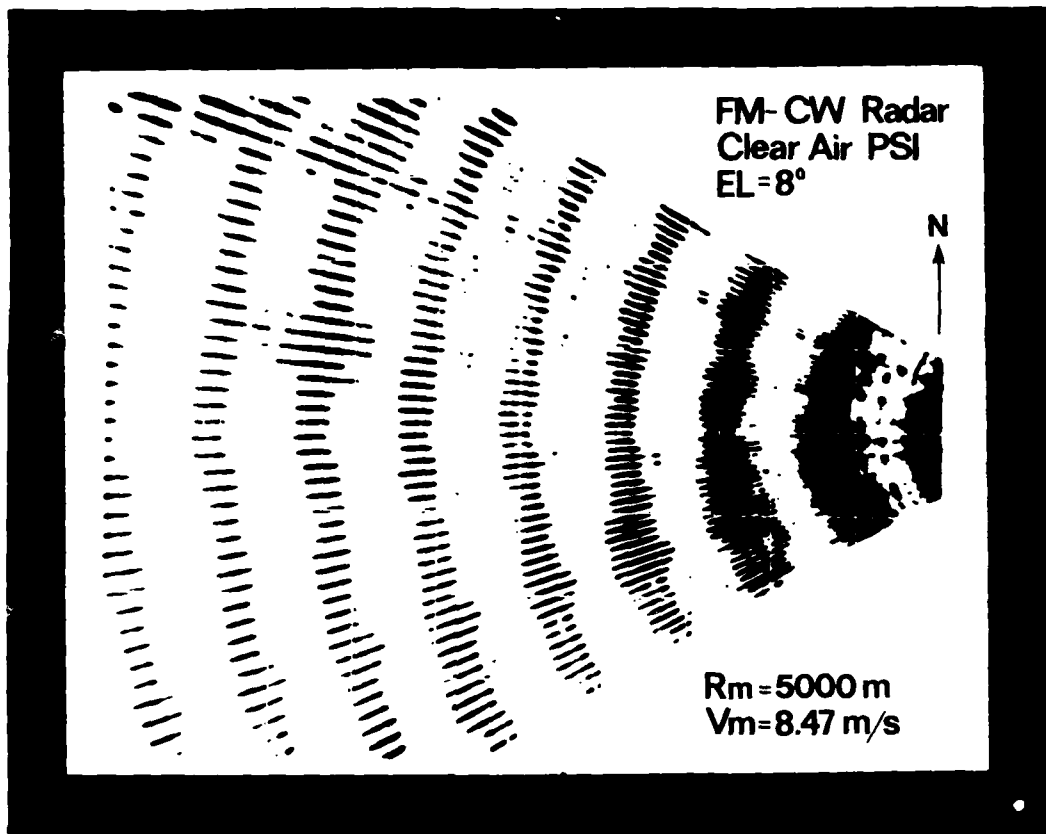


Figure 4.4--PSI display looking westward from BAO site. Area of scan is over the town of Erie.

4.3 Interference from Biological Targets

A radar as sensitive as the FM-CW Doppler can detect many things in the atmosphere. One class of targets that radars can detect is biological targets, mainly birds and insects. As shown by Fig. 3.1, the return from birds is generally stronger than the return from clear air and there does not seem to be any way to discriminate against birds in the main beam of the radar. Fortunately the percentage of time that birds cause saturation is usually very small. On only two occasions have birds been a problem in the operation of the FM-CW Doppler radar. The first was on a single day at a rural location in Colorado. The radar was operating at a 5° elevation angle with a maximum range of 5 km. The beam diameter at this range is about 250 m and the chosen range bin size was 500 m. One target that persisted for about 20 minutes was probably a hawk circling in the beam. The return was such that a data processing algorithm to detect wind shear would

have probably given an erroneous output. This has happened only once and it seems unlikely that this would be a problem near an airport.

The second problem occurred when the radar was located on top of a mountain on White Sands Missile Range. It was close to the edge of a cliff where there were rather intense updrafts. At certain times of the day, large numbers of swallows soared on these updrafts at very short radar ranges (a few hundred meters). This resulted in the radar being saturated for up to fifty percent of the time.

It appears that birds could pose a problem to FM-CW Doppler radar operation if a few birds stayed in the beam or if large numbers pass through the beam. This does not seem likely at airports as we have never experienced a problem with birds at any of the three airports we have operated at.

Insects are also easily detected by FM-CW Doppler radar and, in warm months, they are detected so frequently that they can actually be studied by FM-CW radar, Gossard and Chadwick (1979). Sometimes the return from insects is greater than the return from the clear atmosphere. Also sometimes the insects are closer together than the resolution of the radar and they appear as dense layers. Fortunately however, insects are generally weak fliers and they usually follow the mean flow. An example of this is Bean et al. (1971), where the insect tracks are clearly tracing out the atmospheric motion. During periods of migration, certain large insects do fly with considerable velocity (up to 5 m/s) and wide spatial extent (up to 100 km). This type of condition would perhaps affect a shear detection algorithm, but fortunately these migrations are rare. Usually, the insects act as tracers and make the wind shear measurement easier because they increase the backscattered signal power. In the large range cell case of interest, the insects would increase the backscattered power and spectral width, but would have little effect on the mean velocity or wind shear measurements.

4.4 Interference from Hydrometeors

Hydrometeors, generally in the form of rain, are readily detectable with the FM-CW radar. For most cases of interest, they increase the signal-to-noise ratio and actually make it easier to detect wind shear. In fact, if all hazardous wind shear occurred in the presence of rain, the problem of detecting these hazards

would be quite simply solved with a small pulse radar. However, oftentimes the hazardous region is in clear air and a very sensitive radar is required to detect the hazards.

In the normal mode of operation for detecting hazardous wind shear at airports, the radar would be operating at a fairly low elevation angle somewhat greater than the standard 3° glide slope. In this case, the downward velocity of the rain is nearly transverse to the radar beam so that fall velocity is not a factor. The radar measures only horizontal winds in the mode.

Generally, rain will not cause pre-detection saturation of the FM-CW radar. Figure 3.1 shows the antenna power levels for two cases of rain. A case where the power level was actually measured experimentally is designated "rain signal." This is for a case where the rain extended from the radar out to a range of several km. This is the worst case for pre-detection saturation and the level is still about 20 dB below saturation. Another case where both the radar and the region being investigated are in the rain is presented in Chapter 5. The shear measurement described there was very easily made.

A second rain case that is not difficult for shear measurement is when the radar is outside of the rain and the region of interest is in the rain. Figure 3.1 shows calculated receiving antenna power levels for the case of a 150 m rain cell centered at 1 km. Again the antenna power level, even for the most intense rain, is well below the pre-detection saturation level, so the shear measurement in the rain cell is quite easy.

The case which is not easy is when the measurement is to be made in a clear air region and there is rain in the beam near the clear air region of interest. The main problem here is that the return from the strong target (the rain) is range spread as described in Chapter 3. The spread portions of the rain can then interfere with the desired clear air wind shear measurement. The degree to which this interference can be suppressed is not known. However the numerical results in Chapter 3 using relatively simple techniques show that suppression of up to 50 dB is not unrealistic. One of the major recommendations in Chapter 1 is that the range spreading problem be studied in greater detail so that effective solutions can be developed.

4.5 Interference from Wake Related Return

The clear air return that the FM-CW Doppler radar sees is backscattered from half-wavelength (5 cm) fluctuations in radio refractive-index. Generally these fluctuations are caused by turbulence in the free atmosphere. However, the wake of an aircraft also produces small fluctuations detectable by radar. This was first shown by Noonkester et al. (1974), where it is stated that "the data strongly indicate that the unique echo is created by departing aircraft. The source and nature of the echo is undetermined, however." Later in Noonkester's report, it is stated that "the echo intensity is often sufficient to overdrive the radar like birds or other large targets have been observed to do." If the return is related to the aircraft wake and is strong enough to sometimes saturate the radar, it may provide interference to a wind shear measurement algorithm.

In the fall of 1979, we moved the FM-CW radar to the Rocky Mountain Arsenal which is at the north end of the north-south runway complex of Denver's Stapleton International Airport. One purpose of this experiment was to see if the radar could detect wake-related echoes and if they would be a problem. We found that the radar can readily detect wake-related echoes when the atmospheric conditions are right. When there was a strong cross-wind, we did not detect wake-related echoes. But when there was a light wind along the runway, we detected wake-related echoes for most of the large aircraft. This agrees with the Noonkester et al. (1974) results where they detected 292 wake-related echoes in a one month period at San Diego's Lindberg Field.

On rare occasions, we found that the return from the wake was quite strong and may cause interference to a wind shear detection algorithm. However, we did not find any instance where the wake return saturated the radar. Models of wing-tip vortices show that most of the velocity is transverse to the runway so that a radar looking parallel to the glide slope would be relatively insensitive to any vortex velocity. Most of the time the wake-related return should have predictable features so that data processing algorithms could separate hazardous wind shear from wake vortices. In fact, these two phenomena, hazardous wind shear and hazardous wake vortices, are nearly mutually exclusive as the winds tend to remove the vortices.

The radar signatures of the wake-related echoes detected by Noonkester and Richter (1980) and by us, Campbell et al. (1980) have yet to be fully explained. The Noonkester wake-related echoes were taken in a high resolution, range-only, vertically looking mode while our data are low resolution, range-Doppler, slant looking (elevation 25°) mode. Our data was obtained at the RMA site shown in Fig. 4.1 with the radar looking transverse to the glide slope of the west runway of the north-south runway complex. The west runway glide slope was 500 m away and we operated with a maximum range of 1 km and an elevation angle of 20° to 25° . This resulted in the aircraft being slightly above the beam which means that the wingtip vortex system should drop through the beam according to the conventional models.

Qualitative analysis indicates that with the Doppler mode, we detect two different classes of wake-related echoes. The first is where the echo stays in one range cell and shows a changing velocity, the second is where the echo moves from one range cell to another and shows an unchanging velocity. Examples of these two types of echoes are shown in Fig. 4.5 where the range translating echo is on the right and the changing velocity echo is on the left. The return from the atmosphere shows up as the horizontal dark areas, each of these is the time history of the radial velocity spectrum of the clear air at that range. The vertical dark areas are due to the aircraft passage close to the beam and the resulting saturation of the signal processor. The dark sine wave area on the right is a wake-related return at 500 m range that is alternately changing radial velocity from approximately +8 m/s to -8 m/s with a period of about 20 s. The second type of return is shown on the left where immediately after an aircraft passage, a return moves from 200 m to 700 m with a constant velocity. This velocity can be measured two different ways, range change with time or Doppler frequency shift. Both give an outward radial velocity of about 16 m/s.

Of the two types of wake-related echoes, the range translation type is the most common. Figure 4.6 shows several instances where wake-related echoes of the range translation type are moving both toward and away from the radar. On one occasion, it appears that both types of wake-related echoes were generated by the same aircraft as shown in Fig. 4.7. However, it is somewhat difficult to assign a given wake-related echo to a given aircraft because the traffic on both of the north-south runways was high when the data were taken.

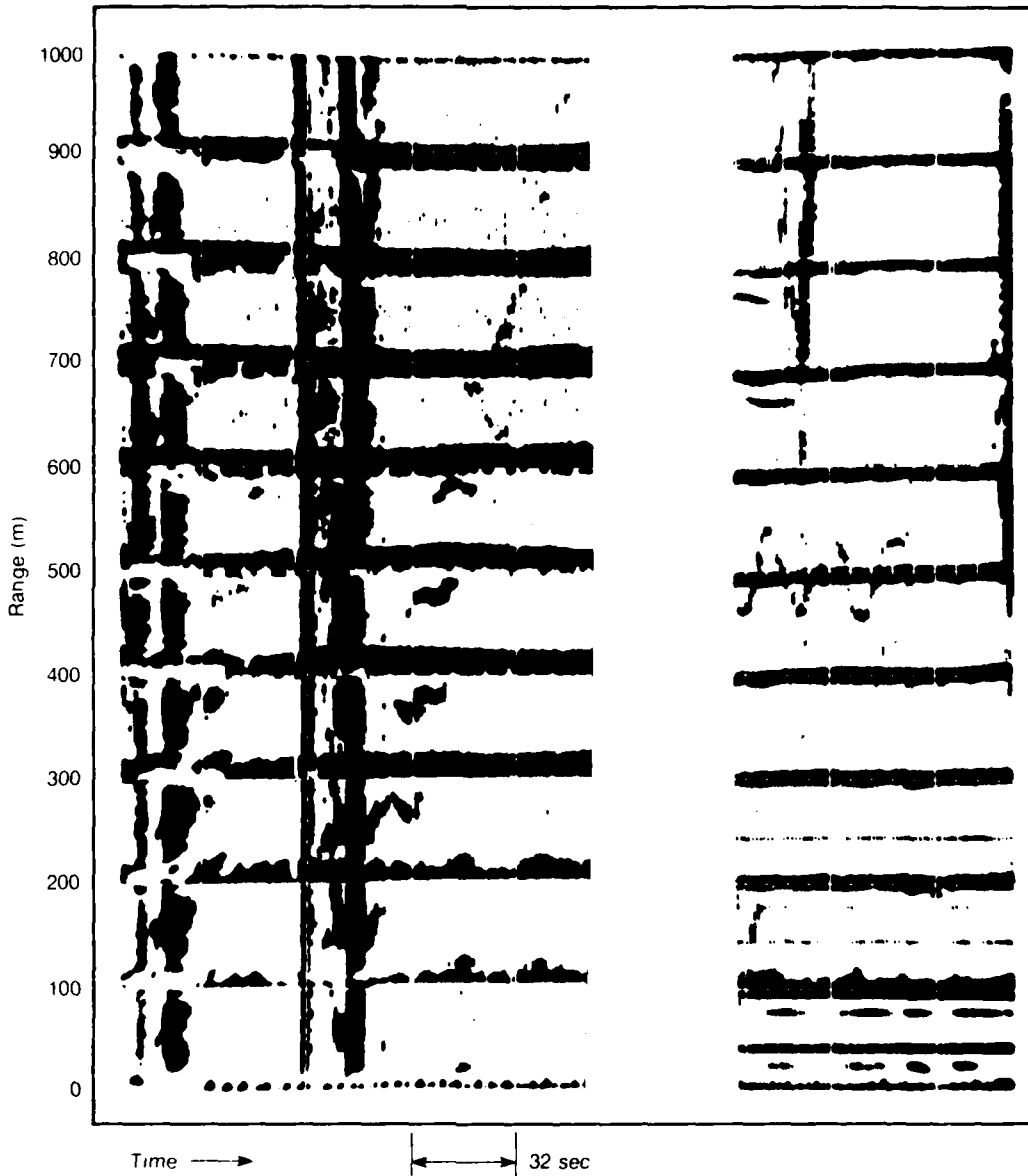


Figure 4.5--Two types of wake-related echoes obtained at RMA site.
Elevation angle is 23° .

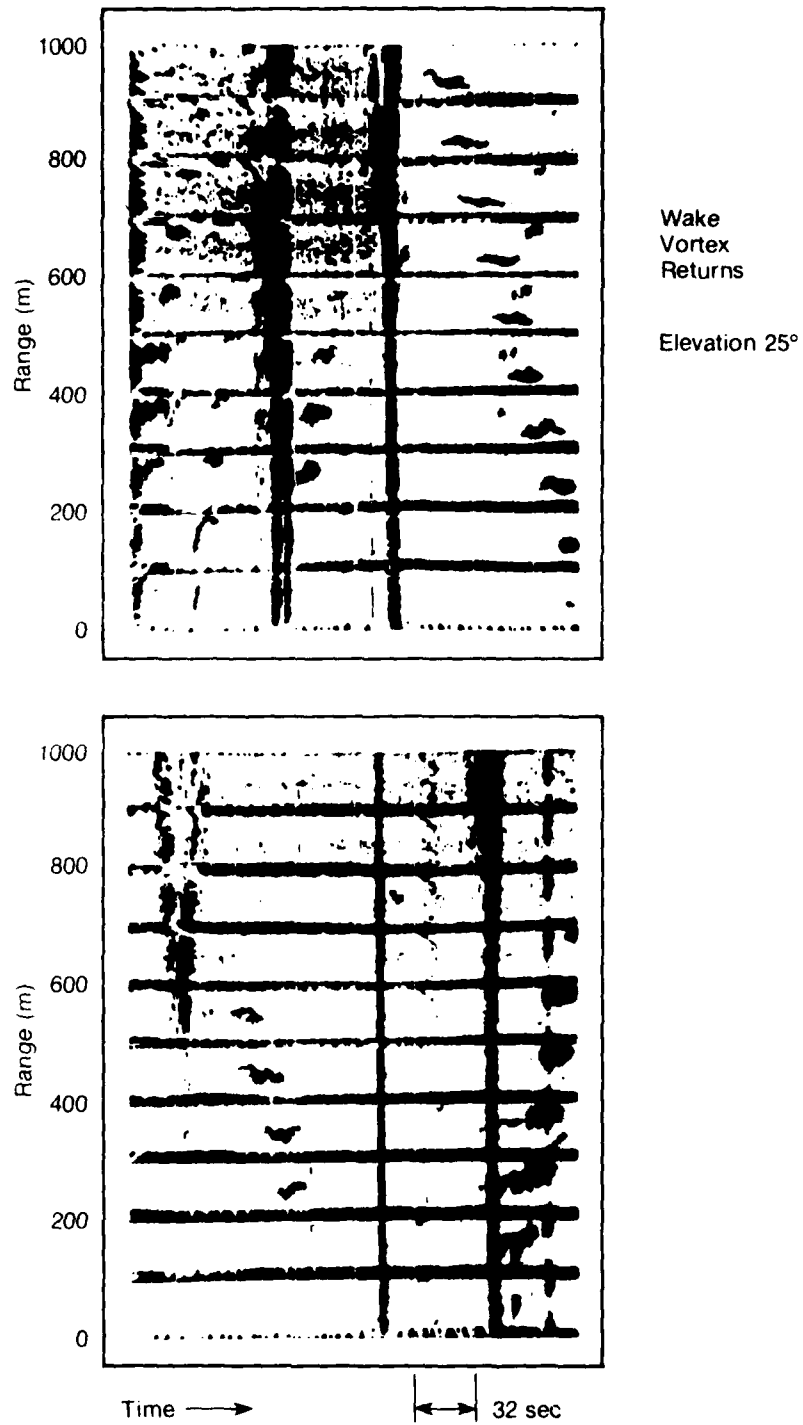


Figure 4.6--Wake-related echoes of the range translation type. Elevation angle is 20°.

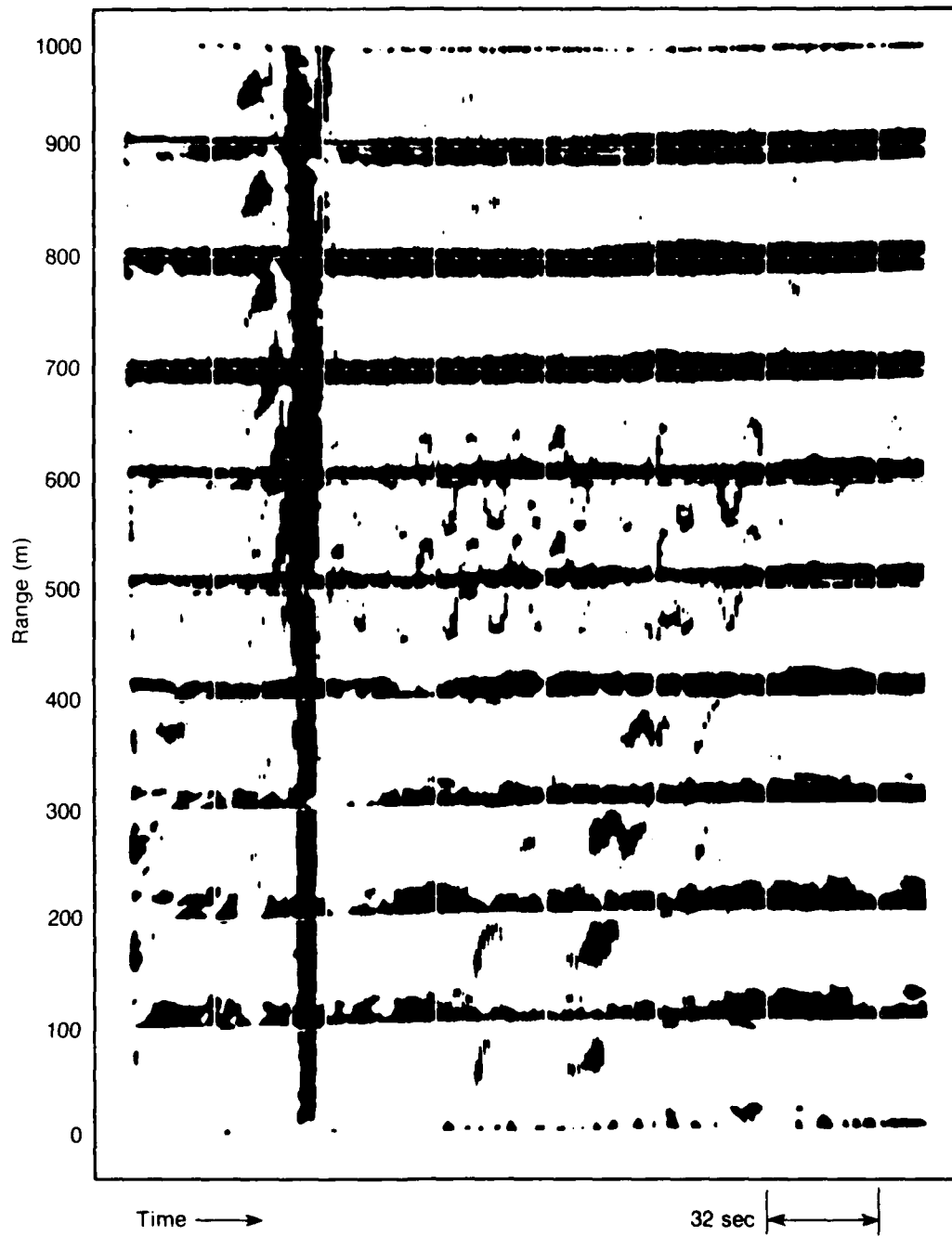


Figure 4.7--Incident where a 727 generated both types of wake-related echoes. Elevation angle is 25°.

On a first examination, our wake-related echoes do not seem to agree with those of Noonkester et al. (1974) and Noonkester and Richter (1980). However the major difference between the two is that the Noonkester data is taken with range cells of two meters while our data has range cells of 100 m. The striking feature of the Noonkester data is the small apparent height fluctuations of an almost perfect sinusoidal nature with periods of about 15 s. If these apparent height fluctuations were present they would not be detected with a 100 m range cell. However, they could be due to an unresolved range-velocity ambiguity which exists in a single-sweep range-only FM-CW radar as used to take the Noonkester data. Since a range only FM-CW radar measures range with a frequency measurement, it cannot measure Doppler frequency unambiguously with range. However, an FM-CW Doppler radar such as ours, which processes many sweeps coherently, can differentiate between range and velocity. Our data does show, for some cases, that the wake-related echo does have velocity changes and, furthermore these velocity changes have about the same period as the apparent range changes in the Noonkester data. We feel that the apparent range changes in the Noonkester data are really velocity changes as in our data. Further, we feel that the two sets of data are essentially describing the same phenomenon relating to an aircraft wake.

The wake-related echoes do not seem to agree with conventional models for wingtip vortices. Clearly, this is an area that needs further research as pointed out in the recommendations in the first chapter.

The ease with which wake-related echoes can be detected indicates that the FM-CW radar may be a viable candidate for detection of hazardous wingtip vortices near crowded approach zones at airports. This is another area which needs further work.

4.6 Summary of Problem Areas

There are some important problem areas which we have identified as needing attention before this type of radar technology can be considered for operational use at airports. We have done preliminary work in each of these problem areas and have shown that the problems are solvable. We have found nothing, either in

the atmosphere or the current state of radar technology, to suggest that a short range, clear air radar would not be extremely useful as a landing aid at airports.

An important and solvable problem is the range spreading associated with large targets. Preliminary numerical results demonstrate that weighting of the return signal prior to processing can significantly reduce the undesirable effects of range spreading. It remains to determine the best way to do this. We were not able to do this because our signal processor does not allow arithmetic operations.

A second problem is to determine quantitative information on siting in the airport environment. This involves using the radar at many different sites near airports. We were not able to do this because our experimental unit is difficult to move from one site to another.

CHAPTER 4 -- BIBLIOGRAPHY

- Gossard, E.E. and R.B. Chadwick (1979), "Studies of insects by high resolution radar," Fourth Conference on Biometeorology, p. 268-271. American Meteorological Society, 45 Beacon St., Boston, Mass. 02108.
- Bean, B.R., R.E. McGavin, R.B. Chadwick and B.D. Warner (1971), "Preliminary results of utilizing the high resolution radar as a boundary-layer probe," Boundary-Layer Meteorology, Vol. 1, p. 466-473.
- Noonkester, V.R., J.H. Richter and D.R. Jensen (1974), "Unique echoes observed by FM-CW radar at a jet airport," Naval Electronics Laboratory Center Technical Note, TN 2787, Sept., 1974. This information is to be identified as tentative and unpublished.
- Noonkester, V.R. and J.H. Richter (1980), "Radar investigations of the clear air," Radio Science, Vol. 15, No. 2, p. 337-353.
- Campbell, W.C., R.B. Chadwick, K.B. Earnshaw, and K.P. Moran (1980), "Low elevation angle wind measurements by FM-CW radar," 19th Convergence on Radar Meteorology, American Meteorological Society, p. 722-726.

CHAPTER 5 -- AIRPORT OPERATION AT OTIS AIR FORCE BASE, MASSACHUSETTS

R.B. Chadwick, K.P. Moran, W.C. Campbell, and T.R. Detman

5.1 Introduction

During May and June of 1980, the FM-CW radar was operated continuously near the AFGL meteorological test site at Otis Air Force Base, Massachusetts. The move across country from Colorado caused some damage and this had to be repaired before the test period could start. Most of the damage was related to the vibration the radar experienced while moving from White Sand Missile Range to Otis AFB. The radar was designed only as an experimental unit and was never meant to be moved long distances. It was with great reluctance that we undertook this move and it was only because of the dedication of the people involved that the operation was not a failure.

One major problem in analyzing the data has developed. The raw data was recorded on magnetic tape and it was planned to analyze and display processed information off-line. However, on a later non-Air Force experiment that the radar was involved in, a break-in and theft occurred and some needed computer equipment was stolen. Because of the inevitable delays and red tape involved in replacing this equipment, we have been unable to perform the planned analysis for this final report. What is presented here are the results of hand graphical analysis on photographic data and on some graphical output of the computer line printer. Because the analysis was done by hand, there may be errors, however every effort has been taken to make these errors as small as possible.

There are two different types of data presented in this chapter. The first set of data was taken on 21 May 1980, a day with considerable rain activity. The main feature of interest here is a persistent shear layer. The second set of data is in the clear air and is from low-angle velocity-azimuth displays (VAD). Wind profiles were calculated from this data and compared with winds taken from the AFGL tower facility at Otis AFB.

5.2 Wind Shear Measurements in Rain

The meteorological situation on 21 May 1980 was that of a stratiform rain reaching to about 4 km. The return was such that the radar would experience post-detection saturation using the receiver amplifier gains normally used for clear-air return. However, there was no pre-detection saturation. The power into the mixer was measured at -30 dBm which is equivalent to a receiving antenna power level of -45 dBm in Fig. 3.1. This level is about 30 dB below the pre-detection saturation level in Fig. 3.1. To prevent the post-detection saturation, we operated the radar with about 20 dB less gain in the audio amplifier which follows the mixer. We did not have to reduce the transmitted power and this shows that a ranging CW radar can operate well in rain at full power.

On 21 May 1980, the rain started about 0645 and continued with uniform intensity until about 1600 when the intensity became much less. Personnel arrived at the radar at 0830 and immediately began equipment check-out, calibration, and power measurements. From 0930 to 1015, data was taken for a rain test at an elevation angle of 60° and a maximum range of 1686 m (maximum height of 1460 m). During this test, no wind shear was detected. From 1033 to 1114, the elevation angle remained at 60° and the maximum range was varied from 14,900 m to 1686 m. This verified that the top of the rain was about 4 km and that no wind shear existed in the rain. An example of the radar output for this constant elevation, constant azimuth operation is shown in Fig. 5.1 and Fig. 5.2 where the elevation

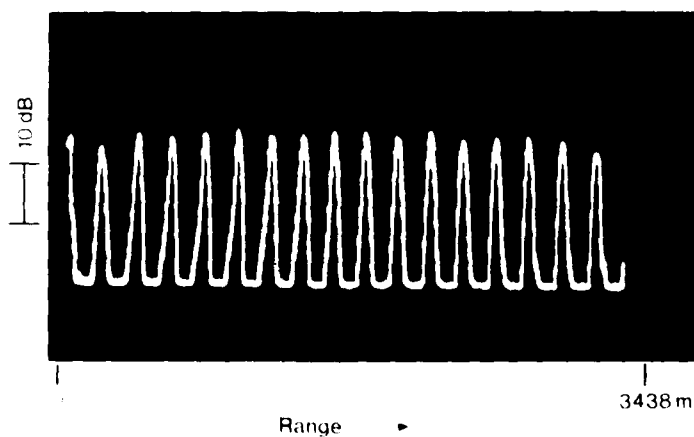


Figure 5.1--Radar output showing 16 adjacent velocity spectra taken in stratiform rain. The range spacing between spectra is 215 m while the velocity scale from one spectrum to the adjacent is 9 m/s.

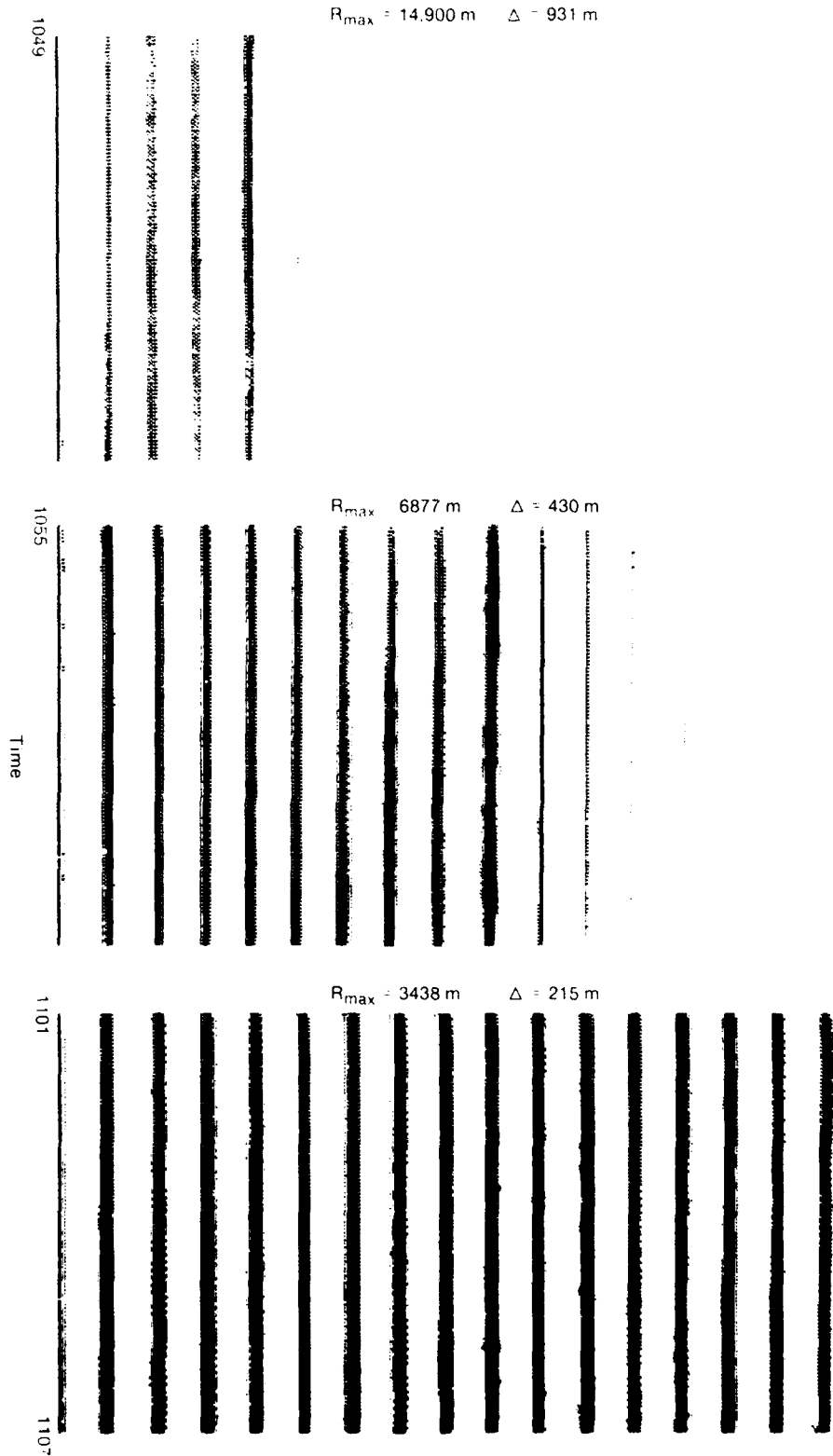


Figure 5.2--Time history of radar output for three different range settings at a constant azimuth and elevation in stratiform rain.

angle is 60° and the azimuth angle is 275° . Figure 5.1 shows a single radar output record which consists of 16 side-by-side radial velocity spectra where each one is from a different 215 m range cell. The maximum range is 3438 m and the maximum height is 2977 m. The uniform spacing shows that there is no wind shear up to 2977 m height. Figure 5.2 shows time histories (over approximately five minutes) for three different ranges where the maximum heights are 12900 m, 5950 m and 2980 m. These data show a very uniform velocity field with no wind shear.

At 1120, the radar crew went for lunch and because of the stratiform rain which had not changed all morning, the radar was left in a standby mode. Then after returning from lunch at 1230, the radar was set to a maximum height of about 1200 m until 1400. So the heights above 1200 m were not monitored from 1110 to 1400 and during this time a strong wind shear developed at about 2000 m as shown below.

Figure 5.3 shows a velocity azimuth display (VAD) which was taken between 1437 and 1449. The maximum range is 14,900 m at an elevation angle of 20° for a maximum height of 5096 m. The standard VAD (with 16 range gates) would show 16 one-cycle segments of sine waves where wind velocity is proportional to sine wave amplitude and wind direction is proportional to sine wave phase. So a VAD in a uniform wind field would consist of constant amplitude, constant phase, one cycle segments of sine waves. The VAD in Fig. 5.3 shows one cycle segments of sine wave, but these change both phase and amplitude with height. A complete wind profile can be obtained from a VAD and the profiles of wind speed and direction are shown in Fig. 5.4. The strong shear layer at about 2 km has developed since 1100. A second VAD at 30° elevation angle and maximum range of 6877 m was taken from 1505 to 1516 and is shown in Fig. 5.5. The profiles derived from this VAD are shown in Fig. 5.6. The shear layer is persistent and seems to be located at 2 km height. The VAD data were reduced to profiles by a graphical technique which involved some subjective judgment to determine the mean velocities. This could account for some of the differences between Fig. 5.4 and 5.6. The main difference appears to be the minimum velocity at the shear layer. The sine wave amplitudes in Fig. 5.5 are difficult to define and measure by graphical technique.

AD-A108 236

NATIONAL OCEANIC AND ATMOSPHERIC ADMINISTRATION BOUL--ETC F/G 17/9
DEVELOPMENT OF A CLEAR AIR RADAR TO DETECT METEOROLOGICAL HAZAR--ETC(U)
SEP 81 R B CHADWICK, K P MORAN, W C CAMPBELL

AFGL-TR-81-0268

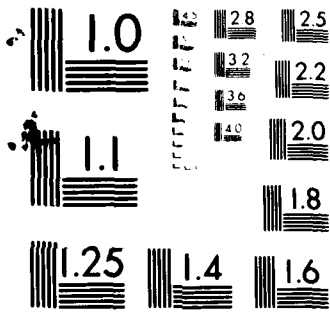
NL

UNCLASSIFIED

2
11
10
9



END
DATE
FILMED
1 82
DTIC



MICROCOPY RESOLUTION TEST CHART
NATIONAL BUREAU OF STANDARDS-1963-A

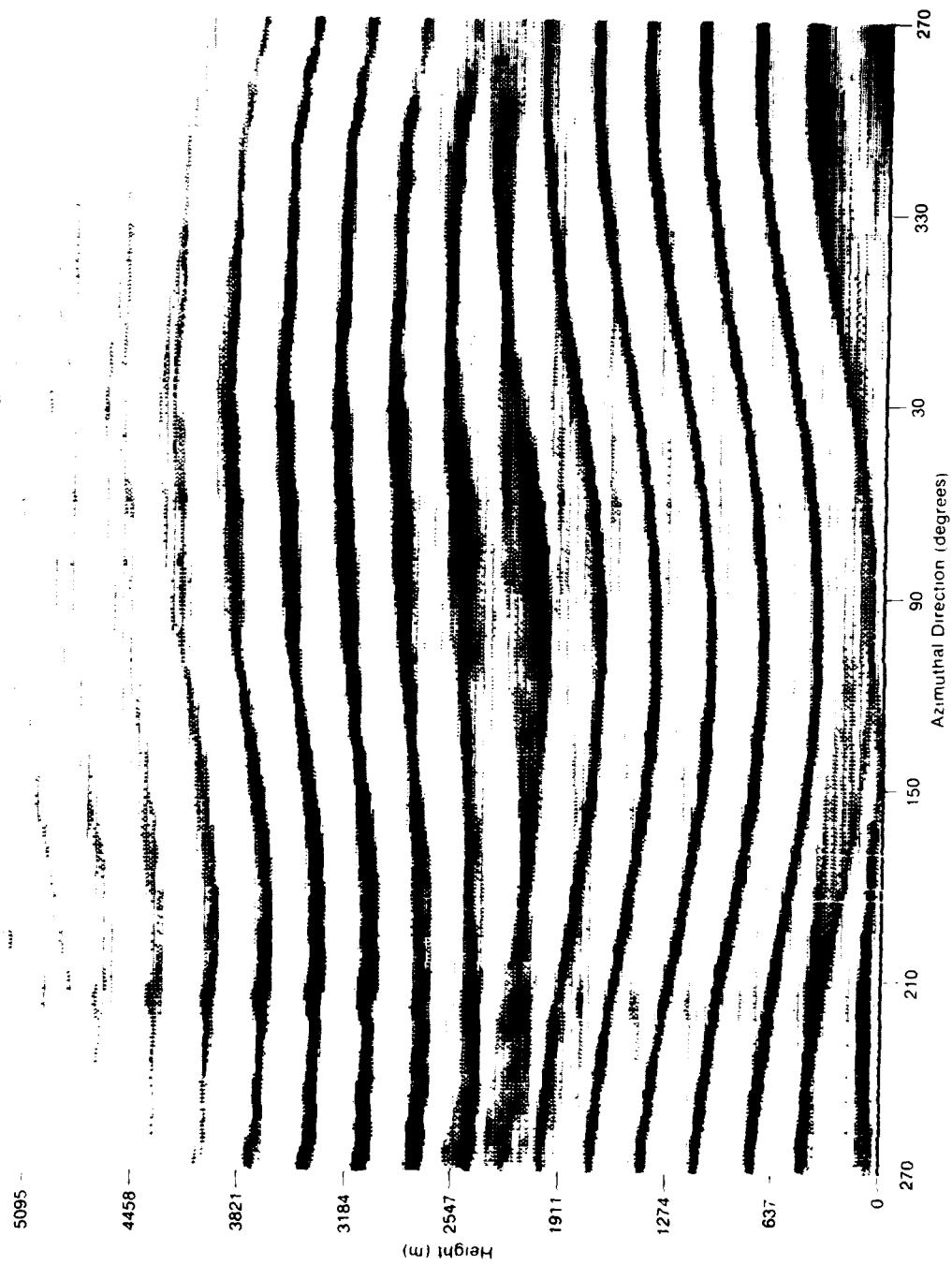


Figure 5.3--Velocity azimuth display in rain with a wind shear layer present.
 Maximum range is 14.9 km and elevation angle is 20°.

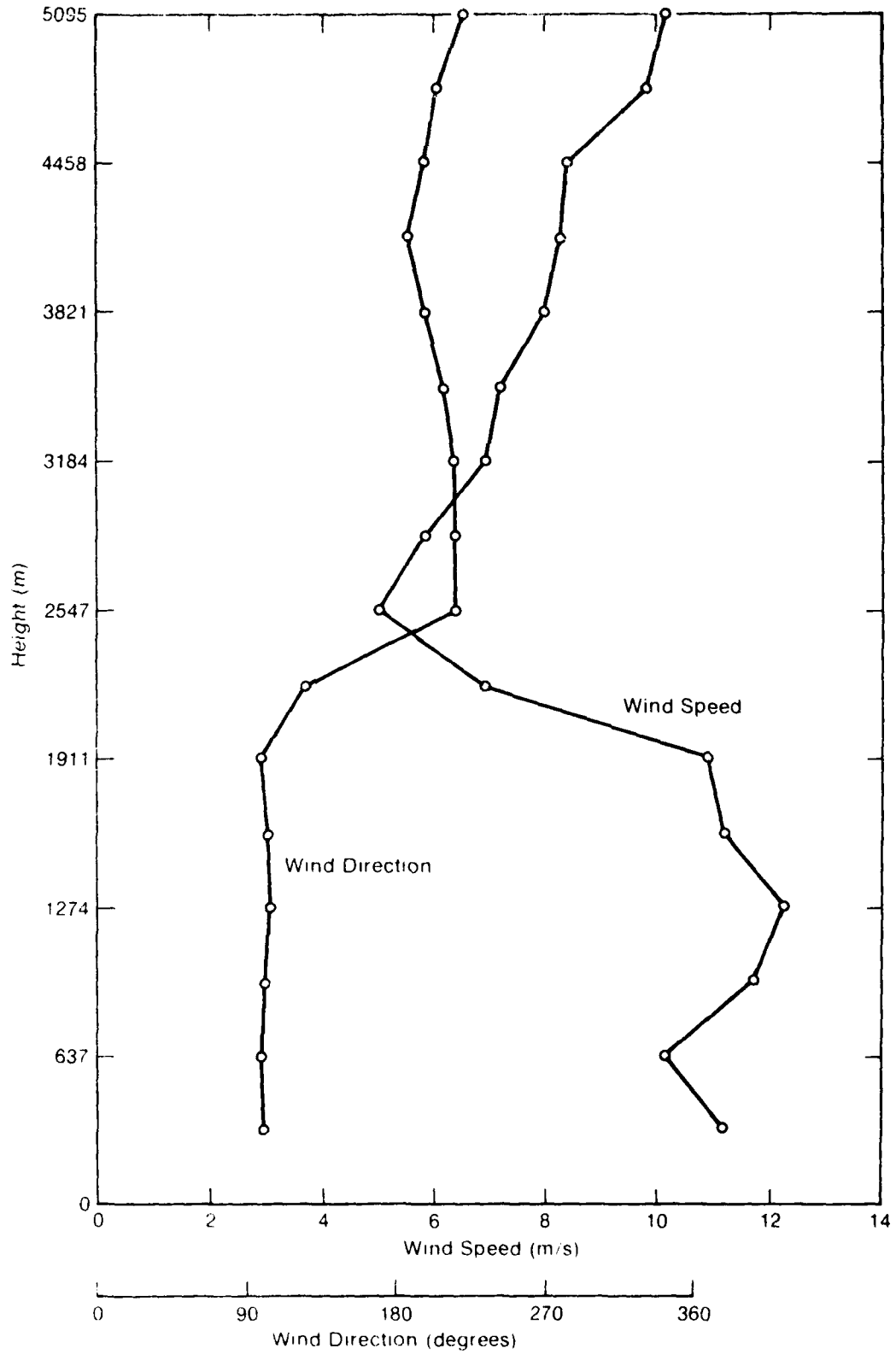


Figure 5.4--Wind profile obtained graphically from VAD in Fig. 5.3.



Figure 5.5--Velocity azimuth display in rain with a wind shear layer present.
 Maximum range is 6877 m and elevation angle is 30°.

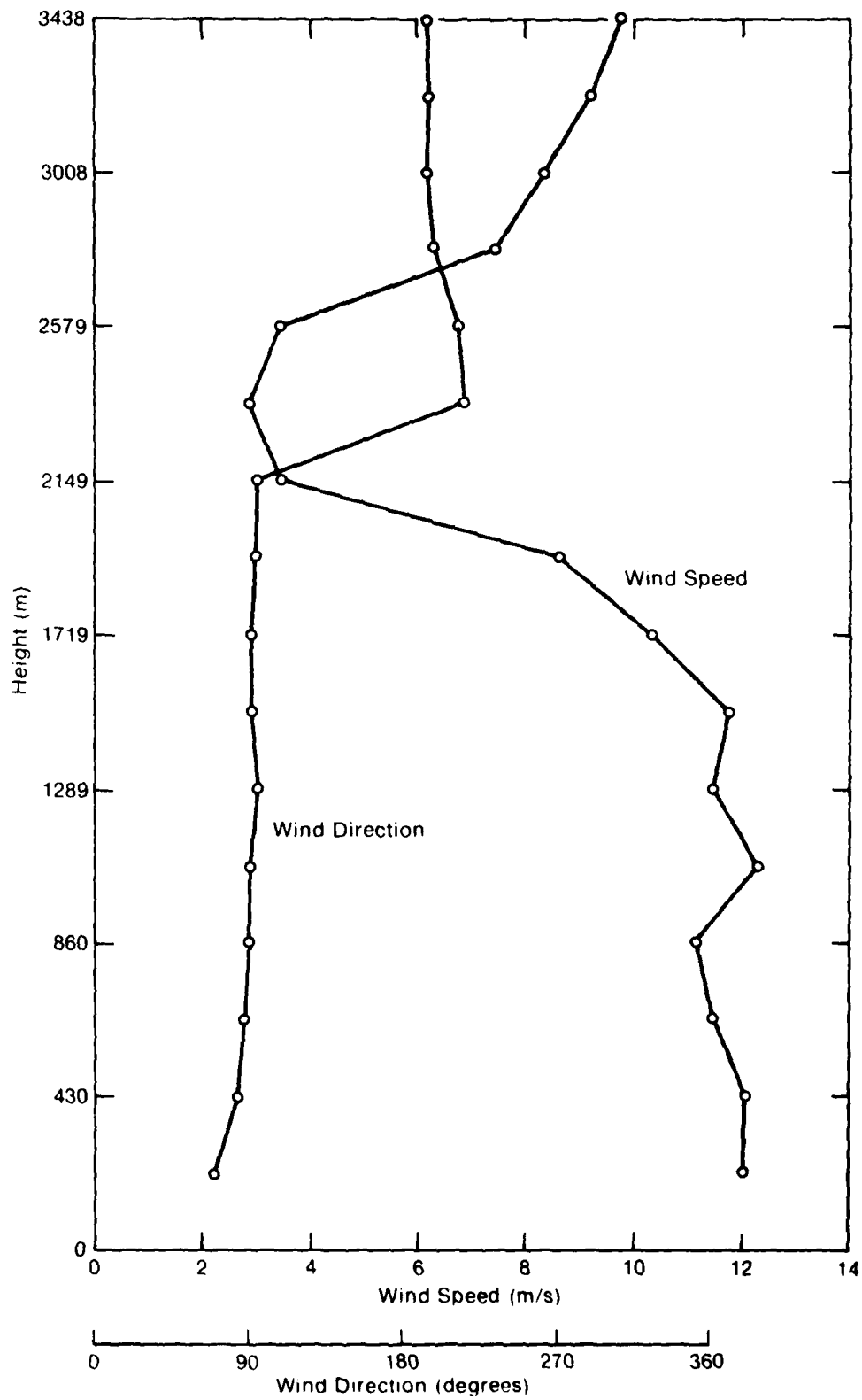


Figure 5.6--Wind profile obtained graphically from VAD in Fig. 5.5.



Figure 5.7--Radar output similar to that in Fig. 5.1 except that a shear layer is present.

It is of interest to compare a single radar output taken in the shear layer with the radar output under uniform winds. Figure 5.7 shows the radar output at the end of the VAD in Fig. 5.5. In this type of display the shear layer is evident mainly by the increased spectral width in the layer. This shows that there is increased small scale turbulence in the layer and this would certainly be noticed by an aircraft descending through the layer. In the case of uniform wind the spectral spacing is constant as shown by Fig. 5.1. For the case of a shear layer, the spectral spacing is constant above and below the layer, but not through it as shown by Fig. 5.7.

The VAD scan holds elevation constant and changes azimuth. Another scan is to hold azimuth constant and change elevation. With a conventional meteorological radar, this is called a Range Height Intensity (RHI) display. In our case, velocity is also indicated, but we will still call this display an RHI.

From 1534 to 1539, an RHI was taken where azimuth was held at 270° and the elevation was increased from 5° to 90° at a uniform rate. The RHI obtained from this scan is shown in Fig. 5.8 where the numbers on the display indicate the height (km) for a zero velocity point. The distinctive feature in Fig. 5.7 is the change in radial velocity as the beam passes through the layer. This outlines the shear layer and shows that it is still at about 2 km height.

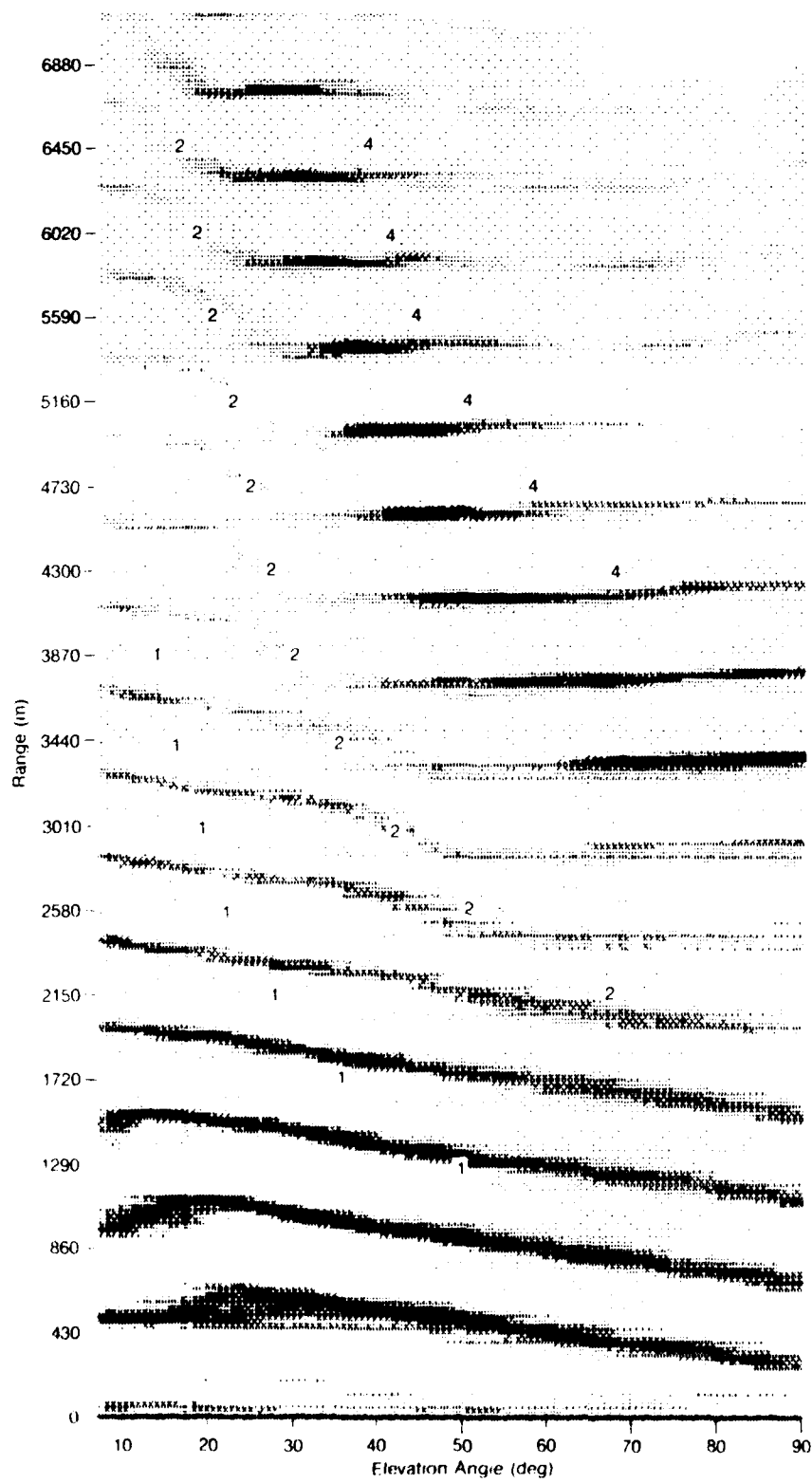


Figure 5.8--Range height intensity display of the wind shear layer. The numbers show heights in km.

An additional feature in Fig. 5.8 is the region of increased return slightly below the 4 km height. This is probably the melting region or "bright band" as it is sometimes called.

The data presented show that the FM-CW radar can detect and map wind shear layers in stratiform rain. These measurements were made at full power and there was no pre-detection saturation. The increased dynamic range was handled by changing the gain in the audio portion of the receiver and in an operational system, this could easily be done automatically.

5.3 Comparison of Tower Measurements and Radar Measurements of Low-Level Winds

The experiment at Otis AFB was conducted to obtain side-by-side comparisons between the radar and a meteorological tower at some location meteorologically different from the high plains of Colorado. The maritime regime of southern Massachusetts provided the first real test of our radar in a humid environment. Because the radio refractive index is determined mainly by the amount of water vapor present, we expected the radar to work better at Otis AFB than in Colorado. This was not the case. The radar did not seem to operate greatly different in the clear air of a maritime regime than in the clear air of a high plains regime. We were able to measure winds in the clear air to slant ranges in excess of 7 km and to heights of 2-3 km which is very similar to the capability of the radar when it is in Colorado. We had hoped to process the data for C_n^2 values measured in Massachusetts and compare them with C_n^2 values measured in Colorado. However, the graphical nature of the analysis precluded these comparisons.

The comparison that we can make are between the winds as measured by the radar and as measured by the tower. The tower is 200 ft high which matches up with the lower five range bins when the radar is at 1000 m maximum range and 7° elevation angle. The tower measurements were made with standard anemometers at heights of 50, 100, 150, and 200 feet. The radar measurements were made by scaling velocities and angles from PSI displays photographed during the experiment. Even though this procedure was done with the maximum possible care, some error will still be present.

On May 27, 28, and 29, many azimuth scans were made to compare with tower measurements. This was a period of clear, sunny days with differing wind conditions. These azimuth scans were generally at elevation angles less than 10° and maximum ranges from 1000 m to 7000 m. Figure 5.9 shows a PSI made during one of the azimuth scans where the scan was between 60° and 150° . The elevation angle in this case is 9.9° and the maximum range is 1064 m and this causes the first four range gates to fall within the tower height. The zero velocity points or range markers show up on the PSI as concentric circles of rings, and radial velocity (at that azimuth) is the departure of the atmospheric return from the zero velocity points. The wind profile from Fig. 5.9 is shown in Fig. 5.10 where the agreement is fairly good, except for the wind speed at the lowest height. Examination of the first range cell in Fig. 5.9 reveals that the atmospheric return and the zero velocity point (or ring) are both fairly wide regions and any graphical technique to find the separation is error prone.

Figure 5.11 shows another PSI taken shortly after the first, except now the azimuth scan is from 60° to 300° at an elevation angle of 7.5° . The reduced elevation angle means that now the lower five range cells are within tower height and the agreement between the tower winds and the radar winds is quite good as shown by Fig. 5.12.

Figure 5.13 shows a PSI taken about three hours later at an elevation of 7° . Again the agreement with the tower is reasonable as shown by Fig. 5.14. Note in Fig. 5.13 that wind shear to the west would be easily recognized as a change in displacement from the zero velocity points.

On the next day, May 28, the PSI in Fig. 5.15 was taken at a 7° elevation angle and a maximum range of 2128 m. In this case, three range cells are within tower height and these show excellent agreement with the tower as shown in Fig. 5.16. During this scan, there was a triggering instability in the display which accounts for the changes in the concentric circles in Fig. 5.15.

A PSI at a much greater range was taken on May 29 and is shown in Fig. 5.17. The maximum range of 6386 m and the elevation angle of 7° means that the first range gate is above the top of the tower. However, a comparison as in Fig. 18 shows that the radar measured winds compare favorably with extrapolated tower winds. Figure 5.17 shows several instances of the range spreading phenomena discussed in Chapter Three.

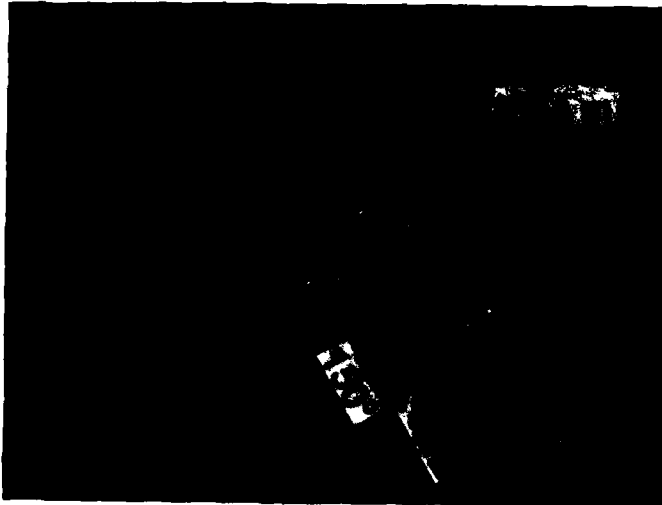


Figure 5.9--Partial PSI taken from azimuth scan of 60° to 150° at elevation angle of 9.9°. The maximum range is 1064 m.

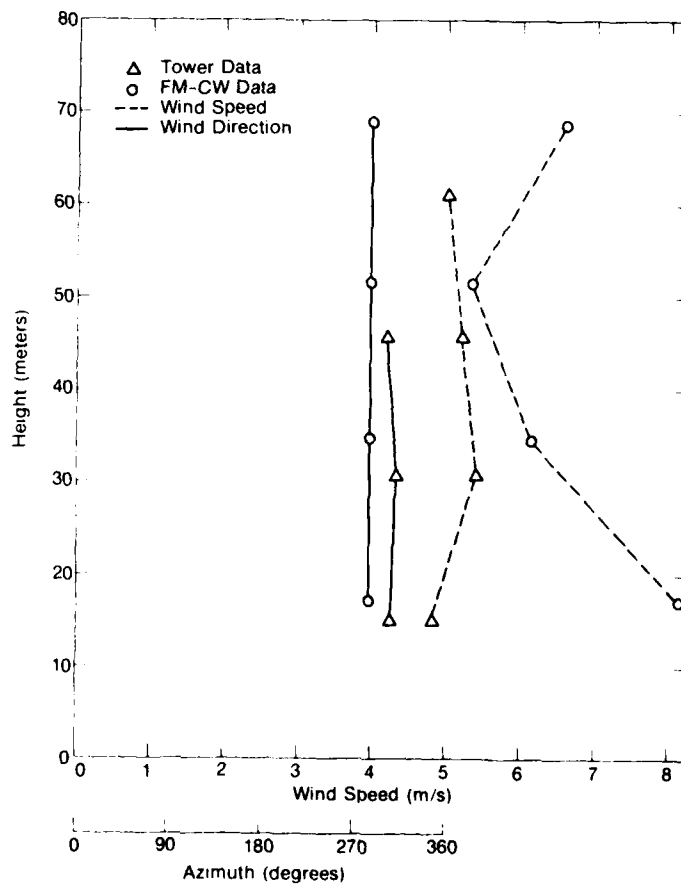


Figure 5.10--Wind profiles as measured by tower and radar. This is for the PSI in Fig. 5.9.

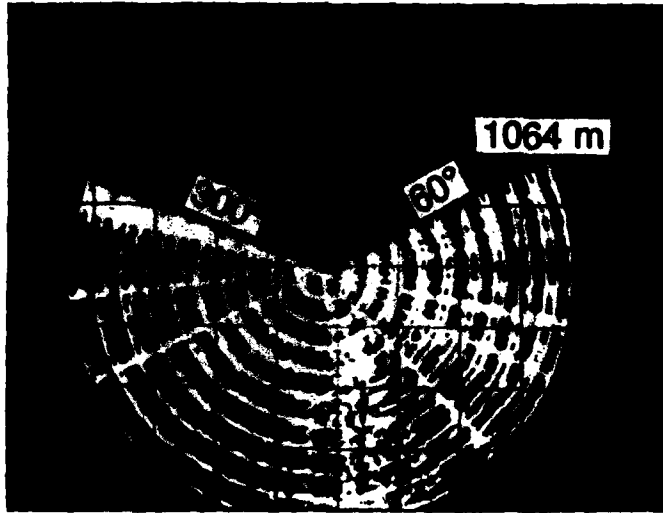


Figure 5.11--PSI taken from azimuth scan of 60° to 300° at an elevation angle of 7.5° and maximum range of 1064 m.

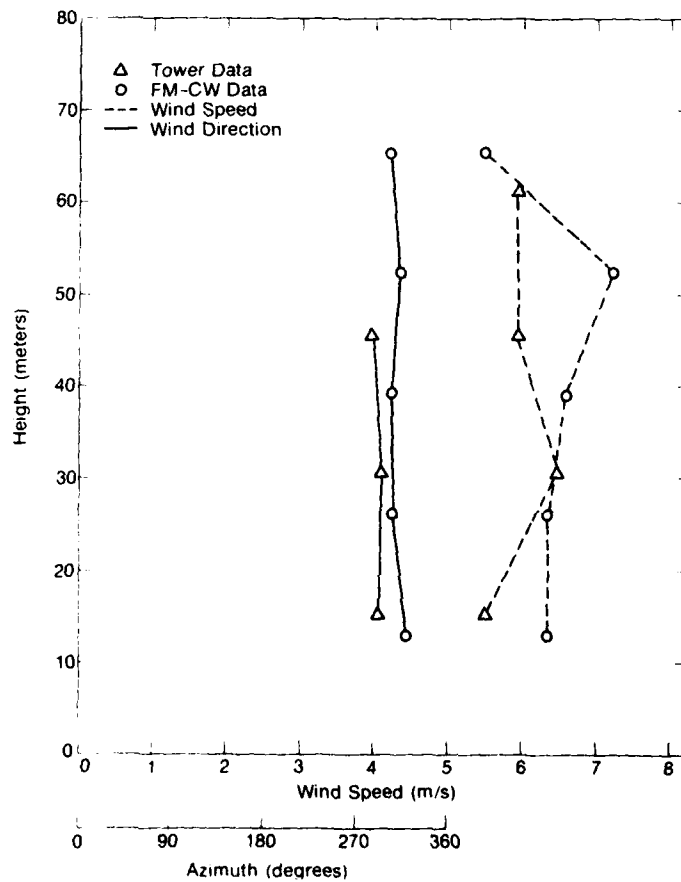


Figure 5.12--Wind profile is measured by tower and radar. This is for the PSI in Fig. 5.11.

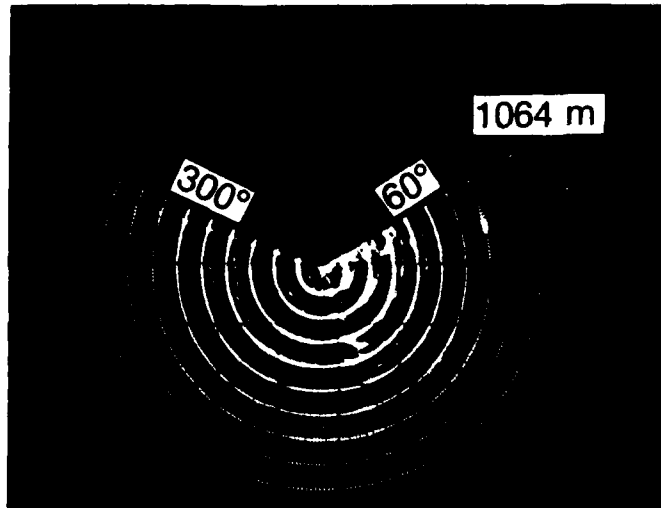


Figure 5.13--PSI taken from azimuth scan of 60° to 300° at an elevation angle of 7° and maximum range of 1064 m.

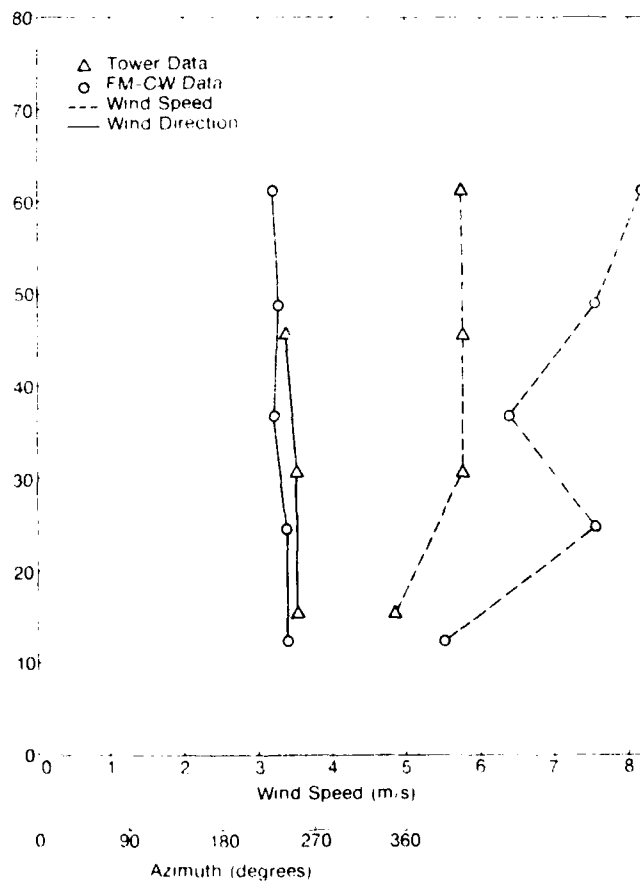


Figure 5.14--Wind profiles as measured by tower and radar. This is for the PSI in Fig. 5.13

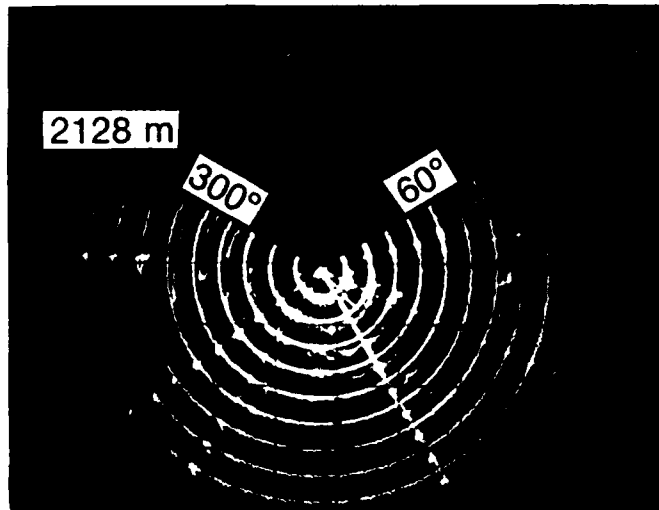


Figure 5.15--PSI taken from azimuth scan of 60° to 300° at an elevation angle of 7° and maximum range of 2128 m.

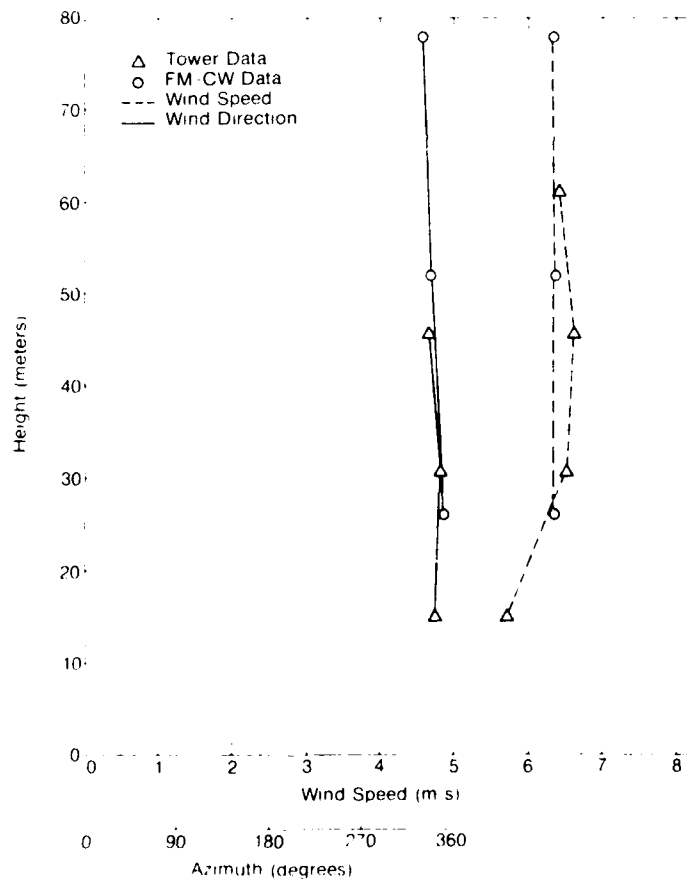


Figure 5.16--Wind profiles as measured by tower and radar. This is for the PSI in Fig. 5.15.

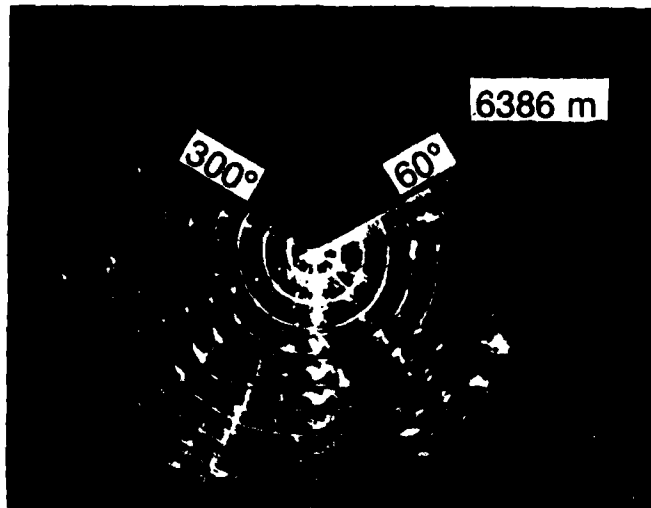


Figure 5.17--PSI taken from azimuth scan of 60° to 300° at an elevation angle of 7° and maximum range of 6386 m.

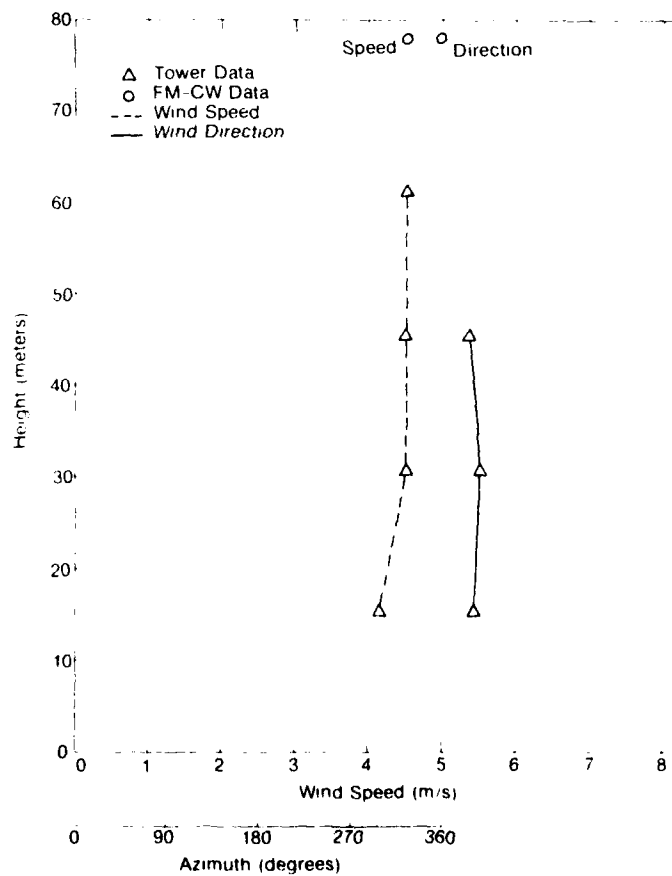


Figure 5.18--Wind profiles as measured by tower and radar. This is for the PSI in Fig. 5.17.

5.4 Summary of Experimental Results

One result of the Otis AFB experiment is that an FM-CW radar can measure winds to significant ranges in maritime air. This was expected. However, we had expected that there would be an increase in capability in the moist maritime air and this did not occur. The range capability of the radar seems to be approximately the same in a maritime regime as in a high plains regime. Clear air wind measurements to ranges of 6 to 10 km seem reasonable.

A second result is that the radar capability increases in stratiform rain. An excellent example of a shear layer in rain was obtained at Otis AFB and was discussed in Section 5.2. In that case, there was no problem with pre-detection saturation, and the post-detection saturation was avoided by reducing the receiver gain, a process that could easily be automated.

There were also numerous comparisons of wind as measured by a tower and the radar. These comparisons show good agreement. What discrepancies there are can perhaps be attributed to the graphical nature of the data reduction.

CHAPTER 6 -- SUMMARY AND OBSERVATIONS

R.B. Chadwick

Low level wind shear became a widely recognized aviation hazard in the 1970's and still represents an unsolved problem. Annual workshops concerned with meteorological inputs to aviation system have been sponsored jointly by NASA, NOAA and the FAA for the past five years and one of the findings of these workshops is that wind shear continues to be a serious problem. In a summary of these five workshops, Frost and Camp (1981), it is stated that "wind shear effects in the terminal area has through all five workshops continued to be one of the most dominant topics of discussion. The 1981 committee reported the re-occurring theme that current wind shear detection and warning systems are inadequate." We feel that the short-range, clear-air radar technology outlined in this report represents a viable approach to solving this problem.

In the past, both acoustic and optical wind measurement techniques have been applied to the wind shear measurement problem and have been rejected for various reasons. An approach based on radar has a very important advantage over both acoustic and optical techniques. Radar is an all-weather approach and, as shown in Chapter Five, rain actually enhances the capability of radar to measure winds. Both the acoustic and optical approaches fail under certain rain conditions. One of the important results of the wind shear detection research over the past several years is that microwave radar is the appropriate remote sensing device to detect hazardous wind shear. In the summary of aviation weather research referred to above, Frost and Camp (1981), state "the application of ground based, pulsed microwave Doppler radar which is located at or near the terminal to provide detection capabilities of wind shear along approach and departure paths is strongly supported. ...The development of Doppler radar technology to detect the wind shear hazard should be continued at an accelerated pace." We feel that an FM-CW radar technique is more appropriate than pulsed techniques because of lower cost, more flexibility, capability of detecting aircraft wake echoes, and a reduced non-thermal radiation hazard.

The work described in this report, is a continuation of that in an earlier Air Force Geophysics Laboratory report, Chadwick et al. (1978). At the start of the period covered by that report it was not known if microwave radar could be used to detect wind shear at airports. The task in that project was to measure the clear air radar return over a one-year period to determine if radar detection of wind shear is feasible. The main conclusion was that it was indeed feasible to detect low level wind shear at airports with microwave radar. A secondary conclusion was that the FM-CW radar was a possible device to detect wind shear but that the technology necessary to operate this type of radar at low elevation angles had to be developed.

The main task for the period covered by the present report was to develop low elevation angle capability for the existing experimental FM-CW radar. The first sub-task to accomplish this was to try and reduce the antenna sidelobes to as low a level as possible without incurring major expense. The approach was to replace the feed horns and this is described in detail in Chapter Two. The present status of the antennas is adequate, but could be improved and possible approaches are outlined in Chapter Two. It is desirable to be able to operate with a single antenna and some results of preliminary research to accomplish this are contained in Chapter Two. It is still not clear if single antenna operation with 100% duty cycle is possible, but we are strongly convinced that single antenna operation with 50% duty cycle is possible.

The second sub-task necessary to achieve low angle capability was to develop techniques for canceling ground returns electronically. This is covered in Chapter Three. The two necessary requirements for canceling ground clutter are a stable transmitted signal and a digital filter to suppress the ground return. Both of these were developed and are discussed in Chapter Three. The results indicate that clutter canceling of 40 dB has been obtained. One problem here is that the antenna assembly is on a conventional sprunged trailer and the antennas move slightly in the wind. These movements are such that the ground clutter changes phase and can not be canceled as readily. Of course, this problem can be solved by a more stable antenna assembly.

Our experiments at various sites have shown that the geographical surroundings of the site are extremely important but are difficult to quantify. This

is discussed in Chapter Four. Another important result in Chapter Four is the ability to detect echoes from aircraft wakes and the possibility that these returns may be useful in detecting hazardous wingtip vortices in the wakes of large aircraft. This raises the possibility of a single, all-weather device to monitor for hazardous wind shear and for hazardous vortex conditions. One of our recommendations in Chapter One is that this possibility be explored.

Results taken at Otis Air Force Base under both rain and clear air conditions are contained in Chapter Five. These results show that the FM-CW radar is capable of working for a wide range of weather conditions. Some changes in baseband receiver gain are necessary, but this type of change could easily be automated.

The present status of FM-CW radar technology as applied to monitoring the airport environment is that an experimental radar exists and has been tested at airports. The results are entirely positive and indicate that further work should be done. The experimental radar was built in 1973-74 using early 1970's technology, and is obsolete in terms of 1980's technology. However, it has been possible to test and prove or disprove many concepts. Some of the recommendations in Chapter One relate to upgrading or replacing the experimental radar. There is no question that the appropriate technology exists to build an FM-CW radar capable of operationally detecting hazardous wind shear. The only question is to whether or not the necessary resources can be brought to bear on this important problem.

CHAPTER 6 -- BIBLIOGRAPHY

1. Frost, W. and D.W. Camp (1981), "Summary of Aviation Weather Research and Development Needs Identified through the Annual Workshops on Meteorological and Environmental Inputs to Aviation Systems," obtainable through D.W. Camp, Space Sciences Laboratory, NASA Marshall Space Flight Center, AL 35812.
2. Chadwick, R.B., K.P. Moran, G.E. Morrison, and W.C. Campbell (1978), "Measurements Showing the Feasibility for Radar Detection of Hazardous Wind Shear at Airports," Tech. Report AFGL-TR-78-0160, Air Force Geophysics Laboratory, Hanscom AFB, Mass. 01731.